IWS1 phosphorylation promotes cell proliferation and predicts poor prognosis in EGFR mutant lung adenocarcinoma patients, through the cell cycle-regulated U2AF2 RNA splicing.

Georgios I. Laliotis[1,2,3], Evangelia Chavdoula[1,2§], Maria D. Paraskevopoulou[4,12§], Abdul Kaba[1,2], Alessandro La Ferlita[1,2,5], Vollter Anastas[1,2,6], Arturo Orlacchio[1,2], Vasiliki Taraslia[4,13], Ioannis Vlachos[7,14], Marina Capece[1,2], Artemis Hatzigeorgiou[7], Dario Palmieri[1,2], Salvatore Alaimo[5], Christos Tsatsanis[8,9], Lalit Sehgal[10], David P. Carbone[11], Vincenzo Coppola[1,2] and Philip N. Tsichlis[1,2*]

[1]The Ohio State University, Department of Cancer Biology and Genetics, Columbus, OH, 43210, [2]The Ohio State University Comprehensive Cancer Center-Arthur G. James Cancer Hospital and Richard J. Solove Research Institute, Columbus, OH, 43210 [3]University of Crete, School of Medicine, Heraklion Crete, 71500, Greece, [4]Molecular Oncology Research Institute, Tufts Medical Center, Boston, MA, 02111 [5]Department of Clinical and Experimental Medicine, Bioinformatics Unit, University of Catania, Catania, 95131, Italy, [6]Tufts Graduate School of Biomedical Sciences, Program in Genetics, Boston, MA, 02111 [7]DIANA-Lab, Hellenic Pasteur Institute, Athens, 11521, Greece, [8]Department of Clinical Chemistry-Biochemistry, School of Medicine, University of Crete, Heraklion 71110, Crete, Greece, [9]Institute for Molecular Biology and Biotechnology, Foundation for Research and Technology Hellas, Heraklion 70013, Greece, [10]Department of Internal Medicine, Division of Hematology, The Ohio State University, Columbus, OH 43210 [11]Department of Internal Medicine, Division of Medical Oncology, The Ohio State University Medical Center, Columbus, OH, 43210

Running Title: IWS1 and U2AF2 RNA splicing in EGFR mutant lung adenocarcinoma.

[§] These authors contributed equally to this work.

Present Address :

[12]Takeda Pharmaceuticals U.S.A, Boston, MA, 02139, USA

[13]Center of Basic Research, Biomedical Research Foundation of the Academy of Athens, 11527, Greece

[14]Beth Israel-Deaconess Medical Center, Department Of Pathology, Harvard Medical School, Boston, MA 02215, USA

*Corresponding author: Philip N. Tsichlis, Department of Cancer Biology and Genetics. The Ohio State University, and the Ohio State University Comprehensive Cancer Center. Columbus Ohio 43210. Email: Philip.tsichlis@osumc.edu

Abstract

Our previous studies have shown that IWS1 (Interacts with Spt6) is a phosphorylation target of AKT and regulates the alternative RNA splicing of *FGFR2*, linking IWS1 with human Non-Small Cell Lung Cancer. To further address the role of IWS1 in alternative RNA splicing in lung cancer, we performed an RNA-seq study using lung adenocarcinoma cells in which IWS1 was knocked down or replaced by its phosphorylation site mutant. The results identified a novel, exon 2 deficient splice variant of the splicing factor U2 Associated-Factor 2 (U2AF2), whose abundance increases, upon the loss of phosphorylated IWS1. This exon encodes part of the U2AF65 Serine-Rich (SR) Domain, which is required for its binding with pre-mRNA Processing factor 19 (Prp19). Here, we show that *U2AF2* exon 2 inclusion depends on phosphorylated IWS1, by promoting histone H3K36 trimethylation and the assembly of LEDGF/SRSF1 splicing complexes, in a cell-cycle specific manner. Inhibition of the pathway results in the downregulation of cell cycle division associated 5 (*CDCA5*), a phosphorylation target and regulator of ERK, leading to G2/M phase arrest, impaired cell proliferation and tumor growth in mouse xenografts models, an effect more pronounced in EGFR mutant cells. Analysis of lung adenocarcinoma samples revealed strong correlations between IWS1 phosphorylation, U2AF2 RNA splicing, and Sororin/p-ERK levels, especially in EGFR, as opposed to K-RAS mutant patients. More importantly, IWS1 phosphorylation and *U2AF2* RNA splicing pattern are positively correlated with tumor stage, grade and metastasis, and associated with poor survival in the same patients. This work highlights the instrumental role of the AKT/p-IWS1 axis to alternative RNA splicing in governing cell cycle progression and tumorigenesis and proposes this axis as a novel drug target in EGFR mutant lung adenocarcinoma, by concomitantly affecting the epigenetic regulation of RNA processing and oncogenic signals.

55 **Introduction**

56 Cells use a variety of mechanisms to regulate the fine-tuning of mRNA expression
57 (Glisovic T. et al., 2008[1]). These co- and post-transcriptional processes are orchestrated by a
58 complex RNA-binding protein network. (Jewer M. et al., 2012[2]). One of the main mechanisms of
59 this regulation is alternative RNA splicing. Most human genes harbor introns which are removed
60 during pre-mRNA splicing (Pan Q. et al., 2008[3]), a common mechanism employed by eukaryotic
61 cells to generate multiple transcripts and expand their functional network of the generated protein
62 products. Thus, regulation of alternative RNA splicing affects cellular fate and function and
63 controls the pathobiology of many diseases, including cancer (Paronetto M.P. et al., 2016[4], Zhang
64 X. et al., 2016[5]). Its importance has been demonstrated in different types of cancer, including non-
65 small cell lung carcinoma (NSCLC) (Coomer A.O. et al., 2019[6]).

66 Non-small cell lung carcinoma (NSCLC) is the 2nd most common cancer, with more than
67 250,000 new cases per year in the US and extremely poor prognosis with <5% 5-year survival
68 (Siegel et al., 2020[7]). NSCLC is further divided into lung adenocarcinoma, squamous cell
69 carcinoma and large cell carcinoma based on histological features. (Yuan M et al, 2019[8]). Notably,
70 up to 69% of NSCLCs harbor mutations in the Epidermal Growth Factor Receptor (EGFR) and
71 Kirsten Rat Sarcoma (KRAS) genes, affecting major downstream oncogenic signal such as the
72 PI3K/AKT and ERK/MAPK pathway (Sequist et al., 2020[9]).

73 Following our original observations linking the alternative RNA splicing of *FGFR-2* with
74 NSCLC (Sanidas et al., 2014[10]), several additional splicing events have been linked to the biology
75 of NSCLC including Bcl-X_L, CD44, Androgen Receptor (AR), HLA-G and PKM, by promoting cell
76 survival, metastasis, chemoresistance, immune surveillance and metabolic advantage,
77 respectively (Li Z. et al., 2016[11], Todaro M. et al., 2014[12], Oltean S. et al., 2014[13], Calabretta S.
78 et al., 2016[14]). Furthermore, another mechanism utilized by lung cancer cells involves the re-
79 programming of alternative splicing through the introduction of de novo mutations which create
80 new splice sites and alternatively spliced isoforms (Vo N.S. et al., 2018[15], Giaj Levra M. et al.,

81 2014[16]). This knowledge has led to an ongoing phase I clinical trial to determine the effects of a
82 modulator of the core splicing function, H3B-8800, in cancer patients (Seiler M., 2018[17]). Thus,
83 deeper comprehension of the molecular regulation of RNA splicing in lung cancer, and other
84 cancer types, is a necessity for proper design of anti-tumor therapies.

85 Mechanistically, alternative RNA splicing is regulated co-transcriptionally and through
86 chromatin modifications in the body of transcribed genes. When the rate of transcription is low, it
87 increases the probability for exons that are not efficiently spliced, to be spliced out of the mature
88 transcript. (Listerman et al., 2012[18]) Chromatin modifications are recognized by readers of
89 epigenetic marks, which orchestrate the assembly of molecular complexes that bind to, and
90 functionally regulate RNA-associated enhancers or repressors of splicing (*cis*-acting RNA
91 sequences). This alters the rate of assembly and the composition of spliceosomal complexes
92 (*trans*-acting RNA Binding Proteins-RBPs) (Luco et al., 2010[19], Pradeepa et al., 2012[20], Oltean
93 S. et al., 2014[10]). Cancer cells utilize this machinery in order to manipulate alternative RNA
94 splicing and promote tumorigenesis. Well studied families of RBPs include the Serine/Rich (SR
95 proteins) and heterogeneous nuclear ribonucleoproteins (hNRNPs). (Chen M. et al., 2009[21]). SR
96 proteins bind RNA exonic splicing enhancers (ESE) and intronic splicing enhancers (ISE) and
97 usually promote exon inclusion. (Obeng et al., 2019[22]). On the contrary, hnRNPs bind to exonic
98 splicing silencers (ESS) and intronic splicing silencers (ISS) and in most cases lead to exon
99 skipping. (Martinez-Contreras et al., 2007[23]). Several reports have shown the role of these RBPs
100 in the regulation of alternative RNA splicing and tumor growth in cancer cells, including Serine
101 Rich Specific Factor 1 (SRSF1) and Polypyrimidine Tract Binding Protein (PTB) (de Miguel et al.,
102 2014[24], Chen M et al., 2012[25], Jin W et al., 2003[26]).

103 One cellular function, which interfaces with the RNA splicing machinery, is the cell cycle
104 regulation (Dominguez et al., 2016[27]). Progression through the cell cycle depends on periodic
105 changes of RNA metabolism, which can be achieved by multiple mechanisms, one of which is
106 the periodic modulation of RNA splicing (Dominguez et al., 2016[27]). On the other hand, alterations

107 in RNA splicing, are regulated by periodic shifts in the expression and the activity of known cell
108 cycle regulators, such as the Aurora kinases (Moore et al., 2010[28]), the large SR domain-
109 containing protein SON (Ahn et al., 2011[29]), the RNA recognition motif (RRM)-containing protein
110 TgRRM1 (Suvorova et al, 2013[30]) and CLK1 (Dominguez et al., 2016[27]), demonstrating the
111 bidirectional relationship of these cellular functions.

112 We have previously shown that the transcription elongation factor IWS1 and the AKT3
113 kinase play a central role in the regulation of the alternative RNA splicing of *FGFR-2*, by promoting
114 the exclusion of exon 8. This exclusion event depends on the phosphorylation of IWS1 by AKT3
115 at Ser720/Thr721. IWS1 binds SPT6, which is attached to the phosphorylated Ser2 of the C-
116 terminal domain (CTD) of RNA polymerase II. SETD2, a histone H3 trimethyl-transferase, binds
117 to the IWS1/Spt6 complex only when IWS1 is phosphorylated at Ser720/Thr721. SETD2 bound
118 to the phosphorylated and CTD-associated IWS1, trimethylates histone H3 at K36 during
119 transcription. The histone H3K36me3 marks in the body of actively-transcribed target FGFR-2
120 gene are recognized by MRG15, which interacts with PTB leading to exclusion of exon 8 in the
121 mature FGFR2 mRNA transcript, affecting cell invasion, migration, cell proliferation and tumor
122 growth in mouse xenografts models. More importantly, we had shown robust expression of IWS1
123 phosphorylation in 21 out of 24 NSCLC samples, which correlates with AKT phosphorylation,
124 introducing the role of IWS1 in lung cancer (Sanidas et al., 2014[10]).

125 Here, to gain insight on the role of IWS1 phosphorylation in the pathogenesis of lung
126 cancer and the epigenetic regulation of alternative RNA splicing genome-wide, we performed
127 RNA-seq studies in lung adenocarcinoma cells NCI-H522, in which IWS1 was knocked down or
128 replaced by its phosphorylation site mutant. The results revealed a novel RNA splice variant of
129 the splicing factor U2 Associated Factor A2 (U2AF2), which lacks exon 2 upon loss of
130 phosphorylated IWS1. U2AF65, its protein product, as a splicing factor binds to the Polypyrimidine
131 (Py)-tract/3' splice site and initiates spliceosome assembly, by promoting the interaction between
132 U2 snRNP and the branchpoint (Shen H. et al., 2004[31]). Several reports have illustrated the role

133 of U2AF65 in lung cancer. Specifically, cancer-associated mutations of *U2AF2* in lung cancer
134 patients alter the affinity of its RNA-Binding Domain with Py-tract (Glasser E. et al., 2017[32]).
135 Furthermore, it has been shown that stabilization of U2AF65 by OTUB2 promotes Warburg effect
136 and tumorigenesis in NSCLC, pointing out the importance of this splicing factor in NSCLC. (Li J.
137 et al., 2018[33]). In this report, our goal was to further investigate the molecular mechanisms that
138 control exon inclusion phenotype induced by IWS1 phosphorylation, to characterize this novel
139 variant and to highlight its significance in lung carcinogenesis.

140 **Results**

141 **IWS1 expression and phosphorylation regulate alternative mRNA splicing.**

142 We have previously reported that IWS1 phosphorylation at Ser 720/Thr721, primarily by
143 AKT3, resulted in the exclusion of exon 8 of *FGFR-2* in the human NSCLC cell lines NCI-H522
144 and NCI-H1299 (Sanidas et al., 2014[10]). To explore the molecular mechanisms driving the IWS1
145 phosphorylation-dependent RNA splicing and gene expression, we performed RNA-Seq to
146 examine the transcriptome of shControl, shIWS1, shIWS1/wild type IWS1 rescue (shIWS1/WT-
147 R) and shIWS1/phosphorylation site IWS1 mutant rescue (shIWS1/MT-R) NCI-H522 cells. First,
148 we confirmed the significant down-regulation of IWS1 expression after the transduction of the
149 cells with lentiviral shIWS1 construct and the rescue of IWS1 knock-down with the Flag-tagged
150 wild type and phosphorylation IWS1 site mutant (**Fig. 1A**). Differential expression analysis of the
151 RNA-seq data, identified 1,621 and 562 differentially expressed genes between shControl and
152 shIWS1 and between shIWS1/WT-R and shIWS1/MT-R cells, respectively ($p \leq 0.01$, FDR ≤ 0.2).
153 340 genes were detected as differentially expressed in both comparisons (**Fig. S1A, S1B**).
154 Moreover, 19 out of the FDR-ranked top 100 differentially expressed genes, in shControl versus
155 shIWS1 cells, were also differentially expressed in shIWS1/WT-R versus shIWS1/MT-R (**Fig.**

156 **S1C**). Gene Set Enrichment analysis (Subramanian et al., 2005[34]), revealed significant
157 enrichment of genes involved in RNA metabolism and regulation of RNA processing (**Fig. S1D**).
158 Using an unbiased approach, we performed differential exon usage analysis of the RNA-
159 seq data, DEXseq (Anders et al., 2012[35]), to determine the effect of IWS1 expression and
160 phosphorylation on RNA splicing. This analysis identified 1,434 (corresponding to 851 genes) and
161 436 (corresponding to 273 genes) differentially employed exons between shControl versus
162 shIWS1 and shIWS1/WT-R versus shIWS1/MT-R cells, respectively ($p \leq 0.05$). The 1,796
163 differentially expressed genes and the 692 genes with differential exon usage in shIWS1 versus
164 shControl cells, exhibited an overlap of 165 genes ($p \leq 0.05$). Similarly, the 858 differentially
165 expressed genes and the 230 genes with differential exon usage, between shIWS1/MT-R and
166 shIWS/WT-R cells revealed an overlap of 44 genes (**Fig. 1B**).
167 Our earlier studies have shown that the IWS1 expression and phosphorylation promote
168 exon exclusion in the *FGFR-2* gene (Sanidas et al., 2014[10]). Therefore, we analysed the exon
169 usage data, and we observed that the most common event associated with the expression and
170 phosphorylation of IWS1, was exon inclusion (**Fig. 1C).** Functional analysis of the IWS1-regulated
171 alternative spliced genes, focused on GO-biological processes, identified significant enrichment
172 of genes involved in RNA processing and RNA splicing, among the top biological processes
173 regulated by IWS1-dependent alternative RNA splicing (**Fig. 1D, 1E**). It is remarkable that the
174 results were similar with the results generated from the functional analysis of the IWS1-dependent
175 differential gene expression. Therefore, these findings imply that the effect of IWS1 on RNA
176 processing may be direct or indirect. The indirect effect may be due to the IWS1 expression and
177 phosphorylation-dependent differential regulation of genes involved in RNA processing.
178 Validation of the RNA-seq, using RT-PCR, showed several examples of alternative RNA
179 splicing of genes which are regulated by IWS1 and IWS1-phosphorylation, via exon inclusion
180 (**Fig. 1, S1G-S1J**). One of these events is the inclusion of exon 2 in the mature mRNA transcript
181 of *U2AF2*, the gene encoding the splicing factor U2AF65. To validate these results, we examined

182 the ratio of exons 2 and 3 (E2/E3 U2AF2) by RT-PCR in NCI-H522 and NCI-H1299 shControl,
183 shIWS1, shIWS1/WT-R and shIWS1/MT-R cells. The results revealed a decrease in the E2/E3
184 ratio in shIWS1 and shIWS1/MT-R cells, relative to shControl cells (**Fig. 1F**). The decrease in the
185 E2/E3 ratio in shIWS1 and shIWS1/MT-R, relative to shControl cells, was confirmed by
186 quantitative RT-PCR (**Fig. S1E**). Whereas the predominant *U2AF2* mRNA transcript in shControl
187 and shIWS1/WT-R cells contains exon 2, the predominant transcript in shIWS1 and shIWS1/MT-
188 R cells, is a novel transcript lacking exon 2. Sequencing data from the isolated PCR products in
189 NCI-H522 shControl and shIWS1 cells validated the exclusion of exon 2 in shIWS1-derived
190 *U2AF2* transcripts (**Fig. 1G**). Notably, the knockdown of IWS1 or the rescue with the non-
191 phosphorylatable site mutant (IWS1/MT-R) did not significantly change the total expression of
192 U2AF2 in NCI-H522 and NCI-H1299 cells. (**Fig. S1F**).

193 To establish whether IWS1 is directly involved in the molecular complex that regulates
194 U2AF2 RNA splicing, in NCI-H522 and NCI-H1299 cells transduced with shControl, shIWS1,
195 shIWS1/WT-R and shIWS1/MT-R, we performed chromatin immunoprecipitation (ChIP) assays.
196 The results revealed that both IWS1 WT and S720A/T721A bind equally well to exon 2 and exon
197 3 of *U2AF2* (**Fig. 1H**). Therefore, IWS1 phosphorylation controls *U2AF2* exon 2 alternative RNA
198 splicing by regulating events occurring after the binding of IWS1 to chromatin.

199 **IWS1 phosphorylation-dependent mRNA splicing of *U2AF2* is regulated by serum and IGF-**
200 **1 via AKT3.**

201 IWS1 is phosphorylated by AKT3, and to a lesser extent by AKT1, at Ser720/Thr721
202 (Sanidas et al., 2014[10]). Since the phosphorylation and activity of the AKT isoforms can be
203 induced by tyrosine-kinase signals, we questioned whether IGF-1 stimulation of serum starved
204 NCI-H522 and NCI-H1299 cells, promotes *U2AF2* exon 2 inclusion along with the expected AKT
205 activation and IWS1 phosphorylation. The results showed that the E2/E3 *U2AF2* ratio indeed
206 parallels the activation of AKT and the subsequent phosphorylation of IWS1 (**Fig. 2A, S2A**). To

207 address whether the *U2AF2* exon 2 inclusion depends on AKT activation, we treated NCI-H522
208 and NCI-H1299 cells growing in serum-containing complete media with 5 μM of the pan-AKT
209 inhibitor MK2206, a dose that fully inhibits all AKT isoforms (Sanidas et al., 2014[10]) .The results
210 confirmed that MK2206 inhibits both AKT (T308 and S473) and IWS1 phosphorylation (S720) and
211 *U2AF2* exon 2 inclusion (**Fig. 2B, S2B).** To determine whether it is the AKT3 isoform, which is
212 responsible for the observed effects of AKT inhibition on the *U2AF2* alternative RNA splicing, we
213 transfected NCI-H522 and NCI-H1299 cells with siAKT3, along with siControl, and we examined
214 its effects on the alternative splicing of *U2AF2* exon 2, using RT-PCR and qRT-PCR. The results
215 phenocopied the inhibition with MK2206 (**Fig. 2C, S2C)**, providing evidence that the physiological
216 regulation of alternative RNA splicing of *U2AF2* by external stimuli depends on the
217 phosphorylation of IWS1 by AKT3.

218 ***U2AF2* Exon 2 inclusion, induced by IWS1 phosphorylation at Ser720/Thr721, depends on**
219 **histone H3K36 trimethylation by SETD2.**

220 We have previously reported that IWS1 phosphorylation by AKT promotes the exclusion
221 of exon 8 from the mature *FGFR-2* mRNA transcript, via a process that depends on histone
222 H3K36 trimethylation by SETD2, and that the latter is recruited to the CTD of RNA Pol II by
223 phosphorylated IWS1 (Sanidas et al., 2014[10]). To determine whether the U2AF2 exon 2 inclusion
224 phenotype is also dependent on histone H3K36 trimethylation, we performed ChIP assays in
225 shControl, shIWS1, shIWS1/WT-R and shIWS1/MT-R NCI-H522 and NCI-H1299 cells,
226 addressing the abundance of H3K36me3 marks on exons 2 and 3 of *U2AF2*, as well as on the
227 *U2AF2* transcriptional start site (TSS) and the *GAPDH* gene, which were used as controls. The
228 results revealed that the knockdown of IWS1 or the replacement with the phosphorylation-site
229 mutant significantly decreased the abundance of H3K36me3 on *U2AF2* exon 2 and 3 (**Fig. 3A**).
230 More importantly, inhibition of AKT, using MK2206, phenocopied the H3K36me3 pattern of
231 phosphorylation-deficient IWS1 mutant (**Fig. 3B**). Since IWS1-phosphorylation recruits SETD2 in

232 C-terminal domain of RNA-pol II, we examined the binding of SETD2 on *U2AF2* and *GAPDH*
233 gene in the same NCI-H522 and NCI-H1299 cells, transduced using a SETD2 lentiviral construct,
234 with a Hemagglutinin (HA)-tag. The results showed a pattern of SETD2 binding, which parallels
235 the IWS1 phosphorylation-dependent pattern of H3K36me3 abundance (**Fig. 3C**), suggesting that
236 H3K36 trimethylation is mediated by SETD2.

237 The preceding data suggested that the enzymatically active SETD2 contributes to the
238 IWS1 phosphorylation-dependent regulation of the *U2AF2* alternative RNA splicing. The role of
239 catalytically-active SETD2 was confirmed by knockdown and rescue experiments in NCI-H522
240 and NCI-H1299 cells. Using RT-PCR and qRT-PCR, we observed that the knockdown of SETD2
241 phenocopies the knockdown of IWS1 on the *U2AF2* RNA splicing, an effect rescued by the wild
242 type SETD2, but not by the SETD2 methyltransferase mutant R1625C, which globally silences
243 H3K36me3 (Hacker et. al., 2016[36]) (**Fig. 3D**). We conclude that the catalytically-active SETD2 is
244 indeed required for the inclusion of exon 2 in the mature *U2AF2* mRNA.

245 Recently, and after the completion of the ChIP experiments, we carried out ChIP-Seq
246 experiments, addressing the binding of IWS1 and SETD2 and the distribution of H3K36me3
247 marks genome-wide in NCI-H522 shIWS1/WT-R and shIWS1/MT-R cells. The unbiased data on
248 the abundance of these markers in the *U2AF2* gene were in general agreement with the ChIP
249 data described above. Specifically, IWS1 was found to bind *U2AF2* E2 independent of its
250 phosphorylation, but SETD2 binding and H3K36me3 abundance on *U2AF2* E2 increased only
251 when IWS1 was phosphorylated (**Fig. 3E**).

252 If the recruitment of SETD2 in C-terminal domain of RNA-pol II depends on the
253 phosphorylation of IWS1, as our data indicate, one would expect that ectopic overexpression of
254 SETD2 would fail to rescue the *U2AF2* alternative RNA splicing phenotype in shIWS1 and
255 shIWS1/MT-R cells. This was confirmed by experiments addressing the rescue of *U2AF2*

256 alternative RNA splicing in NCI-H522 and NCI-H1299 shCon, shIWS1, shIWS1/WT-R and
257 shIWS1/MT-R cells transduced with a SETD2 lentiviral construct, with a Hemagglutinin (HA)-tag
258 (**Fig. S3A**). The failure of SETD2 to rescue the phenotype supports the model of SETD2
259 recruitment by phosphorylated IWS1.

260 However, histone methylation is a dynamic step-by-step process. (Greer et al., 2012[37])
261 and while SETD2 is the only known H3K36 trimethyl-transferase in mammalian cells (Hyun K. et
262 al., 2017[38]), there are several Lysine methyltransferases, which catalyze mono- or di-methylation
263 of histone H3 at K36 and may influence the SETD2 output. Transfection of the NCI-H522 and
264 NCI-H1299 cells with siRNAs targeting a set of methyltransferases that are known to catalyze
265 histone H3K36 mono and di-methylation (NSD1, NSD2 and NSD3), or only di-methylation
266 (SMYD2 and ASHL1) (Lucio-Eterovic et al., 2010[339], Q. Qiao et al., 2010[40], Berdasco et al., 2009[41]
267 , Rahman et al., 2011[42], Brown M.A et al., 2006[43], Gregory G.D. et al., 2007[44]), revealed no
268 contribution to the regulation of the alternative RNA splicing of *U2AF2* (**Fig. S3A**).

269 Conversely, histone methylation is a reversible process (Bannister et al., 2002[45]). The
270 histone H3K36me3 marks are erased by KDM4A and KDM4C, two members of the KDM4 JmjC
271 domain-histone demethylase family (Berry, W.L et al., 2013[46], Cloos, P.A et al., 2007[47], Li, W et
272 al., 2011[48]). Ectopic expression of KDM4A, KDM4B and KDM4C using lentiviral constructs in NCI-
273 H522 and NCI-H1299 cells showed that none of these three altered the IWS1 phosphorylation-
274 dependent alternative RNA splicing pattern of *U2AF2* (**Fig. S3C**). Overall, these data indicate that
275 the reported demethylation of H3K36me3 by members of KDM4/JMJD2 histone demethylase
276 family does not play a significant role in our model.

277

278

279 **The regulation of the alternative RNA splicing of the *U2AF2* exon 2 by IWS1**
280 **phosphorylation, depends on the p52 isoform of the H3K36me3 reader LEDGF.**

281 Based on our preceding studies, the regulation of the *FGFR-2* alternative RNA splicing by
282 IWS1 phosphorylation depends on the reading of the histone H3K36me3 marks by MRG15
283 (Sanidas et al., 2014[10]). To determine whether MRG15 is also the reader of the IWS1-dependent
284 alternative RNA splicing of *U2AF2*, we knocked down MRG15 in both NCI-H522 and NCI-H1299
285 cells. Using RT-PCR and qRT-PCR to monitor the alternative splicing of *U2AF2* in these cells,
286 revealed that it is independent of MRG15 (**Fig. 4A Left panels**). In agreement with this result, the
287 knockdown of the splicing repressor and binding partner of MRG15, PTB, also had no effect on
288 the RNA splicing of *U2AF2* (**Fig. 4A Right panels**), results not surprising since IWS1
289 phosphorylation mediates exon inclusion signals in our model.

290 To identify the factor that controls the IWS1 phosphorylation-dependent exon inclusion of
291 *U2AF2* exon 2, we transfected NCI-H522 and NCI-H1299 cells with siRNAs of the known
292 H3K36me3 readers PHF1 (Cai L. et al., 2013[49]), BRPF1 (Vezzoli et al., 2010[50]), MSH6 (Li F. et
293 al., 2014[51]), GLYR-1 (Vermuelen et al., 2010[52]) and LEDGF (Pradeepa et al., 2012[20]), along with
294 a control siRNA. After validating the significant downregulation of the expression by Western
295 blotting, monitoring the effects of these transfections on E2/E3 *U2AF2* ratio using RT-PCR and
296 qRT-PCR, revealed that only the knockdown of LEDGF phenocopied the knockdown of IWS1 on
297 the alternative RNA splicing of *U2AF2*, suggesting that LEDGF is the sole H3K36me3 reader
298 responsible for the observed phenotype (**Fig. 4B, S4A**). To confirm this conclusion and to
299 determine which isoform of LEDGF may be responsible for the phenotype, we used a lentiviral
300 shRNA construct to knockdown LEDGF, targeting the 3' UTR, and we rescued the knockdown by
301 transducing the cells with lentiviral constructs of the alternatively spliced LEDGF isoforms, p75
302 and p52, with a V5-tag (**Fig. 4C, upper panel**). Monitoring the effects of these transductions by
303 RT-PCR and qRT-PCR, revealed that only the p52 isoform rescues the shLEDGF-induced U2AF2

304 alternative RNA splicing phenotype. Notably, the A51P mutant of p52-LEDGF, which cannot bind
305 Histone H3K36me3 (Shun et al., 2008[53]), failed to rescue the splicing defect, suggesting that the
306 *U2AF2* exon inclusion depends on the reading of the H3K36me3 marks by p52/LEDGF (**Fig. 4C,**
307 **S4B**).

308 The preceding data provide strong genetic evidence that p52/LEDGF regulates the *U2AF2*
309 alternative RNA splicing by reading the IWS1 phosphorylation-dependent histone H3K36me3
310 marks. To validate these observations, chromatin Immunoprecipitation assays for the V5-tagged
311 p52/LEDGF isoform, confirmed that the p52/LEDGF binds *U2AF2* exons 2 and 3 only when IWS1
312 is phosphorylated, observations consistent with SETD2 binding and H3K36me3 abundance (**Fig.**
313 **4D, S4C**).

314 If the p52 isoform of LEDGF regulates the alternative RNA splicing of *U2AF2* by reading
315 the histone H3K36me3 mediated by IWS1-phosphorylation, as suggested by the preceding data,
316 one would expect that overexpression of p52/LEDGF would not rescue the *U2AF2* alternative
317 RNA splicing phenotype in shIWS1 and shIWS1/MT-R cells. This was confirmed by experiments
318 addressing the *U2AF2* RNA splicing in NCI-H522 and NCI-H1299 shControl, shIWS1,
319 shIWS1/WT-R and shIWS1/MT-R cells along with a V5-tagged p52/LEDGF construct (**Fig. S4D**).
320 Altogether, these data support the model based on which p52/LEDGF regulates the alternative
321 RNA splicing of *U2AF2* by reading the histone H3K36 trimethylation on the body of *U2AF2* gene,
322 induced by IWS1 phosphorylation at S720/T721, mediated by SETD2.

323 **The p52 isoform of LEDGF regulates the alternative RNA splicing of *U2AF2*, via its**
324 **interaction with the RNA splicing factor SRSF1.**

325 It has been reported that the p52/LEDGF isoform re-localizes in the nucleus, through
326 signals mediated from its unique C-terminal domain, and interacts with the splicing factor SRSF1,
327 affecting its distribution to alternatively spliced genes. (Pradeepa et al., 2012[20]). To investigate a

328 potential role of SRSF1 in *U2AF2* alternative RNA splicing, we knocked down SRSF1 and we
329 showed that its loss phenocopies the knockdown of IWS1. The dependence of the *U2AF2* exon
330 2 splicing on SRSF1, which was suggested by this result, was confirmed by rescue experiments
331 with wild type SRSF1 (**Fig. 4E, S4E**). We therefore conclude that SRSF1 regulates the alternative
332 RNA splicing of the *U2AF2* exon 2. More importantly, SRSF1 did not rescue the *U2AF2* RNA
333 splicing phenotype induced by shIWS1 or shIWS1/MT-R (**Fig. S4F**), suggesting that it does not
334 function independently. Instead, we hypothesized that it provides the link between IWS1
335 phosphorylation-dependent chromatin modifications and p52/LEDGF binding to the RNA splicing
336 machinery. To test this hypothesis, we performed ChIP experiments addressing the binding of
337 SRSF1 to *U2AF2* exons 2 and 3 in shControl, shIWS1, shIWS1/WT-R and shIWS1/MT-R NCI-
338 H522 and NCI-H1299 cells, transduced with a V5-tagged SRSF1 lentiviral construct. The *U2AF2*
339 TSS and *GAPDH* exon 3 regions were again used as controls. The results confirmed that the
340 binding of SRSF1 to exons 2 and 3 parallels the SETD2 and p52/LEDGF binding along with
341 H3K36me3 abundance and occurs only when IWS1 is phosphorylated (**Fig. 4F, S4G**), providing
342 support to the proposed hypothesis.

343 Based on the preceding data, we hypothesized that the binding of SRSF1 to the
344 chromatin-associated p52/LEDGF should bring it into proximity with the nascent pre-mRNA,
345 facilitating their interaction. Analysis of the U2AF2 mRNA sequence, using the web-based
346 pipeline RBP-map (Paz et al., 2014[55]), identified four potential SRSF1 binding sites (2 in U2AF2
347 exon 2 and 2 in exon 3) (**Fig. S4I**), providing additional support to this hypothesis. To
348 experimentally address the proposed model, we carried out RNA-IP (RIP) experiments in the
349 same shControl, shIWS1, shIWS1/WT-R and shIWS1/MT-R NCI-H522 and NCI-H1299 cells,
350 focusing on the binding of SRSF1 to the *U2AF2* exon 2, intron 2 and exon 3. The results confirmed
351 that SRSF1 binds primarily to exon 2, but only in the shControl and shIWS1/WT-R cells, which
352 parallels its chromatin binding to the H3K36me3-bound p52/LEDGF (**Fig. 4G, S4H**).

353 Based on the data presented in Figure 3 and Figure 4, we propose that IWS1
354 phosphorylation by AKT is required for the recruitment of SETD2 to CTD of RNA Pol II. The latter
355 promotes the trimethylation of histone H3 at K36 on the body of *U2AF2* and perhaps other target
356 genes. This facilitates the recruitment of the histone H3K36me3-interacting protein p52/LEDGF
357 and its binding partner SRSF1, resulting in exon inclusion of *U2AF2* exon 2. (**Fig. 4H**)

358 **The novel U2AF65 splice variant lacking exon 2, does not interact with Prp19.**

359 The predominant novel splice variant of the *U2AF2* mRNA that we identified in shIWS1
360 and shIWS1/MT-R cells, lacks exon 2, which encodes part of the N-terminal SR domain of
361 U2AF65 (**Fig 5A**). This domain is responsible for the interaction of U2AF65 with several factors
362 that contribute to mRNA splicing, 3' cleavage and polyadenylation (Millevoi et al., 2006[57], Shen
363 H, et al., 2004[58]). One of these factors is Prp19, a component of the seven-member ubiquitin
364 ligase complex Prp19C (S.P Chan et al., 2003[59], S.P Chan et al., 2005[60], R. Hogg et al., 2010[61],
365 Chanarat S. et al., 2013[62]).
366 Using co-immunoprecipitation experiments in HEK-293T cells engineered to express the
367 exon-2 containing U2AF65α or the exon 2-excluded U2AF65β variants, with a V5-tag, we
368 confirmed that only the U2AF65α splice variant interact with the endogenous Prp19 (**Fig. 5B**).
369 More important, consistent with the previous results, immunoprecipitation of endogenous U2AF65
370 in NCI-H522 and NCI-H1299 shControl, shIWS1, shIWS1/WT-R and shIWS1-MT-R cells,
371 revealed impaired U2AF65-Prp19 interaction in shIWS1 and shIWS1/MT-R cells, which express
372 primarily U2AF65β, while maintaining interaction with its U2-heterodimer partner, U2AF35 (**Fig.
373 5B, S5A**). These data confirmed that the interaction of U2AF65 with Prp19 depends on the
374 sequence encoded by *U2AF2* exon 2, whose inclusion is regulated by IWS1 phosphorylation.
375

376 **The splicing of the *U2AF2* mRNA downstream of IWS1 phosphorylation, regulates the**
377 ***CDCA5* mRNA splicing and expression of Sororin.**

378 Based on previous reports, U2AF65 binds RNA Pol II, leading to an U2AF65-dependent
379 recruitment of Prp19 to the newly synthetized pre-mRNA and promoting proper co-transcriptional
380 splicing activation (C.J David et. al., 2011[63]). Furthermore, it had been shown that U2AF65 and
381 Prp19 are necessary for the pre-mRNA splicing and accumulation of Sororin, a component of the
382 cohesin complex, which is encoded by *CDCA5* (Watrin et. al., 2014[64]). Given that aberrant splicing
383 of *U2AF2* in shIWS1 and shIWS1/MT-R cells resulted in the loss of the interaction between
384 U2AF65 and Prp19, we hypothesized that the pre-mRNA splicing of *CDCA5* in these cells will be
385 impaired. We therefore employed qRT-PCR to examine the ratio of spliced and unspliced *CDCA5*
386 mRNA in the same cells. The results confirmed that the mRNA splicing of *CDCA5* was impaired
387 in both the shIWS1 and shIWS1/MT-R cells, with no significant change in the spliced/unspliced
388 ratios of the control *GUSB* mRNA (Watrin et. al., 2014[64]) (**Fig. 5D, S5B, S5C upper panels).** The
389 splicing defect was rescued by U2AF65α but not by U2AF65β. (**Fig. 5E, S5D upper panels**).

390 To determine how IWS1 phosphorylation regulates *CDCA5* RNA splicing, we performed
391 RNA Immunoprecipitation (RIP) experiments in shControl, shIWS1, shIWS1/WT-R and
392 shIWS1/MT-R NCI-H522 and NCI-H1299 cells. The results confirmed that both spliced variants
393 of U2AF65 bind equally well *CDCA5* pre-mRNA, as well as the control *GUSB* pre-mRNA, as
394 expected (**Fig. 5D, 5E, S5C, S5D middle panels**) (Shen H. et al., 2004[31]). However, Prp19
395 binding to the same pre-mRNA regions of *CDCA5* was significantly impaired in shIWS1 and
396 shIWS1/MT-R cells, which predominantly express the U2AF65β isoform (**Fig. 5D, S5C lower**
397 **panels**). Consistently, the impaired Prp19 binding to *CDCA5* pre-mRNA was rescued by
398 U2AF65α, but not U2AF65β (**Fig. 5E, S5D lower panels**).

399 Given that only spliced mRNAs are transported out of the nucleus, we also examined the
400 abundance of cytosolic *CDCA5* mRNA in shControl, shIWS1, shIWS1/WT-R, shIWS1/MT-R and

401 shIWS1 rescues with U2AF65α or U2AF65β. To this extent, we fractionated the nuclear and
402 cytosolic compartments of these NCI-H522 and NCI-H1299 cells. Then, using western blotting,
403 we confirmed the validity of the fractionation by the expected expression of Lamin A/C and
404 GAPDH only in the nuclear and cytosolic protein compartment, respectively (**Fig. S5E**). The
405 results also confirmed that the mature CDCA5 mRNA in the cytoplasm was downregulated as
406 expected, and that the RNA transport deficiency is rescued by U2AF65α, but not U2AF65β (**Fig.
407 5F**).

408 To determine whether the *CDCA5* RNA splicing defect in shIWS1 and shIWS1/MT-R NCI-
409 H522 and NCI-H1299 cells prevents the expression of its protein product, Sororin, we examined
410 its expression along with the expression of IWS1, p-IWS1, U2AF65 and Prp19, by western
411 blotting. The results confirmed that the expression of Sororin parallels IWS1 phosphorylation as
412 it was impaired in shIWS1 and shIWS1/MT-R NCI-H522 and NCI-H1299 cells. The low expression
413 of Sororin in shIWS1 was rescued by U2AF65α, but not by U2AF65β (**Fig. 5G, S5F upper
414 panels**). Taken together, these data confirm that IWS1 phosphorylation via the alternative RNA
415 splicing of *U2AF2*, is ultimately responsible for the regulation of the mRNA splicing of *CDCA5*.

416 **Sororin and p-ERK, form a novel positive feedback loop, which is activated by IWS1
417 phosphorylation and promotes the expression of CDK1 and Cyclin B1.**

418 It has been previously shown that the downregulation of Sororin leads to reduced ERK
419 phosphorylation, in human Colorectal Cancer (CRC) and human Hepatocellular Carcinoma
420 (HCC) (Wang J., et al., 2018[65], A. Zhen et. al., 2019[66]). Since the IWS1 phosphorylation-
421 dependent *U2AF2* alternative RNA splicing regulates the abundance of Sororin, we hypothesized
422 reduced ERK phosphorylation in NCI-H522 and NCI-H1299 shIWS1 and shIWS1/MT-R cells. This
423 was confirmed by experiments showing that ERK phosphorylation at Y202/T204 was reduced in
424 shIWS1 and shIWS1/MT rescue cells, while total ERK was not. The observed reduction of p-ERK

425 levels in shIWS1 cells was rescued by U2AF65α, but not by U2AF65β (**Fig. 5G, S5F lower**
426 **panels**), confirming the p-IWS1/Sororin/p-ERK axis in lung adenocarcinoma.

427 Sororin is a known target of ERK, which phosphorylates the protein at S79 and S209
428 (Nguyen et. al., 2010[67]). Interestingly, whereas the wild type Sororin and the Sororin
429 phosphomimetic mutant S79E/T209E (Sororin DM-E) rescued the phosphorylation of ERK in
430 shIWS1 cells, the S79A/S209A (Sororin DM-A) mutant did not (**Fig 5G and S5F Lower panels**).
431 This suggests a novel Sororin-ERK phosphorylation positive feedback loop in lung
432 adenocarcinoma, which is controlled by the AKT-dependent IWS1 phosphorylation, and the
433 *U2AF2* alternative RNA splicing.

434 Based on previous observations, down-regulation of Sororin leads to impaired expression
435 of CDK1 and Cyclin B1 (Wang J., et al., 2018[65], A. Zhen et. al., 2019[66]). To this extent, we
436 hypothesized that IWS1 phosphorylation regulates the expression of CDK1 and Cyclin B1,
437 through the regulation of *U2AF2* RNA splicing and the abundance of Sororin. Consistent with the
438 preceding data, western blotting revealed reduced levels of CDK1 (Y15) phosphorylation, CDK1
439 and Cyclin B1 levels in shIWS1 and shIWS1/MT-R cells. More importantly, the downregulation of
440 these molecules in shIWS1 cells was rescued by U2AF65α, but not by U2AF65β, wild type Sororin
441 and Sororin DM-E but not by Sororin DM-A (**Fig. 5G, S5F lower panels**). These data indicate
442 that the Sororin-ERK phosphorylation feedback loop, downstream of IWS1 phosphorylation,
443 controls the expression of CDK1 and Cyclin B1, through a process depending on U2AF2
444 alternative RNA splicing.

445 **IWS1 phosphorylation controls the ERK phosphorylation levels, in cells harboring EGFR**
446 **and K-RAS mutations, through U2AF2 RNA splicing.**

447 *EGFR* and *K-RAS* are frequently mutated in human lung adenocarcinoma and promote
448 downstream pro-oncogenic signals through the phosphorylation of ERK (Guo et al., 2020[68], Wee
449 et al., 2017[69]). We therefore addressed the role of IWS1 phosphorylation and *U2AF2* alternative

450 RNA splicing on Sororin and ERK phosphorylation in lung adenocarcinoma cells harboring *K-*
451 *RAS* (A549 and NCI-H460) and *EGFR* (NCI-H1975, PC-9, NCI-H1650) mutations. The results
452 showed that *U2AF2* alternative RNA splicing pattern is independent of the mutational status. (**Fig.**
453 **5H, upper and lower left panels**) Notably, the knockdown of IWS1 downregulated the
454 expression of Sororin and ERK phosphorylation (**Fig. 5H, upper panel**). These data were striking,
455 because they showed that the effect of Sororin on ERK phosphorylation is dominant over the
456 effect of *K-RAS* and *EGFR* mutations. Surprisingly, the reduction of ERK phosphorylation induced
457 by the loss of IWS1 phosphorylation was more robust in *EGFR* as opposed to the *K-RAS* mutated
458 cells (**Fig. 5H, lower right panels)**. Altogether, this data suggests that IWS1 phosphorylation
459 controls the *U2AF2* alternative RNA splicing independent of the cellular mutational status and
460 shows robust reduction of the Sororin/ERK phosphorylation axis in lung adenocarcinoma cell
461 lines, harboring *EGFR* mutations.

462 **IWS1 phosphorylation promotes cell proliferation by controlling the Sororin/ERK**
463 **phosphorylation feedback loop, through *U2AF2* RNA splicing.**

464 Given that the Sororin/ERK phosphorylation positive feedback loop, activated by IWS1
465 phosphorylation, promotes the expression of CDK1 and Cyclin B1, we hypothesized that the
466 stimulation of cell proliferation by IWS1, we had observed previously (Sanidas et al., 2014[10]), may
467 depend on the activation of the *U2AF2* RNA splicing-regulated Sororin/ERK phosphorylation loop.
468 To address this hypothesis, we examined the rate of proliferation of shControl, shIWS1,
469 shIWS1/Sororin WT, shIWS1/Sororin DM-A and shIWS1/Sororin DM-E NCI-H522 and NCI-
470 H1299 cells growing under standard culture conditions. The results showed that cell proliferation
471 was inhibited by shIWS1. The observed inhibition was rescued by wild type Sororin and Sororin
472 DM-E but not by the Sororin DM-A. Significantly, the proliferative effect of the Sororin DM-E was
473 more robust than the proliferative effect of wild type (wt) Sororin **(Fig. 6A).** Western blotting
474 revealed reduced expression of the cell proliferation marker PCNA in NCI-H522 and NCI-H1299

475 shIWS1 cells, which was rescued by U2AF65α, but not U2AF65β, confirming that the regulation
476 of cell proliferation depends on the novel *U2AF2* RNA splicing pattern (**Fig. 6B**).

477 As we pointed out above, the loss of phosphorylated IWS1 results in more robust
478 downregulation of ERK phosphorylation in *EGFR* as opposed to *K-RAS* mutated lung
479 adenocarcinoma cells (**Fig. 5H**), suggesting that the *EGFR* mutated cells would be more sensitive
480 to the knockdown of IWS1. This was confirmed by experiments showing reduced cell proliferation
481 of A549 (*K-RAS* mutant) and NCI-H1975 (*EGFR* mutant) shIWS1 cells. More importantly, in
482 parallel with the data of the reduction of ERK phosphorylation, *EGFR* mutated cell line NCI-
483 H1975, demonstrates the highest reduction in cell proliferation induced by the loss of IWS1 (**Fig.
484 S6A**). Additional support was provided by experiments showing that the shIWS1-induced
485 downregulation of PCNA was more robust in *EGFR* (NCI-H1975, NCI-H1650) as opposed to *K-
486 RAS* mutated (A549, NCI-H460) cells. (**Fig. 6C, S6B**). Moreover, the PCNA downregulation in
487 these cell lines was rescued by U2AF65α, but not the U2AF65β, suggesting that the U2AF2 RNA
488 splicing affects cell proliferation in *K-RAS* and *EGFR*-mutated cells (**Fig. 6D, S6B).** Altogether,
489 these data suggest that IWS1 phosphorylation controls cell proliferation through the regulation
490 Sororin/ERK phosphorylation mediated by *U2AF2* RNA splicing.

491 To determine whether IWS1 phosphorylation stimulates cell proliferation by promoting
492 progression through the G2/M phase of the cell cycle, we stained log phase cultures of shControl,
493 shIWS1 NCI-H522, NCI-H1299, A549 and NCI-H1975 cells with Propidium Iodide (PI) and we
494 examined the percentage of cells in different phases of the cell cycle by flow-cytometry. The
495 results confirmed that the knockdown of IWS1 induced prolonged G2/M phase of the cell cycle,
496 an effect less pronounced in *K-RAS* mutant cell line, A549 **(Fig. 6E).** Altogether, data presented
497 in figures 5 and 6 suggest that the *EGFR* mutated lung adenocarcinoma cell lines are more
498 sensitive than *K-RAS* mutant cells upon the loss of IWS1 phosphorylation.

499 **IWS1 phosphorylation and novel *U2AF2* splice variant fluctuate during progression**
500 **through the cell cycle.**

501 The preceding findings suggest that an RNA splicing event, regulated by the AKT-
502 mediated phosphorylation of IWS1, plays a critical role in cell cycle progression. Given that the
503 expression and activity of molecules critically involved in the regulation of the cell cycle, tend to
504 fluctuate as cells transit from one cell cycle phase to the next (Kent et al., 2019[70]), we examined
505 the expression and phosphorylation of IWS1, the *U2AF2* alternative RNA splicing pattern and the
506 expression of SETD2, Sororin and the trimethylation of histone H3K36 in G1, S and G2/M in NCI-
507 H1299 cells. To this end, using carboxyfluorescein succinimidyl ester (CFSE)-like DNA dyes, cells
508 were stained in G1, S and G2/M phase and they were fractionated by FACS sorting (Begum et
509 al, 2013[71]). Western blotting of these fractions confirmed that IWS1, phospho-IWS1, SETD2,
510 histone H3K36me3 and Sororin are indeed upregulated in S and G2/M. As specific cell cycle
511 phase markers, Cyclin E1 (G1 phase), CDC25A (S phase) and phosphorylated Histone H3 (S10)
512 were used, validating the integrity of the fractionation **(Fig. 6F lower panels)**. More importantly,
513 IWS1 expression and phosphorylation occurred more during S phase, whereas Sororin, SETD2
514 and Histone H3K36me3 levels were more robust during G2/M phase, as previously reported
515 (Watrin et al., 2014[64], Dronamraju et al., 2018[72]) **(Fig. 6F upper panels).** Furthermore, using RNA
516 extracts from the same cells, RT-PCR experiments revealed an *U2AF2* RNA exon inclusion
517 pattern which parallels the expression of IWS1 during the cell cycle **(Fig. 6F).** Furthermore, qRT-
518 PCR confirmed that the expression of *IWS1* and *CDCA5* in the RNA level parallels their protein
519 expression, with no change of total *U2AF2* levels (**Fig. 6G**).

520 Chromatin Immuno-Cleavage (ChIC) experiments revealed increased binding of IWS1 on
521 *U2AF2* exon 2 and 3 during S and G2/M phase, with significantly more binding during S phase
522 (**Fig. 6H upper panel**). Consistently, the binding of SETD2, the abundance of H3K36me3 and

523 the E2/E3 *U2AF2* ratio parallel the levels and the binding of IWS1 on *U2AF2* gene, although total
524 SETD2 and H3K36me3 are more abundant during G2/M phase (**Fig. 6H, 6I**).
525 Overall, these data provide strong evidence for the model in which IWS1, whose
526 expression increases during S and G2/M, recruits SETD2 to CTD of RNA-Pol II, following
527 phosphorylation by AKT. RNA-Pol II-associated SETD2 trimethylates histone H3 at K36 during
528 transcriptional elongation, resulting in the assembly of p52/LEDGF-SRSF1 complexes which
529 promote the inclusion of exon 2 in the *U2AF2* mRNA. Subsequently, the U2AF65α isoform along
530 with Prp19, facilitate the proper splicing of *CDCA5* pre-mRNA, leading to Sororin accumulation
531 during S and G2/M phase. Finally, Sororin forms a positive feedback loop with ERK
532 phosphorylation, and controls the progression through the cell cycle in lung adenocarcinoma. The
533 events described in this model define a molecular mechanism of a novel splice variant which is
534 epigenetically regulated during the cell cycle, feeding back into its regulation (**Fig. 6J, S6C**).

535 **IWS1 phosphorylation controls tumor growth *in vivo*, by regulating the U2AF2/Sororin/ERK**
536 **axis.**

537 Based on our preceding studies, the loss of IWS1 and IWS1 phosphorylation impair tumor
538 growth in a mouse xenograft model (Sanidas et al., 2014[10]). To further validate and expand this
539 observation, we knocked down IWS1 in NCI-H1299 and A549 cells and we injected them
540 subcutaneously, along with shControl cells, in immunocompromised NSG mice. The animals were
541 monitored for tumor development and were sacrificed 4 and 6 weeks later, respectively. The
542 results revealed that the knockdown of IWS1 reduced tumor weight and volume (**Fig. 7A**). They
543 also showed that the reduction of tumor growth induced by the loss of IWS1 was less pronounced
544 in A549 cells, harboring *K-RAS* mutations (**Fig. 7B**). The weak growth reduction of tumors derived
545 from shIWS1 A549 cells, paralleled the weak inhibition of ERK phosphorylation (**Fig 5H**) and cell
546 proliferation (**Fig S6A**) induced by the knockdown of IWS1 in these cells.

547 The preceding data confirmed that the knockdown of IWS1 reduces tumor growth.
548 Following confirmation, we proceeded to address the mechanism of the growth inhibition, which
549 had not been adequately addressed in our earlier studies. First, we confirmed the efficiency of
550 the IWS1 knockdown, by probing western blots of tumor cell lysates with anti-IWS1 and anti-
551 phospho-IWS1 (S720) antibodies (**Fig. 7C**). Following this, we employed RT-PCR and qRT-PCR
552 on RNA derived from these tumors, to address the usage of exon 2 in the *U2AF2* mRNA. The
553 results confirmed that the knockdown of IWS1 has no effect on the total *U2AF2* mRNA levels
554 (**Fig. S7A**), but promotes the exclusion of exon 2 from *U2AF2* mRNA (**Fig. 7C, upper panels,**
555 **7D**). Probing both tumor lysates and tissue sections with antibodies to regulators and targets of
556 the Sororin/ERK feedback loop, confirmed that the activity of the loop is reduced in tumors derived
557 from shIWS1 cells (**Fig. 7C, lower panels, S7B**). Measuring the abundance of the PCNA and Ki-
558 67 proliferation markers by western blotting (PCNA), or Immunohistochemistry (Ki-67), also
559 confirmed the reduced expression of these markers in the shIWS1 tumors (**Fig. 7C, lower panels,**
560 **7E**).
561 Quantitative analyses of the western blot (p-ERK and PCNA) and IHC data (Ki-67) (**Fig.**
562 **7F**), showed that the reduction of all these markers was less pronounced in the *K-RAS* mutant
563 A549 tumors suggesting that these cells are more resistant to the loss of IWS1. Altogether, these
564 results are in agreement with the less pronounced effect of shIWS1 in the tumor growth in A549-
565 derived tumors (**Fig. 7B**) and with the less pronounced effect of shIWS1 in p-ERK levels (**Fig.**
566 **5H**), cell proliferation in culture and degree of G2/M arrest in these cells (**Fig. 6**).

567 **The AKT3/p-IWS1/U2AF2 axis is active in human lung adenocarcinoma and affects the**
568 **clinical outcome of *EGFR* mutant patients.**

569 To determine whether the pathway activated by IWS1 phosphorylation leading to Sororin
570 expression and ERK phosphorylation is active in human lung adenocarcinoma (LUAD), we
571 examined the expression and phosphorylation of several components of this axis, along with the

572 alternative RNA splicing pattern of *U2AF2* in a set of 40 human LUAD samples. For 30 of these
573 tumors, Normal Adjacent Tissue (NAT) was also available and it was tested on parallel with the
574 matching tumor sample. (**Fig. 8A**). More importantly, the exon 2-containing *U2AF2* transcript was
575 more abundant in tumor versus normal samples, with no change in total levels of *U2AF2*. (**Fig.**
576 **S8A**). Overall, these results confirmed that the pathway was active in the tumors, but not in the
577 NAT.

578 Human LUAD frequently harbors *K-RAS* or *EGFR* mutations and data presented in this
579 report suggest that lung adenocarcinoma cells harboring *EGFR* mutations are more sensitive to
580 the loss of IWS1, as opposed to *K-RAS* mutant cells (**Fig. 5 and Fig. 6**). We therefore used
581 monoclonal antibodies, which selectively recognize *K-RAS* and *EGFR* mutant forms (Kim et al.,
582 2015[74]), and we identified tumors harboring these mutations (**Fig. 8A**). Comparison of the
583 correlation coefficients of IWS1 and phosphorylated IWS1 with the E2/E3 *U2AF2* and all the
584 components of the downstream Sororin/ERK phosphorylation pathway, revealed strong
585 correlations in the entire cohort with more robust correlations in the *EGFR* than the *K-RAS* mutant
586 tumors (**Fig. 8B**). Strikingly, the levels of IWS1 phosphorylation and abundance of exon 2-
587 containing *U2AF2* isoform exhibit strong correlation with more aggressive clinical stage and
588 defines poor survival in the entire patients' and the *EGFR* mutant cohort, but not in the *K-RAS*
589 mutated group (**Fig. 8C, 8D**).

590 The preceding data were confirmed by IHC, using sections of a commercially available
591 tissue microarray (TMA) of 50 LUAD with paired NAT. The TMA samples were probed with
592 antibodies against p-IWS1, Sororin, p-ERK, p-CDK1 and EGFR E746-A750 deletion (**Fig. S8B,**
593 **S8C**). The results confirmed that the pathway is more active in the tumors, compared to the NAT
594 samples **(Figure S8D).** Notably, IWS1 phosphorylation expression exhibits strong correlations
595 with the components of the Sororin/ERK axis, with more robust correlations in the *EGFR* mutant
596 tumors (**Fig. S8E**). Consistently, the results also showed that the activity of the pathway correlates
597 with clinical stage and histological grade **(Fig. S8F, S8G).** In addition to confirming the western

598 blot data in our set of LUAD patients, the IHC data also demonstrate that the activity of the
599 pathway can be monitored clinically in human tumors by IHC.

600 The data generated from the analysis of our LUAD samples and the TMA were confirmed
601 by data in publicly available databases. Analysis of the data derived from Tumor Cancer Genome
602 Atlas (TCGA), revealed correlations between *IWS1* or *SRSF1*, *U2AF2* E2 and other components
603 of the IWS1 phosphorylation pathway (**Fig. 8E**). The results also showed that the *U2AF2* E2/E3
604 ratio and the expression of *CDCA5* mRNA were significantly upregulated in TCGA LUAD patients
605 with high IWS1, compared to the low IWS1 group (**Fig. S8H**). Consistently, IWS1 expression
606 correlates with more aggressive tumor stage in tumors harboring *EGFR* but not *K-RAS* mutations
607 (**Fig. S8I**).

608 Based on recent reports, 55% of lung adenocarcinoma patients relapse and up to 40% of
609 them develop metastatic disease. (Popper et al., 2016[75], West et al., 2020[76]). Given that the IWS1
610 phosphorylation controls oncogenic signals and plays a critical role in patients with lung
611 adenocarcinoma, as suggested in this report, we questioned whether the IWS1-mediated axis is
612 associated to clinical relapse or metastasis in LUAD patients. Analysis of a relapse-related
613 molecular signature database GSE13213 (Tomida et al., 2009[77]), revealed increased expression
614 of the IWS1/Sororin axis in relapsing patients harboring *EGFR*, but not with *K-RAS* mutations
615 (**Fig. 8F, S8J**). We therefore conclude that the activation of the IWS1 phosphorylation pathway
616 may also contribute to the relapse of lung adenocarcinoma, especially with *EGFR* mutations.
617 Furthermore, analysis of RNA-seq data derived from dissected brain metastatic lesions from lung
618 adenocarcinoma patients (GSE141685), revealed increased expression of the components of
619 IWS1/Sororin axis in the metastatic as opposed to primary lung adenocarcinoma lesions.
620 Importantly, the *U2AF2* mRNA E2/E3 ratio was also elevated in the metastatic tumors, while the
621 E8/E9 ratio of the *FGFR2* mRNA was reduced (**Fig. S8K and S8L**), in agreement with our earlier
622 observations, showing that IWS1 phosphorylation promotes *FGFR2* exon 8 skipping (Sanidas et
623 al, 2014[10]). Analysis of the RNA-Seq data in the TCGA LUAD dataset, which contains information

624 on cancer-associated mutations, confirmed the link between IWS1 expression and metastatic
625 disease, but also showed that IWS1 is again upregulated in tumors derived from patients with
626 metastatic disease, and harboring *EGFR*, but not *K-RAS* mutations (**Fig. S8M**).
627 As expected from the preceding data, IWS1 expression, *U2AF2* exon 2 inclusion and *FGFR2*
628 exon 8 exclusion, are indicators of poor prognosis in patients with lung adenocarcinomas in the
629 TCGA LUAD dataset, harboring *EGFR*, but not *K-RAS* mutations (**Fig. 8H**). In addition, the
630 survival of patients with lung adenocarcinomas in the same dataset, expressing high levels of
631 IWS1, was reduced if the tumors also harbored a mutated *EGFR* (**Fig. S8N**). Confirmatory to
632 these observations, was the finding that the synergy between IWS1 expression and *EGFR*
633 mutations, was also observed in the GSE13213/GSE26939 dataset (**Fig. S8O**).
634 Altogether, these data come in agreement with the *in vitro* (**Fig. 5 and Fig. 6**) and *in vivo*
635 (**Fig. 7**) data provided in this report, that indicate that the p-AKT/p-IWS1 axis through the
636 epigenetic regulation of *U2AF2* alternative RNA splicing and oncogenic signals, defines poor
637 survival in lung adenocarcinoma patients harboring *EGFR* mutations.

638 **Discussion**

639 **Regulation of the Sororin/ERK phosphorylation loop from IWS1 phosphorylation**

640 Our studies implicate IWS1 phosphorylation as a regulator of oncogenic signals in lung
641 adenocarcinoma through alternative RNA splicing. We report a novel *U2AF2* splice variant in lung
642 adenocarcinoma which lacks exon 2 upon loss of phosphorylated IWS1. This signaling pathway
643 is initiated by the AKT3-dependent phosphorylation of IWS1, which induces the epigenetic
644 regulation of *U2AF2* alternative RNA splicing, through H3K36me3-mediated signals (**Fig. 3**). The
645 shift in the alternative RNA pattern controls the interaction of U2AF65 with Prp19. These two
646 factors regulate the pre-mRNA splicing of *CDCA5* and the expression of its protein product,
647 Sororin, co-transcriptionally (**Fig. 5**). Our data provide insight for the existence of a novel

648 Sororin/ERK phosphorylation feedback loop in lung adenocarcinoma, which is regulated by the
649 alternative RNA splicing of *U2AF2*. Notably, the Sororin-dependent regulation of ERK
650 phosphorylation by IWS1 is dominant over the ERK-activating *EGFR* mutations and has a major
651 impact in the biology of these cells harboring such mutations **(Fig. 5 and Fig. 6)**. Sororin is a
652 member of the cohesin complex, a seven member protein complex which plays a central role in
653 sister chromatid cohesion and higher chromosomal architecture during meiosis (Ishiguro et al.,
654 2019[78]). This molecular Sororin/ERK phosphorylation switch controls cell proliferation and the
655 progression through the G2/M phase of the cell cycle (**Fig. 6**). Defects in Sororin expression lead
656 to the activation of spindle assembly checkpoint, delaying the progression through the G2/M
657 phase (Dreier et al., 2011[79]). Given that loss of IWS1 reduced the expression of Sororin, this could
658 explain the G2/M phase delay observed in shIWS1 cells (**Fig. 6**) How the ERK-phosphorylated
659 Sororin promotes the phosphorylation and activation of ERK is currently unknown. Our working
660 hypothesis is that the phosphorylation and activation of ERK is due to signals induced by the
661 interaction of Sororin with its partners in the cohesin complex. If this is the case, the cell may use
662 this mechanism to sense the successful progression from prometaphase to metaphase, in order
663 to activate a molecular switch. This enhances the phosphorylation of Sororin, facilitating
664 progression through the G2/M phase of the cell cycle. In addition, data presented in this report
665 show that the loss of IWS1 leads to impaired expression of CDK1 and Cyclin B1, a phenotype
666 regulated through the Sororin/ERK phosphorylation loop (**Fig. 5**). On the other hand, our data
667 indicate strong correlation of *CDCA5*, *CDK1* and *CCNB1* mRNA levels in LUAD patients, derived
668 from TCGA database (**Fig. 8**) These observations indicate that the induction of Cyclin B1 and
669 CDK1 by Sororin is most likely at the level of transcription. A potential mechanism for this
670 transcriptional regulation, controlled by IWS1, was suggested by earlier studies showing that the
671 Cohesin complex interacts with the Mediator complex. The Mediator-Cohesin complexes are
672 loaded by the NIBPL Cohesin loading factor to enhancers and core promoters of target genes.
673 Enhancer and core promoter-associated complexes promote loop formation between these

674 segments, and regulate transcription (Kagey et al., 2010[80]). The contribution of this and other
675 mechanisms on the regulation of Cyclin B1 and CDK1 expression is under investigation.

676 **Regulation of RNA processing in multiple layers**

677 Another important conclusion, based on the data presented in this report, is that RNA
678 splicing is a process regulated at multiple levels. IWS1 phosphorylation directly regulates the
679 alternative RNA splicing of *U2AF2*, via a H3K36me3-mediated mechanism (**Fig. 3**) and thus,
680 introducing a new layer of RNA splicing regulation. This shift in alternative RNA splicing pattern
681 affects the binding and formation of the U2AF65/Prp19 interacting complex, required for the
682 efficient splicing of *CDCA5*, which ultimately controls pro-oncogenic ERK phosphorylation signals
683 (**Fig. 5, Fig. 6**). The reason for the multilayered control of RNA splicing by a single RNA splicing
684 regulator could be that this allows a limited number of available pathways to converge, in different
685 combinations, on a large number of RNA splicing events and differentially regulate them. To this
686 extent, our data provide insight on the novel importance of the AKT/IWS1 phosphorylation axis
687 on the fine-tuning of the global epigenetic regulation of RNA splicing cellular program, governing
688 cell cycle regulation and tumor progression.

689 **IWS1 phosphorylation and U2AF2 splicing are regulated through the cell cycle, feeding**
690 **back to its regulation, enhancing tumor proliferation.**

691 Given that the cell cycle is an integrated system and that cell cycle regulatory mechanisms
692 tend to also be cell cycle-regulated, we examined and confirmed that IWS1 expression and
693 phosphorylation fluctuate through the cell cycle, regulating *U2AF2* RNA splicing. The mechanism
694 of the expression of IWS1 is under investigation. The increased activity of the pathway may also
695 occur due to cell cycle-dependent changes in the activity of AKT. Earlier reports have shown that
696 CDK2-Cyclin A2 complex is activated in S phase and phosphorylates AKT at Ser477/Thr479 (Liu

697 et al., 2014[73]), which further enhances the activity of IWS1 pathway. Furthermore, our results
698 show that the epigenetic complexes assembled upon the phosphorylation of IWS1 on *U2AF2*
699 gene, are regulated in a cell-cycle specific manner. These results come in agreement with
700 previous reports stating that spliceosomal assembly is also regulated through the cell-cycle,
701 implying an extra layer of alternative RNA splicing regulation. (Karamysheva et al., 2015[81],
702 Hofmann et al., 2010[82]). More importantly, our results reveal that IWS1 phosphorylation
703 epigenetically controls the dynamics of a novel *U2AF2* splice variant through the cell cycle and
704 regulates the levels of Sororin, which subsequently feeds back to the regulation of the cell cycle
705 and tumor proliferation, through enhancement of ERK oncogenic signals (**Fig. 6**).

706 **Interpretation of the same histone modification signal through different epigenetic**
707 **complexes, affecting lung adenocarcinoma development.**

708 Data presented in this report showed that signals originate from AKT phosphorylation may
709 regulate alternative RNA splicing of target genes by different mechanisms, through IWS1
710 phosphorylation. Our previous findings had shown that IWS1 phosphorylation regulates the
711 alternative RNA splicing of *FGFR2* by promoting the exclusion of exon 8 from the mature
712 transcript. (Sanidas et al., 2014[10]) Here we show that, similar to the *FGFR2*, the exon inclusion of
713 *U2AF2* exon 2, is also under the control of the SETD2-dependent histone H3K36 trimethylation
714 in the body of the actively transcribed genes. However, the reader of the histone H3K36me3 mark
715 is the p52 isoform of LEDGF which interacts with the RNA-binding protein SRSF1, as opposed to
716 the MRG15/PTB complex. Therefore, although the transduction signal and the regulatory
717 chromatin modification mark is the same for both the exon inclusion and exclusion signals, the
718 effector complexes assembled around H3K36me3, that are responsible for the effects on RNA
719 splicing differ. Interestingly, both the IWS1 phosphorylation splicing targets affect lung
720 adenocarcinoma development. On the one hand, the *FGFR2* exon exclusion pattern promotes
721 invasion and EMT (Sanidas et al., 2014[10]) and to the other hand, *U2AF2* exon inclusion pattern

722 promotes oncogenic and survival signals, converging towards more aggressive phenotype and
723 clinical profile in lung adenocarcinoma patients, especially with *EGFR* mutations. This isoform
724 specific aggressive clinical phenotype, comes in agreement with recent reports in the literature
725 describing the existence of a cancer-specific splicing addiction network, in which cancer-related
726 isoforms, in our case *U2AF2* and *FGFR2*, manipulate and maintain oncogenic and invasion
727 signals (Bonnal et al., 2020[83], Wang and Aifantis, 2020[84]).

728 **The clinical impact of the p-IWS1/U2AF2 axis in *EGFR* mutant lung adenocarcinoma.**

729 Throughout this report, we provide evidence that IWS1 phosphorylation, through the
730 epigenetic regulation of *U2AF2* alternative RNA splicing, represents an important oncogenic
731 signal in *EGFR* mutant lung adenocarcinoma. Based on consistent results in cell lines (**Fig. 6**),
732 animals (**Fig. 7**) and human tumor samples (**Fig. 8**), we showed the major impact of IWS1
733 phosphorylation on proliferation, tumor growth and, eventually, clinical outcome in *EGFR* mutant
734 lung adenocarcinoma patients. Since, the PI3K/AKT axis is triggered by the *EGFR* mutated
735 landscape, and as our data suggest, the activity of the IWS1 phosphorylation/U2AF2/Sororin axis
736 would be increased (**Fig. 8**), further inducing the activation and maintenance of the tumorigenic
737 ERK phosphorylation signals. To this extent, signals derived from the AKT/IWS1 phosphorylation
738 pathway facilitates and maintains the oncogenic addiction of these tumors which depends on ERK
739 phosphorylation. Furthermore, our data indicate that IWS1 phosphorylation and the RNA splicing
740 pattern of its targets, *U2AF2* and *FGFR2*, selectively correlates not only with tumor grade, stage
741 and patient survival, but also with metastasis and with relapse (**Fig. 8**). Based on these findings,
742 we propose two translational applications for the IWS1 phosphorylation pathway described in this
743 report. First, *EGFR* mutant lung adenocarcinoma patients may benefit from a dual inhibition of
744 EGFR and specific AKT1/3 inhibitors (not currently investigated) or dual AKT/MEK inhibition
745 (MK2206-AZD6244 : NCT01306045), limiting the ERK oncogenic addiction. Secondly, the IWS1
746 phosphorylation-dependent cancer splicing addiction can be manipulated by synergistic use of

747 EGFR Tyrosine Kinase Inhibitors, inhibitors of the AKT/IWS1 axis and the use of highly isoform-
748 specific antisense oligonucleotides and pharmacologic modulators of splicing machinery (Obeng
749 et al., 2019[85]), which are currently under clinical trials (NCT03901469, NCT02711956,
750 NCT02268552, NCT02908685).

751 Collectively, our results suggest that IWS1 phosphorylation by AKT acts as an epigenetic
752 switch that, through H3K36me3-mediated signals, regulates RNA splicing in lung
753 adenocarcinoma maintaining the oncogenic and splicing addiction, and may serve as a novel
754 precision-medicine marker and important drug target in EGFR mutant lung adenocarcinoma.
755

756 **Materials and methods**

757 **Cells and culture conditions, growth factors and inhibitors**

758 Cells, Growth factors, inhibitors, siRNAs and shRNAs, retroviral and lentiviral constructs and
759 experimental protocols are described in detail in the supplemental experimental procedures.
760 Experimental protocols include stimulation with growth factors, transfection with siRNAs, retroviral
761 and lentiviral packaging, and cellular transduction with retroviral and lentiviral constructs.

762 **Cell Proliferation assay, Cell cycle analysis and FACS-sorting of cells in different phases**
763 **of the cell cycle**

764 Cell proliferation of cells growing under normal culture conditions was monitored using the
765 Incucyte S3 Live-Cell Imaging and Analysis System (Essen Biosciences, Ann Arbor, MI).
766 Captured data were analyzed using the native analysis software. The cell cycle distribution of
767 exponentially growing cells was monitored by FACS analysis of ethanol-fixed, propidium iodide
768 stained, cell cultures. To separate cells in different phases of the cell cycle for further analysis,
769 NCI-H1299 cells were stained with Vybrant™ DyeCycle™ Ruby Stain (Thermo Fisher, Cat. No.

770 V10309) and they were sorted using the BD FACS Aria III cell sorter (BD Biosciences, San Jose,
771 CA). For details on all the above, see Supplemental Experimental Procedures.

772

773

774 **RNA-seq analysis**

775 Detailed descriptions of total RNA isolation from NCI-H522 cells, library preparation, RNA
776 sequencing methodology and data analyses are presented in the Supplemental Experimental
777 Procedures

778 **Immunoblotting and Protein Immunoprecipitation**

779 Cells were lysed with RIPA buffer and cell lysates were resolved by electrophoresis in SDS-PAGE
780 and analyzed by immunoblotting. Protein immunoprecipitation was carried out, following
781 established protocols (Mohammed, H. et al, 2016[86]), with modifications. Images were acquired
782 and analyzed, using the Li-Cor Fc Odyssey Imaging System (LI-COR Biosciences, Lincoln, NE).
783 For the lists of antibodies used for immunoprecipitation and western blotting and for other details,
784 see Supplemental Experimental Procedures.

785 **Cloning and site-directed mutagenesis**

786 The cDNA clones used in experiments in this report were purchased from multiple sources. Open
787 reading frames of all the cDNAs were subcloned in lentiviral vectors. Point mutations were
788 introduced into the open reading frames of these clones by site-directed mutagenesis. For details
789 see Supplemental Experimental Procedures.

790 **Subcellular Fractionation**

791 Cell pellets were fractionated into nuclear and cytoplasmic fractions, which were used to measure
792 the relative abundance of proteins and RNAs in the nucleus and the cytoplasm. For details, see
793 Supplemental Experimental Procedures.
794

795 **RT-PCR and qRT-PCR**

796 Total RNA was isolated using the PureLink RNA Kit (Invitrogen, Cat. No 12183018A). Isolated
797 RNA was analyzed by real-time RT-PCR for the expression of the indicated mRNAs. The mRNA
798 levels were normalized based on the levels of GAPDH (internal control). The primer sets used
799 are listed in the Supplemental Experimental Procedures.

800 **Chromatin Immunoprecipitation-Sequencing (ChIP-Seq), ChIP and Chromatin Immuno-**
801 **Cleavage (ChIC)**

802 The distribution of chromatin-bound IWS1 and SETD2 and the distribution of histone H3K36me3
803 genome-wide were addressed by ChIP-Seq experiments. The binding of IWS1 and SETD2 and
804 the abundance of histone H3K36me3 on the *U2AF2* locus, were addressed by chromatin
805 immunoprecipitation or chromatin Immuno-cleavage (Skene et al., 2018[87]). The latter was
806 employed for experiments with FACS-sorted cells in different phases of the cell cycle. For details,
807 regarding the sorting, the ChIP/ChIC protocols, ChIP-seq library preparation and analysis, see
808 Supplemental Experimental Procedures.

809 **RNA Immunoprecipitation**

810 The binding of RNA binding proteins to regions of the U2AF2, CDCA5 and GUSB pre-mRNAs
811 was addressed by RNA Immunoprecipitation. For details, see Supplemental Experimental
812 Procedures.

813 **Tumor xenografts.**

814 NOD.*Cg-Prkdc*^{scid} *Il2rg*^{tm1Wjl}/SzJ (NSG) mice were injected subcutaneously with $2x10^6$ or $5x10^6$
815 shControl or shIWS1 NCI-H1299 and A549 cells, and they were monitored for 4 and 6 weeks,
816 respectively. Tumor metrics, protein and RNA extraction and tumor immunohistochemistry are
817 described in detail in the Supplemental Experimental Procedures. All mouse experiments were
818 reviewed and approved by the Institutional Animal Care and Use Committee (IACUC) of the Ohio
819 State University.

820 **Human Tumor Samples.**

821 Thirty Lung Adenocarcinoma samples with matching normal adjacent tissue were obtained from
822 the Tissue Bank of The Ohio State University. Ten additional lung adenocarcinomas without
823 matching normal tissue had been obtained earlier from the tissue bank of Tufts Medical Center.
824 The latter had been used also in an earlier study on the role of IWS1 in NSCLC (Sanidas et al.,
825 2014[10]). Protein and RNA extraction, and correlations of the abundance of IWS1 and the inclusion
826 of Exon 2 in the U2AF2 mRNA with tumor stage and patient survival were carried out as described
827 in the Supplemental Experimental Procedures.

828 **Immunohistochemistry**

829 **Human lung adenocarcinoma tissue arrays (US Biomax, Cat. No. LC1504) and tumor**
830 **xenografts from immunodeficient mice, were stained with antibodies. Antibody staining,**
831 **image acquisition and signal intensity measurements, along with the correlation of IWS1**
832 **signal intensity with tumor grade and stage, are described in the Supplemental**
833 **Experimental Procedures.**

834 **TCGA/dataset analysis**

835 TCGA data were downloaded from https://portal.gdc.cancer.gov/ and analysed as described in
836 the Supplemental Experimental Procedures. The microarray and RNA-seq analysis for the
837 publicly available datasets GSE13213, GSE26939 and GSE141685 are outlined in the
838 Supplemental Experimental Procedures.

839 **Data availability**

840 All the source data derived from this report have been deposited in the Mendeley Dataset (Laliotis
841 et al., 2020[88]). Raw RNA-Seq and ChIP-Seq data of NCI-H522 cell lines, transduced with lentiviral
842 constructs of shControl, shIWS1, shIWS1/WT-R or shIWS1/MT-R will be deposited in Gene
843 Expression Omnibus (GEO).

844 **Acknowledgments**

845 The authors wish to thank all the members of the Tsichlis Lab for helpful discussions. We also
846 thank Dr Samir Achaya, Dr Joal Beane and Dr Esmerina Tilli for reviewing the manuscript before
847 the submission. This work was supported by the NIH grant R01 CA186729 to P.N.T., the NIH
848 grant R01 CA198117 to P.N.T and V.C, by start-up funds from the OSUCCC to P.N.T,, from the
849 National Center for Advancing Translational Sciences grant KL2TR002734 to L.S. G.I.L is
850 supported by the Pelotonia Post-Doctoral fellowship from OSUCCC.

851

852 **References**

853

854 1. Glisovic, T., Bachorik, J.L., Yong, J. and Dreyfuss, G., 2008. RNA-binding proteins and
855 post-transcriptional gene regulation. *FEBS letters*, *582*(14), pp.1977-1986.
856 2. Jewer, M., Findlay, S.D. and Postovit, L.M., 2012. Post-transcriptional regulation in cancer
857 progression. *Journal of cell communication and signaling*, *6*(4), pp.233-248.

858 3. Pan, Q., Shai, O., Lee, L.J., Frey, B.J. and Blencowe, B.J., 2008. Deep surveying of
859 alternative splicing complexity in the human transcriptome by high-throughput
860 sequencing. *Nature genetics*, *40*(12), p.1413.
861 4. Paronetto, M.P., Passacantilli, I. and Sette, C., 2016. Alternative splicing and cell survival:
862 from tissue homeostasis to disease. *Cell Death & Differentiation*, *23*(12), pp.1919-1929.
863 5. Zhang, X., Chen, M.H., Wu, X., Kodani, A., Fan, J., Doan, R., Ozawa, M., Ma, J., Yoshida,
864 N., Reiter, J.F. and Black, D.L., 2016. Cell-type-specific alternative splicing governs cell
865 fate in the developing cerebral cortex. *Cell*, *166*(5), pp.1147-1162.
866 6. Coomer, A.O., Black, F., Greystoke, A., Munkley, J. and Elliott, D.J., 2019. Alternative
867 splicing in lung cancer. *Biochimica et Biophysica Acta (BBA)-Gene Regulatory*
868 *Mechanisms*.
869 7. Siegel, R.L., Miller, K.D. and Jemal, A., 2016. Cancer statistics, 2016. *CA: a cancer journal*
870 *for clinicians*, *66*(1), pp.7-30.
871 8. Yuan, M., Huang, L.L., Chen, J.H., Wu, J. and Xu, Q., 2019. The emerging treatment
872 landscape of targeted therapy in non-small-cell lung cancer. *Signal Transduction and*
873 *Targeted Therapy*, *4*(1), pp.1-14.
874 9. Sequist, L.V., Neal, J.W., Jett, J.R. and Ross, M.E., 2016. Personalized, genotype directed
875 therapy for advanced non-small cell lung cancer. *UpToDate, UpToDate*.
876 10. Sanidas, I., Polytarchou, C., Hatziapostolou, M., Ezell, S.A., Kottakis, F., Hu, L., Guo, A.,
877 Xie, J., Comb, M.J., Iliopoulos, D. and Tsichlis, P.N., 2014. Phosphoproteomics screen
878 reveals akt isoform-specific signals linking RNA processing to lung cancer. *Molecular cell*,
879 *53*(4), pp.577-590.
880 11. Li, Z., Li, Q., Han, L., Tian, N., Liang, Q., Li, Y., Zhao, X., Du, C. and Tian, Y., 2016. Pro-
881 apoptotic effects of splice-switching oligonucleotides targeting Bcl-x pre-mRNA in human
882 glioma cell lines. *Oncology reports*, *35*(2), pp.1013-1019.

883 12. Todaro, M., Gaggianesi, M., Catalano, V., Benfante, A., Iovino, F., Biffoni, M., Apuzzo, T.,
884 Sperduti, I., Volpe, S., Cocorullo, G. and Gulotta, G., 2014. CD44v6 is a marker of
885 constitutive and reprogrammed cancer stem cells driving colon cancer metastasis. *Cell*
886 *stem cell*, *14*(3), pp.342-356.
887 13. Oltean, S. and Bates, D.O., 2014. Hallmarks of alternative splicing in cancer. *Oncogene*,
888 *33*(46), pp.5311-5318.
889 14. Calabretta, S., Bielli, P., Passacantilli, I., Pilozzi, E., Fendrich, V., Capurso, G., Delle Fave,
890 G. and Sette, C., 2016. Modulation of PKM alternative splicing by PTBP1 promotes
891 gemcitabine resistance in pancreatic cancer cells. *Oncogene*, *35*(16), pp.2031-2039.
892 15. Vo, N.S., Reynolds, S.M., Zhao, Y., Climente-González, H., Chai11, S., Wang, F.,
893 Varghese, R., Huang, M., Liang, W.W., Wyczalkowski, M.A. and Sengupta, S., Systematic
894 Analysis of Splice-Site-Creating Mutations in Cancer.
895 16. Giaj Levra, M., Andre Olaussen, K., Novello, S. and Soria, J.C., 2014. PARP inhibitors: an
896 interesting pathway also for non-small cell lung cancer?. *Current pharmaceutical design*,
897 *20*(24), pp.3875-3882.
898 17. Seiler, M., Yoshimi, A., Darman, R., Chan, B., Keaney, G., Thomas, M., Agrawal, A.A.,
899 Caleb, B., Csibi, A., Sean, E. and Fekkes, P., 2018. H3B-8800, an orally available small-
900 molecule splicing modulator, induces lethality in spliceosome-mutant cancers. *Nature*
901 *medicine*, *24*(4), p.497.
902 18. Listerman, I., Sapra, A.K. and Neugebauer, K.M., 2006. Cotranscriptional coupling of
903 splicing factor recruitment and precursor messenger RNA splicing in mammalian cells.
904 *Nature structural & molecular biology*, *13*(9), p.815.
905 19. Luco, R.F., Pan, Q., Tominaga, K., Blencowe, B.J., Pereira-Smith, O.M. and Misteli, T.,
906 2010. Regulation of alternative splicing by histone modifications. *Science*, *327*(5968),
907 pp.996-1000.

908 20. Pradeepa, M.M., Sutherland, H.G., Ule, J., Grimes, G.R. and Bickmore, W.A., 2012.
909 Psip1/Ledgf p52 binds methylated histone H3K36 and splicing factors and contributes to
910 the regulation of alternative splicing. *PLoS genetics*, *8*(5).
911 21. Chen, M. and Manley, J.L., 2009. Mechanisms of alternative splicing regulation: insights
912 from molecular and genomics approaches. *Nature reviews Molecular cell biology*, *10*(11),
913 pp.741-754.
914 22. Obeng, E.A., Stewart, C. and Abdel-Wahab, O., 2019. Altered RNA Processing in Cancer
915 Pathogenesis and Therapy. *Cancer discovery*, *9*(11), pp.1493-1510.
916 23. Martinez-Contreras, R., Cloutier, P., Shkreta, L., Fisette, J.F., Revil, T. and Chabot, B.,
917 2008. 8 hnRNP proteins and splicing control. *Advances in Experimental Medicine &*
918 *Biology*, *623*, p.123.
919 24. de Miguel, F.J., Sharma, R.D., Pajares, M.J., Montuenga, L.M., Rubio, A. and Pio, R.,
920 2014. Identification of alternative splicing events regulated by the oncogenic factor SRSF1
921 in lung cancer. *Cancer research*, *74*(4), pp.1105-1115.
922 25. Chen, M., David, C.J. and Manley, J.L., 2012. Concentration-dependent control of
923 pyruvate kinase M mutually exclusive splicing by hnRNP proteins. *Nature structural &*
924 *molecular biology*, *19*(3), p.346.
925 26. Jin, W., Bruno, I.G., Xie, T.X., Sanger, L.J. and Cote, G.J., 2003. Polypyrimidine tract-
926 binding protein down-regulates fibroblast growth factor receptor 1 α-exon inclusion.
927 *Cancer research*, *63*(19), pp.6154-6157.
928 27. Dominguez, D., Tsai, Y.H., Weatheritt, R., Wang, Y., Blencowe, B.J. and Wang, Z., 2016.
929 An extensive program of periodic alternative splicing linked to cell cycle progression. *Elife*,
930 *5*, p.e10288.
931 28. Moore, M.J., Wang, Q., Kennedy, C.J. and Silver, P.A., 2010. An alternative splicing
932 network links cell-cycle control to apoptosis. *Cell*, *142*(4), pp.625-636.

933 29. Ahn, E.Y., DeKelver, R.C., Lo, M.C., Nguyen, T.A., Matsuura, S., Boyapati, A., Pandit, S.,
934 Fu, X.D. and Zhang, D.E., 2011. SON controls cell-cycle progression by coordinated
935 regulation of RNA splicing. *Molecular cell*, *42*(2), pp.185-198.
936 30. Suvorova, E.S., Croken, M., Kratzer, S., Ting, L.M., de Felipe, M.C., Balu, B., Markillie,
937 M.L., Weiss, L.M., Kim, K. and White, M.W., 2013. Discovery of a splicing regulator
938 required for cell cycle progression. *PLoS Genet*, *9*(2), p.e1003305.
939 31. Shen, H. and Green, M.R., 2004. A pathway of sequential arginine-serine-rich domain-
940 splicing signal interactions during mammalian spliceosome assembly. *Molecular cell*,
941 *16*(3), pp.363-373.
942 32. Glasser, E., Agrawal, A.A., Jenkins, J.L. and Kielkopf, C.L., 2017. Cancer-associated
943 mutations mapped on high-resolution structures of the U2AF2 RNA recognition motifs.
944 *Biochemistry*, *56*(36), pp.4757-4761.
945 33. Li, J., Cheng, D., Zhu, M., Yu, H., Pan, Z., Liu, L., Geng, Q., Pan, H., Yan, M. and Yao,
946 M., 2019. OTUB2 stabilizes U2AF2 to promote the Warburg effect and tumorigenesis via
947 the AKT/mTOR signaling pathway in non-small cell lung cancer. *Theranostics*, *9*(1), p.179.
948 34. Subramanian, A., Tamayo, P., Mootha, V.K., Mukherjee, S., Ebert, B.L., Gillette, M.A.,
949 Paulovich, A., Pomeroy, S.L., Golub, T.R., Lander, E.S. and Mesirov, J.P., 2005. Gene
950 set enrichment analysis: a knowledge-based approach for interpreting genome-wide
951 expression profiles. *Proceedings of the National Academy of Sciences*, *102*(43),
952 pp.15545-15550.
953 35. Anders, S., Reyes, A. and Huber, W., 2012. Detecting differential usage of exons from
954 RNA-seq data. *Nature Precedings*, pp.1-1.
955 36. Hacker, K.E., Fahey, C.C., Shinsky, S.A., Chiang, Y.C.J., DiFiore, J.V., Jha, D.K., Vo,
956 A.H., Shavit, J.A., Davis, I.J., Strahl, B.D. and Rathmell, W.K., 2016. Structure/Function
957 analysis of recurrent mutations in SETD2 protein reveals a critical and conserved role for

958 a SET domain residue in maintaining protein stability and histone H3 Lys-36 trimethylation.
959 *Journal of Biological Chemistry*, *291*(40), pp.21283-21295.
960 37. Greer, E.L. and Shi, Y., 2012. Histone methylation: a dynamic mark in health, disease and
961 inheritance. *Nature Reviews Genetics*, *13*(5), p.343.
962 38. Hyun, K., Jeon, J., Park, K. and Kim, J., 2017. Writing, erasing and reading histone lysine
963 methylation. *Experimental & molecular medicine*, *49*(4), p.e324.
964 39. Lucio-Eterovic, A.K., Singh, M.M., Gardner, J.E., Veerappan, C.S., Rice, J.C. and
965 Carpenter, P.B., 2010. Role for the nuclear receptor-binding SET domain protein 1 (NSD1)
966 methyltransferase in coordinating lysine 36 methylation at histone 3 with RNA polymerase
967 II function. *Proceedings of the National Academy of Sciences*, *107*(39), pp.16952-16957.
968 40. Qiao, Q., Li, Y., Chen, Z., Wang, M., Reinberg, D. and Xu, R.M., 2011. The structure of
969 NSD1 reveals an autoregulatory mechanism underlying histone H3K36 methylation.
970 *Journal of Biological Chemistry*, *286*(10), pp.8361-8368.
971 41. Berdasco, M., Ropero, S., Setien, F., Fraga, M.F., Lapunzina, P., Losson, R., Alaminos,
972 M., Cheung, N.K., Rahman, N. and Esteller, M., 2009. Epigenetic inactivation of the Sotos
973 overgrowth syndrome gene histone methyltransferase NSD1 in human neuroblastoma
974 and glioma. *Proceedings of the National Academy of Sciences*, *106*(51), pp.21830-21835.
975 42. Rahman, S., Sowa, M.E., Ottinger, M., Smith, J.A., Shi, Y., Harper, J.W. and Howley, P.M.,
976 2011. The Brd4 extra terminal domain confers transcription activation independent of
977 pTEFb by recruiting multiple proteins, including NSD3. *Molecular and cellular biology*,
978 *31*(13), pp.2641-2652.
979 43. Brown, M.A., Sims, R.J., Gottlieb, P.D. and Tucker, P.W., 2006. Identification and
980 characterization of Smyd2: a split SET/MYND domain-containing histone H3 lysine 36-
981 specific methyltransferase that interacts with the Sin3 histone deacetylase complex.
982 *Molecular cancer*, *5*(1), p.26.

983 44. Gregory, G.D., Vakoc, C.R., Rozovskaia, T., Zheng, X., Patel, S., Nakamura, T., Canaani,
984 E. and Blobel, G.A., 2007. Mammalian ASH1L is a histone methyltransferase that
985 occupies the transcribed region of active genes. *Molecular and cellular biology*, *27*(24),
986 pp.8466-8479.
987 45. Bannister, A.J., Schneider, R. and Kouzarides, T., 2002. Histone methylation: dynamic or
988 static?. *Cell*, *109*(7), pp.801-806.
989 46. Berry, W.L. and Janknecht, R., 2013. KDM4/JMJD2 histone demethylases: epigenetic
990 regulators in cancer cells. *Cancer research*, *73*(10), pp.2936-2942.
991 47. Cloos, P.A., Christensen, J., Agger, K., Maiolica, A., Rappsilber, J., Antal, T., Hansen,
992 K.H. and Helin, K., 2006. The putative oncogene GASC1 demethylates tri-and
993 dimethylated lysine 9 on histone H3. *Nature*, *442*(7100), p.307.
994 48. Li, W., Zhao, L., Zang, W., Liu, Z., Chen, L., Liu, T., Xu, D. and Jia, J., 2011. Histone
995 demethylase JMJD2B is required for tumor cell proliferation and survival and is
996 overexpressed in gastric cancer. *Biochemical and biophysical research communications*,
997 *416*(3-4), pp.372-378.
998 49. Cai, L., Rothbart, S.B., Lu, R., Xu, B., Chen, W.Y., Tripathy, A., Rockowitz, S., Zheng, D.,
999 Patel, D.J., Allis, C.D. and Strahl, B.D., 2013. An H3K36 methylation-engaging Tudor motif
1000 of polycomb-like proteins mediates PRC2 complex targeting. *Molecular cell*, *49*(3),
1001 pp.571-582.
1002 50. Vezzoli, A., Bonadies, N., Allen, M.D., Freund, S.M., Santiveri, C.M., Kvinlaug, B.T.,
1003 Huntly, B.J., Göttgens, B. and Bycroft, M., 2010. Molecular basis of histone H3K36me3
1004 recognition by the PWWP domain of Brpf1. *Nature structural & molecular biology*, *17*(5),
1005 pp.617-619.
1006 51. Li, F., Mao, G., Tong, D., Huang, J., Gu, L., Yang, W. and Li, G.M., 2013. The histone
1007 mark H3K36me3 regulates human DNA mismatch repair through its interaction with
1008 MutSα. *Cell*, *153*(3), pp.590-600.

1009 52. Vermeulen, M., Eberl, H.C., Matarese, F., Marks, H., Denissov, S., Butter, F., Lee, K.K.,
1010 Olsen, J.V., Hyman, A.A., Stunnenberg, H.G. and Mann, M., 2010. Quantitative interaction
1011 proteomics and genome-wide profiling of epigenetic histone marks and their readers. *Cell*,
1012 *142*(6), pp.967-980.
1013 53. Shun, M.C., Botbol, Y., Li, X., Di Nunzio, F., Daigle, J.E., Yan, N., Lieberman, J., Lavigne,
1014 M. and Engelman, A., 2008. Identification and characterization of PWWP domain residues
1015 critical for LEDGF/p75 chromatin binding and human immunodeficiency virus type 1
1016 infectivity. *Journal of virology*, *82*(23), pp.11555-11567.Singh, P.K., Plumb, M.R., Ferris,
1017 A.L., Iben, J.R., Wu, X., Fadel, H.J., Luke, B.T., Esnault, C., Poeschla, E.M., Hughes, S.H.
1018 and Kvaratskhelia, M., 2015. LEDGF/p75 interacts with mRNA splicing factors and targets
1019 HIV-1 integration to highly spliced genes. *Genes & development*, *29*(21), pp.2287-2297.
1020 54. Ferris, A.L., Wu, X., Hughes, C.M., Stewart, C., Smith, S.J., Milne, T.A., Wang, G.G.,
1021 Shun, M.C., Allis, C.D., Engelman, A. and Hughes, S.H., 2010. Lens epithelium-derived
1022 growth factor fusion proteins redirect HIV-1 DNA integration. *Proceedings of the National*
1023 *Academy of Sciences*, *107*(7), pp.3135-3140.
1024 55. Paz, I., Kosti, I., Ares Jr, M., Cline, M. and Mandel-Gutfreund, Y., 2014. RBPmap: a web
1025 server for mapping binding sites of RNA-binding proteins. *Nucleic acids research*, *42*(W1),
1026 pp.W361-W367.
1027 56. Anczuków, O., Akerman, M., Cléry, A., Wu, J., Shen, C., Shirole, N.H., Raimer, A., Sun,
1028 S., Jensen, M.A., Hua, Y. and Allain, F.H.T., 2015. SRSF1-regulated alternative splicing
1029 in breast cancer. *Molecular cell*, *60*(1), pp.105-117.
1030 57. Millevoi, S., Loulergue, C., Dettwiler, S., Karaa, S.Z., Keller, W., Antoniou, M. and Vagner,
1031 S., 2006. An interaction between U2AF 65 and CF Im links the splicing and 3′ end
1032 processing machineries. *The EMBO journal*, *25*(20), pp.4854-4864.

1033 58. Shen, H. and Green, M.R., 2004. A pathway of sequential arginine-serine-rich domain-
1034 splicing signal interactions during mammalian spliceosome assembly. *Molecular cell*,
1035 *16*(3), pp.363-373.
1036 59. Chan, S.P., Kao, D.I., Tsai, W.Y. and Cheng, S.C., 2003. The Prp19p-associated complex
1037 in spliceosome activation. *Science*, *302*(5643), pp.279-282.
1038 60. Chan, S.P. and Cheng, S.C., 2005. The Prp19-associated complex is required for
1039 specifying interactions of U5 and U6 with pre-mRNA during spliceosome activation.
1040 *Journal of Biological Chemistry*, *280*(35), pp.31190-31199.
1041 61. Hogg, R., McGrail, J.C. and O'Keefe, R.T., 2010. The function of the NineTeen Complex
1042 (NTC) in regulating spliceosome conformations and fidelity during pre-mRNA splicing.
1043 62. Chanarat, S. and Sträßer, K., 2013. Splicing and beyond: the many faces of the Prp19
1044 complex. *Biochimica et Biophysica Acta (BBA)-Molecular Cell Research*, *1833*(10),
1045 pp.2126-2134.
1046 63. David, C.J., Boyne, A.R., Millhouse, S.R. and Manley, J.L., 2011. The RNA polymerase II
1047 C-terminal domain promotes splicing activation through recruitment of a U2AF65–Prp19
1048 complex. *Genes & development*, *25*(9), pp.972-983.
1049 64. Watrin, E., Demidova, M., Watrin, T., Hu, Z. and Prigent, C., 2014. Sororin pre-mRNA
1050 splicing is required for proper sister chromatid cohesion in human cells. *EMBO reports*,
1051 *15*(9), pp.948-955.
1052 65. Wang, J., Xia, C., Pu, M., Dai, B., Yang, X., Shang, R., Yang, Z., Zhang, R., Tao, K. and
1053 Dou, K., 2018. Silencing of CDCA5 inhibits cancer progression and serves as a prognostic
1054 biomarker for hepatocellular carcinoma. *Oncology reports*, *40*(4), pp.1875-1884.
1055 66. Shen, A., Liu, L., Chen, H., Qi, F., Huang, Y., Lin, J., Sferra, T.J., Sankararaman, S., Wei,
1056 L., Chu, J. and Chen, Y., 2019. Cell division cycle associated 5 promotes colorectal cancer
1057 progression by activating the ERK signaling pathway. *Oncogenesis*, *8*(3), p.19.

1058 67. Nguyen, M.H., Koinuma, J., Ueda, K., Ito, T., Tsuchiya, E., Nakamura, Y. and Daigo, Y.,
1059 2010. Phosphorylation and activation of cell division cycle associated 5 by mitogen-
1060 activated protein kinase play a crucial role in human lung carcinogenesis. *Cancer*
1061 *research*, *70*(13), pp.5337-5347
1062 68. Guo, Y.J., Pan, W.W., Liu, S.B., Shen, Z.F., Xu, Y. and Hu, L.L., 2020. ERK/MAPK
1063 signalling pathway and tumorigenesis. *Experimental and Therapeutic Medicine*, *19*(3),
1064 pp.1997-2007.
1065 69. Wee, P. and Wang, Z., 2017. Epidermal growth factor receptor cell proliferation signaling
1066 pathways. *Cancers*, *9*(5), p.52.
1067 70. Kent, L.N. and Leone, G., 2019. The broken cycle: E2F dysfunction in cancer. *Nature*
1068 *Reviews Cancer*, *19*(6), pp.326-338.
1069 71. Begum, J., Day, W., Henderson, C., Purewal, S., Cerveira, J., Summers, H., Rees, P.,
1070 Davies, D. and Filby, A., 2013. A method for evaluating the use of fluorescent dyes to
1071 track proliferation in cell lines by dye dilution. *Cytometry Part A*, *83*(12), pp.1085-1095.
1072 72. Dronamraju, R., Jha, D.K., Eser, U., Adams, A.T., Dominguez, D., Choudhury, R., Chiang,
1073 Y.C., Rathmell, W.K., Emanuele, M.J., Churchman, L.S. and Strahl, B.D., 2018. Set2
1074 methyltransferase facilitates cell cycle progression by maintaining transcriptional fidelity.
1075 *Nucleic acids research*, *46*(3), pp.1331-1344.
1076 73. Liu, P., Begley, M., Michowski, W., Inuzuka, H., Ginzberg, M., Gao, D., Tsou, P., Gan, W.,
1077 Papa, A., Kim, B.M. and Wan, L., 2014. Cell-cycle-regulated activation of Akt kinase by
1078 phosphorylation at its carboxyl terminus. *Nature*, *508*(7497), pp.541-545.
1079 74. Kim, C.H., Kim, S.H., Park, S.Y., Yoo, J., Kim, S.K. and Kim, H.K., 2015. Identification of
1080 EGFR mutations by immunohistochemistry with EGFR mutation–specific antibodies in
1081 biopsy and resection specimens from pulmonary adenocarcinoma. *Cancer research and*
1082 *treatment: official journal of Korean Cancer Association*, *47*(4), p.653.

1083 75. Popper, H.H., 2016. Progression and metastasis of lung cancer. *Cancer and Metastasis*
1084 *Reviews*, *35*(1), pp.75-91.
1085 76. West, H.J., Shaw, A.T. and Schild, S.E., 2018. Brain metastases in non-small cell lung
1086 cancer.
1087 77. Tomida, S., Takeuchi, T., Shimada, Y., Arima, C., Matsuo, K., Mitsudomi, T., Yatabe, Y.
1088 and Takahashi, T., 2009. Relapse-related molecular signature in lung adenocarcinomas
1089 identifies patients with dismal prognosis. *Journal of clinical oncology*, *27*(17), pp.2793-
1090 2799.
1091 78. Ishiguro, K.I., 2019. The cohesin complex in mammalian meiosis. *Genes to Cells*, *24*(1),
1092 pp.6-30.
1093 79. Dreier, M.R., Bekier, M.E. and Taylor, W.R., 2011. Regulation of sororin by Cdk1-
1094 mediated phosphorylation. *Journal of cell science*, *124*(17), pp.2976-2987.
1095 80. Kagey, M.H., Newman, J.J., Bilodeau, S., Zhan, Y., Orlando, D.A., van Berkum, N.L.,
1096 Ebmeier, C.C., Goossens, J., Rahl, P.B., Levine, S.S. and Taatjes, D.J., 2010. Mediator
1097 and cohesin connect gene expression and chromatin architecture. *Nature*, *467*(7314),
1098 pp.430-435.
1099 81. Karamysheva, Z., Díaz-Martínez, L.A., Warrington, R. and Yu, H., 2015. Graded
1100 requirement for the spliceosome in cell cycle progression. *Cell Cycle*, *14*(12), pp.1873-
1101 1883.
1102 82. Hofmann, J.C., Husedzinovic, A. and Gruss, O.J., 2010. The function of spliceosome
1103 components in open mitosis. *Nucleus*, *1*(6), pp.447-459.
1104 83. Bonnal, S.C., López-Oreja, I. and Valcárcel, J., 2020. Roles and mechanisms of
1105 alternative splicing in cancer—implications for care. *Nature Reviews Clinical Oncology*,
1106 pp.1-18.
1107 84. Wang, E. and Aifantis, I., 2020. RNA Splicing and Cancer. *Trends in Cancer*.

1108 85. Obeng, E.A., Stewart, C. and Abdel-Wahab, O., 2019. Altered RNA Processing in Cancer
1109 Pathogenesis and Therapy. *Cancer discovery*, *9*(11), pp.1493-1510.
1110 86. Mohammed, H., Taylor, C., Brown, G.D., Papachristou, E.K., Carroll, J.S. and D'santos,
1111 C.S., 2016. Rapid immunoprecipitation mass spectrometry of endogenous proteins
1112 (RIME) for analysis of chromatin complexes. *Nature protocols*, *11*(2), p.316.
1113 87. Skene, P.J., Henikoff, J.G. and Henikoff, S., 2018. Targeted in situ genome-wide profiling
1114 with high efficiency for low cell numbers. *Nature protocols*, *13*(5), p.1006.
1115 88. Laliotis, Georgios I.; Chavdoula, Evangelia; Paraskevopoulou, Maria D.; Kaba, Abdul; La
1116 Ferlita, Alessandro; Anastas, Vollter; Orlacchio, Arturo; Taraslia, Vasiliki; Vlachos,
1117 Ioannis; Hatzigeorgiou, Artemis; Capece, Marina; Palmieri, Dario; Sehgal, Lalit; Carbone,
1118 David P.; Coppola, Vincenzo; Tsichlis, Philip N.; Alaimo, Salvatore; Tsatsanis, Christos
1119 (2020), “IWS1 phosphorylation promotes cell proliferation and predicts poor prognosis in
1120 EGFR mutant lung adenocarcinoma patients, through the cell cycle-regulated U2AF2 RNA
1121 splicing.”, Mendeley Data, v2

1122
1123

1124

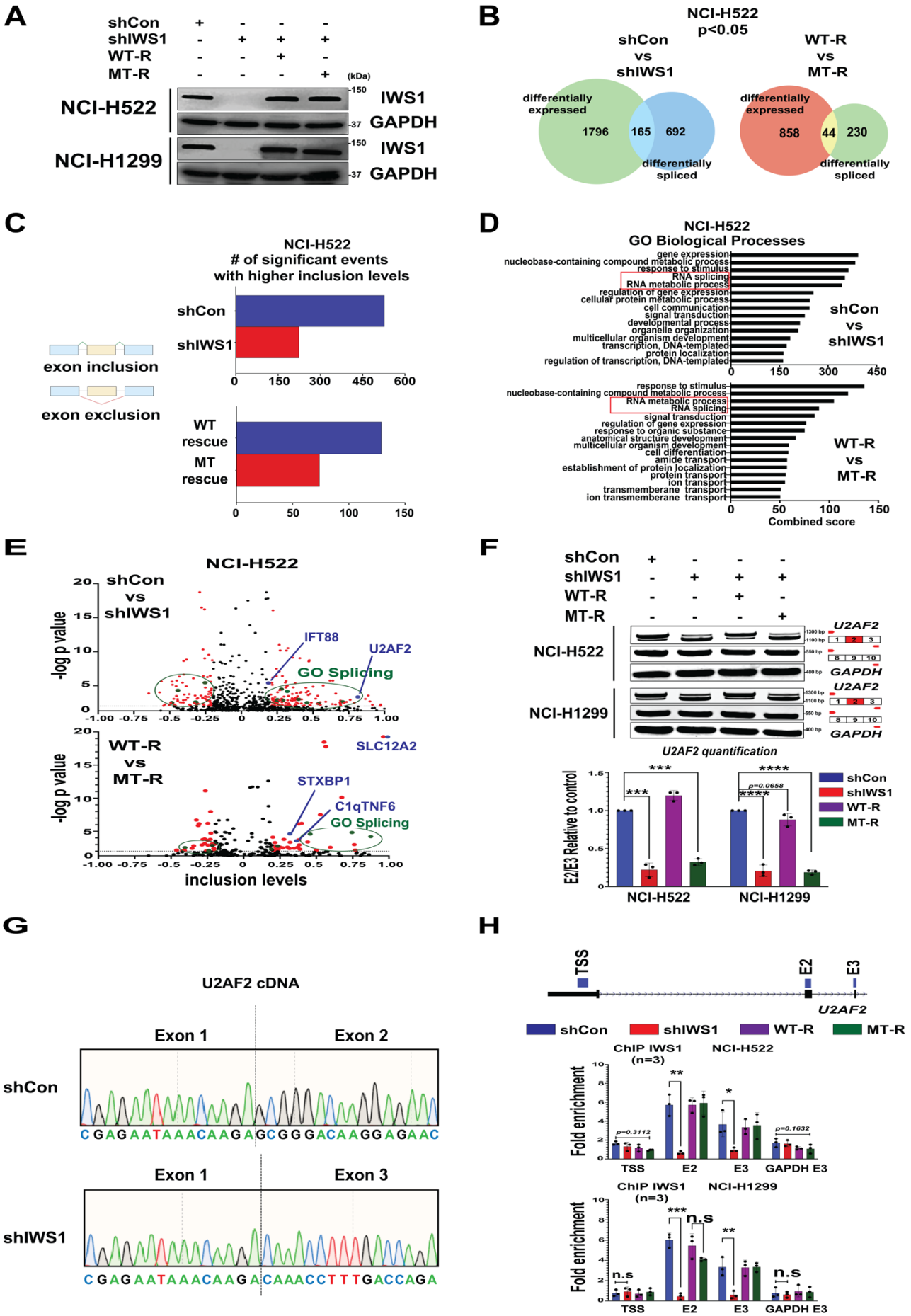
A
shCon
shIWS1
WT-R
MT-R
(kDa)
NCI-H522
NCI-H1299
IWS1
GAPDH
B
NCI-H522
p<0.05
shCon vs shIWS1
WT-R vs MT-R
differentially expressed
differentially spliced
1796
165
692
858
44
230
C
NCI-H522
# of significant events with higher inclusion levels
exon inclusion
exon exclusion
shCon
shIWS1
WT rescue
MT rescue
D
NCI-H522
GO Biological Processes
shCon vs shIWS1
WT-R vs MT-R
Combined score
E
NCI-H522
shCon vs shIWS1
WT-R vs MT-R
-log p value
inclusion levels
IFT88
U2AF2
GO Splicing
SLC12A2
STXBP1
C1qTNF6
F
U2AF2
GAPDH
U2AF2 quantification
E2/E3 Relative to control
shCon
shIWS1
WT-R
MT-R
p=0.0658
G
U2AF2 cDNA
Exon 1
Exon 2
Exon 3
shCon
shIWS1
CGAGAATAAACAAGAGCGGGACAAGGAGAAC
CGAGAATAAACAAGACAAACCTTTGACCAGA
H
TSS
E2
E3
U2AF2
ChIP IWS1 (n=3)
NCI-H522
NCI-H1299
Fold enrichment
GAPDH E3
p=0.3112
p=0.1632
n.s

1126 **Figure 1. IWS1 expression and/or phosphorylation regulate alternative mRNA splicing**

1127 **A**. Western blots of lysates of NCI-H522 and NCI-H1299 cells, transduced with the indicated constructs,
1128 were probed with anti-IWS1 and anti-GAPDH (control) antibodies. **B.** Overlaps between differentially-
1129 expressed and differentially spliced genes in shControl and shIWS1 or shIWS1/WT-R and shIWS1/MT-R
1130 NCI-H522 cells ($p<0.05$) are illustrated, using Venn diagrams. **C**. Bar graphs show the number of alternative
1131 splicing events with exon inclusion (inclusion level >20%) in shControl versus shIWS1 (upper panel) and
1132 shIWS1/WT-R versus shIWS1/MT-R (lower panel) NCI-H522 cells. The comparisons were limited to
1133 alternative splicing events with a p value < 0.05. This shows that IWS1 phosphorylation promotes exon
1134 inclusion (see diagram on the left) in multiple alternatively spliced genes. **D.** GO analysis, based on
1135 differences in the abundance of alternative splicing events in shControl versus shIWS1 (upper panel) and
1136 shIWS1/WT-R versus shIWS1/MT-R (lower panel) NCI-H522 cells. Comparisons were limited to alternative
1137 splicing events whose abundance changes significantly with the expression or phosphorylation of
1138 IWS1($p<0.05$). Red boxes highlight gene sets involved in the regulation of RNA processing. **E.** Volcano
1139 plots of the -log p value vs the exon inclusion levels of all the exon inclusion and exon exclusion alternative
1140 splicing events, detected by DEXseq in the comparisons between shControl and shIWS1 (upper panel), or
1141 shIWS1/WT-R and shIWS1/MT-R (lower panel) NCI-H522 cells. The statistically significant events
1142 ($p<0.05$) with an inclusion level of >0.2 or <-0.2 are shown in red. Statistically significant events in genes in
1143 the GO functions RNA splicing or RNA metabolic processes are shown in green. Alternatively-spliced IWS1
1144 targets validated in this report are shown in blue. (*U2AF2, IFT88, SLC12A2, C1qTNF6, STXBP1)*. The
1145 validation of these through RT-PCR is shown in Figure S1. **F.** *IWS1 phosphorylation regulates U2AF2*
1146 *alternative mRNA splicing.* (Upper panel) RT-PCR of *U2AF2*, using oligonucleotide primers that map in
1147 exons 1 and 3 or exons 8 and 10 (*U2AF2* expression control). RNA transcripts containing or lacking exon
1148 2 are distinguished based on the size of the amplified cDNA derived from these transcripts. RT-PCR was
1149 carried out using RNA derived from shControl, shIWS1 shIWS1/WT-R and shIWS1/MT-R NCI-H522 and
1150 NCI-H1299 cells. *GAPDH* was used as the loading control. (Lower panel) The relative abundance of the
1151 amplified cDNA bands in the upper panel was determined, and the ratio between exons E2 and E3 was
1152 calculated relative to the ratio in shControl cells, which was given the arbitrary value of 1. **G.** Sequencing
1153 chromatograms showing the junction between exons 1 and 2 and exons 1 and 3 in the two alternatively
1154 spliced *U2AF2* RNA transcripts. **H.** *IWS1 binds exons 2 and 3, but not the transcription start site (TSS) of*
1155 *the U2AF2 gene.* (Upper) UCSC browser snapshot showing exons 1, 2 and 3 of the human *U2AF2* gene.
1156 The map position of the PCR primer sets used in the ChIP experiments in this figure is indicated by blue
1157 marks. (Lower) ChIP assays addressing the binding of IWS1 on the *U2AF2* and *GAPDH* genes in shControl,
1158 shIWS1 shIWS1/WT-R and shIWS1/MT-R NCI-H522 and NCI-H1299 cells. Bars show the mean fold
1159 enrichment (anti-IWS1 IP, vs IgG control IP) in IWS1 binding, in shIWS1 relative to shControl cells or in
1160 shIWS1/MT-R relative to shIWS1/WT-R cells ±SD. Data were normalized relative to the input (2%)**.** All
1161 assays were done in triplicate, on three biological replicates. n.s : non-significant *$p<0.05$, **$p<0.01$,
1162 ***$p<0.001$, ****$p<0.0001$. (one-side unpaired t-test)

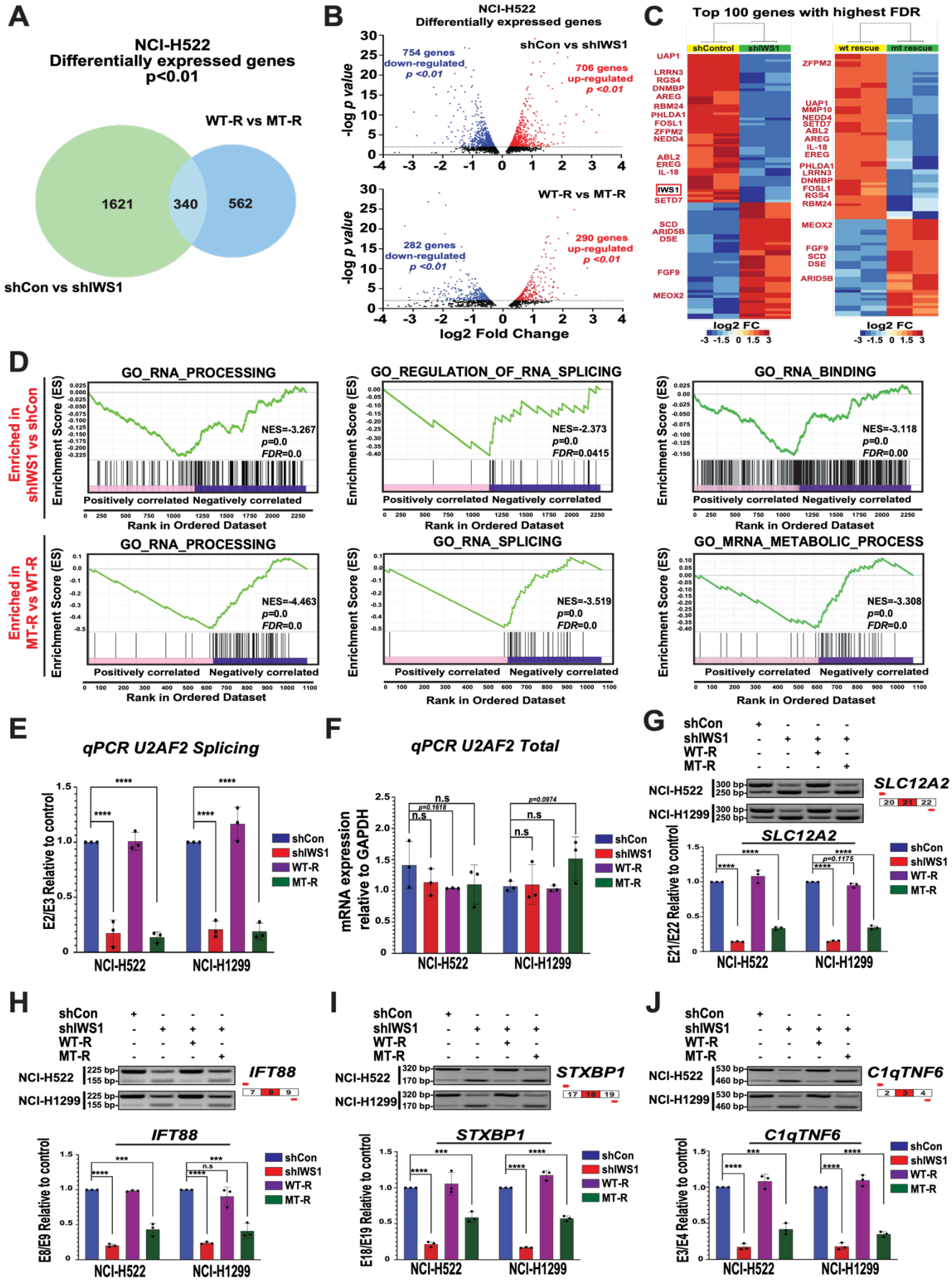
A
NCI-H522
Differentially expressed genes
p<0.01
WT-R vs MT-R
1621
340
562
shCon vs shIWS1
B
NCI-H522
Differentially expressed genes
shCon vs shIWS1
754 genes
down-regulated
p <0.01
706 genes
up-regulated
p <0.01
WT-R vs MT-R
282 genes
down-regulated
p <0.01
290 genes
up-regulated
p <0.01
-log p value
log2 Fold Change
C
Top 100 genes with highest FDR
shControl
shIWS1
wt rescue
mt rescue
UAP1
LRRN3
RGS4
DNMBP
AREG
RBM24
PHLDA1
FOSL1
ZFPM2
NEDD4
ABL2
EREG
IL-18
IWS1
SETD7
SCD
ARID5B
DSE
FGF9
MEOX2
MMP10
SETD7
log2 FC
D
GO_RNA_PROCESSING
NES=-3.267
p=0.0
FDR=0.0
GO_REGULATION_OF_RNA_SPLICING
NES=-2.373
p=0.0
FDR=0.0415
GO_RNA_BINDING
NES=-3.118
p=0.0
FDR=0.00
GO_RNA_PROCESSING
NES=-4.463
p=0.0
FDR=0.0
GO_RNA_SPLICING
NES=-3.519
p=0.0
FDR=0.0
GO_MRNA_METABOLIC_PROCESS
NES=-3.308
p=0.0
FDR=0.0
Enriched in shIWS1 vs shCon
Enriched in MT-R vs WT-R
Enrichment Score (ES)
Positively correlated
Negatively correlated
Rank in Ordered Dataset
E
qPCR U2AF2 Splicing
E2/E3 Relative to control
NCI-H522
NCI-H1299
shCon
shIWS1
WT-R
MT-R
F
qPCR U2AF2 Total
mRNA expression relative to GAPDH
n.s
p=0.1618
p=0.0974
G
SLC12A2
E21/E22 Relative to control
p=0.1175
H
IFT88
E8/E9 Relative to control
I
STXBP1
E18/E19 Relative to control
J
C1qTNF6
E3/E4 Relative to control

1163

Figure S1 (relative to Figure 1). IWS1 expression and/or phosphorylation regulate alternative mRNA splicing

A. Venn diagram shows the genes that are differentially expressed in shControl versus shIWS1 or shIWS1/WT-R versus shIWS1/MT-R NCI-H522 cells ($p<0.01$) and the overlap between the two sets. **B.** Volcano plots of all the differentially expressed genes in shControl versus shIWS1 (upper panel) and shIWS1/WT-R versus shIWS1/MT-R NCI-H522 cells (lower panel). Genes upregulated or downregulated with a p value <0.01 are shown in red and blue, respectively. **C.** Heatmaps of the top 100 differentially expressed genes (highest FDR) in shIWS1 relative to shControl and in shIWS1/MT-R relative to shIWS1/WT-R NCI-H522 cells. Genes present in both sets are shown in red. The abundance of IWS1 was significantly lower in shIWS1 cells, relative to the shControl cells, as expected (red box). **D.** Gene Set Enrichment Analysis (GSEA) of genes differentially expressed in shControl versus shIWS1 (upper panels) and in shIWS1/WT-R versus shIWS1/MT-R (lower panels) NCI-H522 cells demonstrates significant enrichment in genes involved in RNA processing. (NES–normalized enrichment score, FDR–false discovery ratio) **E.** *IWS1 expression and phosphorylation regulate the alternative splicing of the U2AF2 exon 2.* Quantitative RT-PCR showing the *E2/E3* ratio in the *U2AF2* mRNA transcripts in shControl, shIWS1, shIWS1/WT-R and shIWS1/MT-R NCI-H522 and NCI-H1299 cells. Bars show the E2/E3 ratio (mean ± SD) in all the cell lines, normalized relative to the shControl. **F.** Quantitative RT-PCR, showing the abundance of all the *U2AF2* mRNA transcripts in shControl, shIWS1, shIWS1/WT-R and shIWS1/MT-R NCI-H522 and NCI-H1299 cells. Bars show the total *U2AF2* mRNA (mean ± SD) relative to *GAPDH*. **G., H., I.** and **J**. IWS1 expression and phosphorylation regulate the alternative RNA splicing of *SLC12A2* (exon 21), *IFT88* (exon 8), *STXBP1* (exon 18) and *C1qTNF6* (exon 3). In all cases, IWS1 promotes exon inclusion. Upper panels show the electrophoresed products of the corresponding RT-PCR reactions. These products were quantified and the ratios of the alternatively spliced to non-alternatively spliced adjacent exons were normalized relative to the ratio in the shControl cells. Bars show the relative exon ratios (mean ± SD) in shControl, shIWS1, shIWS1/WT-R and shIWS1/MT-R NCI-H522 and NCI-H1299 cells. Assays were done in triplicate, on three biological replicates. n.s : non-significant *$p<0.05$, **$p<0.01$, ***$p<0.001$, ****$p<0.0001$. (one-side unpaired t-test)

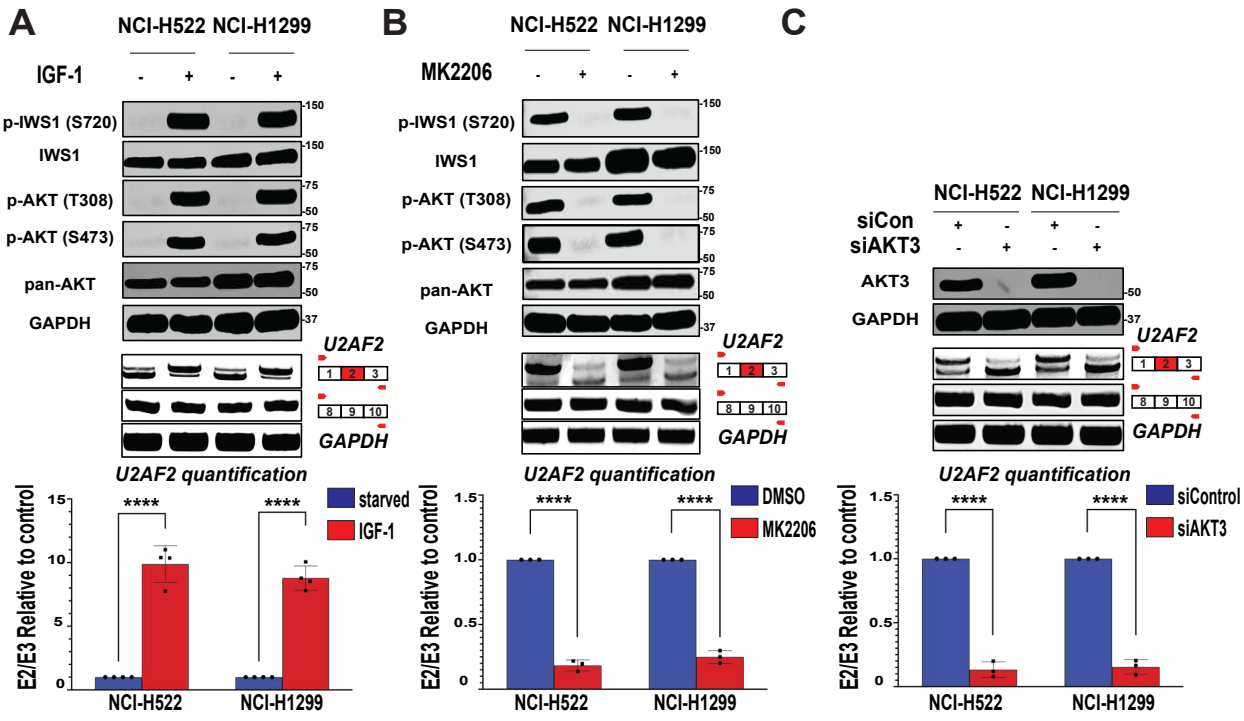

1201

1202 **Figure 2. IWS1 phosphorylation-dependent mRNA splicing of *U2AF2* is regulated by serum and IGF-**
1203 **1-induced signals transduced by AKT**

1204 **A.** *IGF-1 promotes the IWS1-dependent U2AF2 exon 2 (E2) inclusion.* (Upper panel) Following serum
1205 starvation for 24 hours, NCI-H522 and NC-H1299 cells were stimulated with IGF-1 or harvested. Four hours
1206 later, the stimulated cells were lysed, and all the lysates were probed with the indicated antibodies. (Middle
1207 panel) RT-PCR with mRNA derived from the cells shown in the upper panel and oligonucleotide primers
1208 mapping to exons 1 and 3 of the *U2AF2* gene, show that IGF1-induced signals promote *U2AF2* exon 2
1209 inclusion. (Lower panel) The *U2AF2* gene *E2/E3* ratio was calculated following quantification of the RT-
1210 PCR products in the middle panel. The bars show this ratio (mean± SD) in IGF-1 stimulated NCI-H522 and
1211 NCI-H1299 cells relative to the ratio in untreated serum-starved cells. **B.** *U2AF2 exon 2 (E2) inclusion*
1212 *depends on AKT.* (Upper panel) NCI-H522 and NCI-H1299 cell lysates, harvested following a 4 hr treatment
1213 with MK2206 (5μM) or DMSO, were probed with the indicated antibodies. (Middle panel) RT-PCR reactions,
1214 using mRNA derived from the cells in the upper panel and oligonucleotide primers mapping in *U2AF2* exons
1215 1 and 3 show that inhibiting AKT inhibits the inclusion of exon 2 in mature *U2AF2* mRNA transcripts in both
1216 cell lines. (Lower panel) The *U2AF2* mRNA *E2/E3* ratio was calculated following quantification of the RT-
1217 PCR products in the middle panel. The bars show this ratio (mean± SD) in MK2206-treated (5μM) NCI-
1218 H522 and NCI-H1299 cells relative to the ratio in DMSO-treated cells. **C.** *U2AF2 exon 2 (E2) inclusion*
1219 *depends on AKT3***.** (Upper panel) NCI-H522 and NCI-H1299 cell lysates, harvested 48 hr after transfection
1220 with siAkt3 or siControl, were probed with the indicated antibodies. (Middle panel) RT-PCR reactions, using
1221 mRNA derived from the cells in the upper panel and oligonucleotide primers mapping in *U2AF2* exons 1

1222 and 3 show that knocking down Akt3 inhibits the inclusion of exon 2 in mature *U2AF2* mRNA transcripts in
1223 both cell lines. (Lower panel) The *U2AF2* mRNA *E2/E3* ratio was calculated following quantification of the
1224 RT-PCR products in the middle panel. The bars show this ratio (mean±SD) in *siAKT3*-transfected NCI-
1225 H522 and NCI-H1299 cells relative to the ratio in mock-transfected cells. All experiments in this figure were
1226 done in triplicate, on three biological replicates. n.s. : non-significant *p<0.05, **p<0.01, ***p<0.001,
1227 ****p<0.0001. (one-side unpaired t-test).
1228
1229

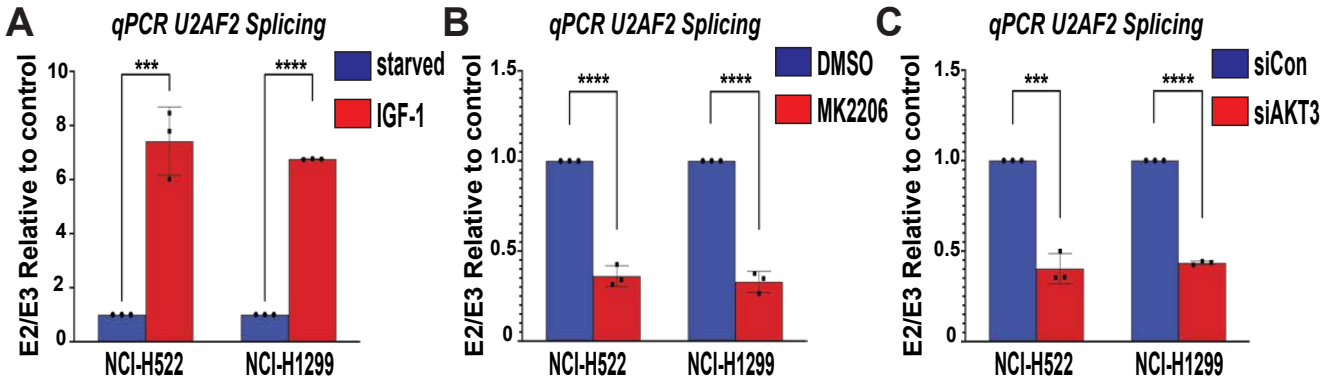

1230

1231 **Figure S2 (relative to Figure 2). IWS1 phosphorylation-dependent mRNA splicing of *U2AF2* is**
1232 **regulated by serum and IGF-1-induced signals transduced by AKT**

1233 **A. B. and C.** The *U2AF2* mRNA E2/E3 ratio in the cells in figure 2 was also measured by quantitative RT-
1234 PCR. Bars show the E2/E3 ratio in IGF-1, MK2206 and siAKT3-treated cells relative to the control
1235 cells. Error bars indicate SD. All experiments in this figure were done on three biological replicates, in
1236 triplicate. n.s. : non-significant *p<0.05, **p<0.01, ***p<0.001, ****p<0.0001. (one-side unpaired t-test)
1237
1238
1239
1240
1241
1242
1243
1244
1245
1246
1247
1248
1249

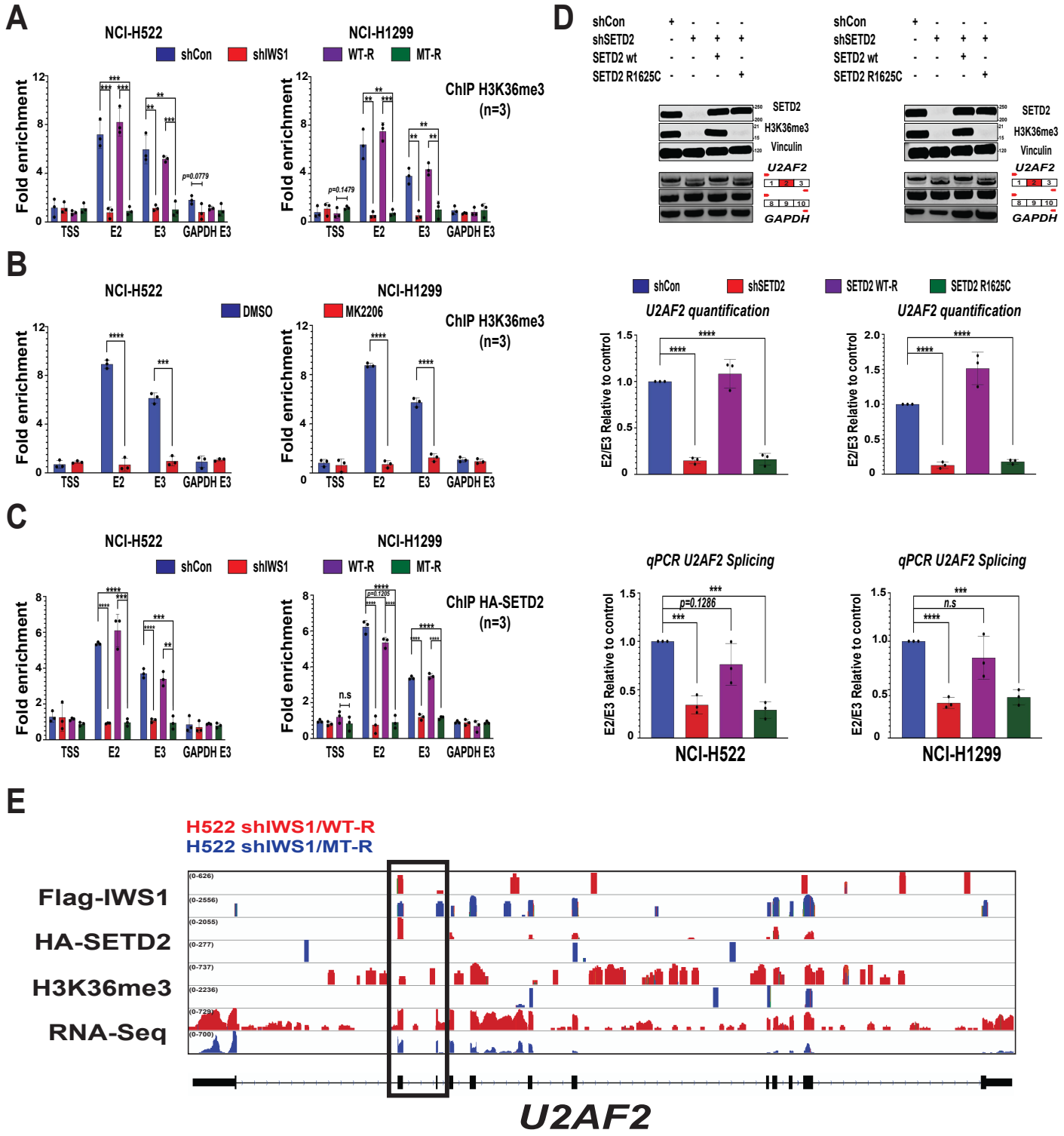
A
NCI-H522
NCI-H1299
shCon
shIWS1
WT-R
MT-R
ChIP H3K36me3
(n=3)
Fold enrichment
TSS
E2
E3
GAPDH E3
p=0.0779
p=0.1479
B
DMSO
MK2206
U2AF2 quantification
E2/E3 Relative to control
shSETD2
SETD2 WT-R
SETD2 R1625C
C
ChIP HA-SETD2
(n=3)
p=0.1206
n.s
qPCR U2AF2 Splicing
p=0.1286
D
SETD2
H3K36me3
Vinculin
U2AF2
GAPDH
E
H522 shIWS1/WT-R
H522 shIWS1/MT-R
Flag-IWS1
HA-SETD2
H3K36me3
RNA-Seq
U2AF2

1255 **Figure 3. *U2AF2* Exon 2 inclusion, induced by IWS1 phosphorylation at Ser720/Thr721, depends on**
1256 **H3K36 trimethylation by SETD2.**

1257 **A.** ChIP assays showing the abundance of H3K36me3 on the *U2AF2* and *GAPDH* genes in shControl,
1258 shIWS1 shIWS1/WT-R and shIWS1/MT-R NCI-H522 (left) and NCI-H1299 cells (right). Bars show the
1259 mean fold enrichment in H3K36me3 (anti-H3K36me3 IP, vs IgG control IP) in the indicated regions of the
1260 *U2AF2* gene, in shControl, shIWS1, shIWS1/WT-R and shIWS1/MT-R cells ±SD. Data were normalized
1261 relative to the input (2%). **B.** *AKT inhibition interferes with the H3K36me3 trimethylation in the U2AF2 gene*.
1262 ChIP assays showing the abundance of H3K36me3 on the *U2AF2* and *GAPDH* genes in NCI-H522 (left)
1263 and NCI-H1299 cells (right), before and after the treatment with MK2206 (5μM) or DMSO. The bars show
1264 the mean fold enrichment of H3K36me3 (anti-H3K36me3 IP, vs IgG control IP) in the indicated regions of
1265 the *U2AF2* gene, in shControl, shIWS1 shIWS1/WT-R and shIWS1/MT-R cells ±SD. Data were normalized
1266 relative to the input (2%). **C.** ChIP assays showing the binding of HA-SETD2 to the indicated regions of the
1267 *U2AF2* and *GAPDH* genes, in shControl, shIWS1 shIWS1/WT-R and shIWS1/MT-R NCI-H522 (left) and
1268 NCI-H1299 cells (right), transduced with a lentiviral HA-SETD2 construct. The bars show the mean fold
1269 enrichment in SETD2 binding (anti-HA IP, vs IgG control IP) in the indicated regions of the *U2AF2* gene, in
1270 shControl, shIWS1, shIWS1/WT-R and shIWS1/MT-R cells ±SD. Data were normalized relative to the input
1271 (2%). The expression of HA-SETD2 is presented in Figure S3A. **D.** *The IWS1-regulated alternative RNA*
1272 *splicing of U2AF2, depends on enzymatically active SETD2*. (Upper panel) Lysates of NCI-H522 (left) and
1273 NCI-H1299 (right) cells transduced with shControl or shSETD2 lentiviral constructs and shSETD2 cells
1274 rescued with wild type SETD2, or the catalytically inactive SETD2 R1625C mutant were probed with the
1275 indicated antibodies. RT-PCR, using RNA derived from these cells and oligonucleotide primers mapping in
1276 *U2AF2* exons 1 and 3, revealed that the inclusion of exon 2 in the mature U2AF2 mRNA transcripts depends
1277 on the expression of enzymatically active SETD2. (Middle panel) The RT-PCR products in the experiment
1278 in the upper panel were quantified. Bars show the E2/E3 ratio relative to the shControl, which was given
1279 the value of 1. (Lower panel) The ratio of the *U2AF2* exons 2 and 3 was determined by quantitative RT-
1280 PCR, using the mRNA isolated from the cells in the upper panel. Again, bars show the E2/E3 ratio relative
1281 to the shControl. Error bars indicate SD. All experiments in this figure were done on three biological
1282 replicates, in triplicate. n.s : non-significant *p<0.05, **p<0.01, ***p<0.001, ****p<0.0001. (one-side unpaired
1283 t-test) **E.** Snapshots of the integrative genomic viewer showing the distribution of Flag-IWS1, HA-SETD2,
1284 and histone H3K36me3 marks, within the *U2AF2* gene, obtained from a ChIP-Seq analysis, along with the
1285 distribution of RNA reads obtained from the RNA-seq analysis of shIWS1/WT-R and shIWS1/MT-R NCI-
1286 H522 cells. Scale represents reads per million (RPM). Snapshots of peaks detected in both biological
1287 replicates are shown. The black box outlines *U2AF2* exons 2 and 3 and the adjacent regions.

1288
1289
1290
1291

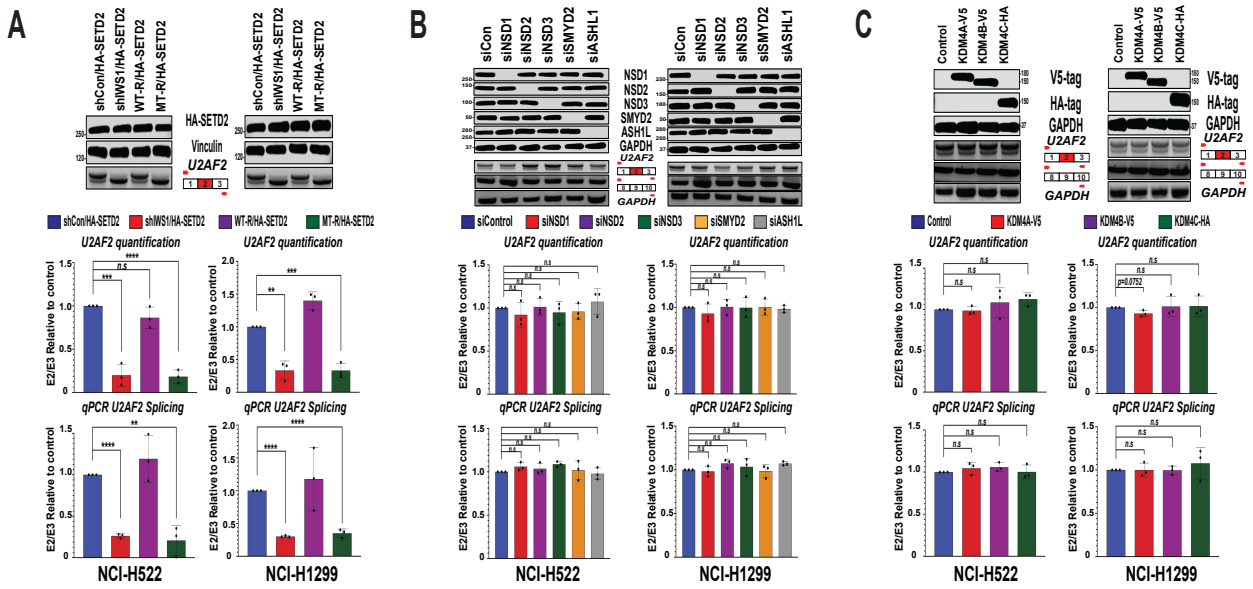

Figure S3 (relative to Figure 3). *U2AF2* Exon 2 inclusion, induced by IWS1 phosphorylation at Ser720/Thr721, depends on H3K36 trimethylation by SETD2.

A. *SETD2 does not rescue the shIWS1 and shIWS1/MT-R U2AF2 alternative splicing phenotype.* (Upper panels-First two lines) Lysates of shControl, shIWS1 shIWS1/WT-R and shIWS1/MT-R NCI-H522 and NCI-H1299 cells, transduced with a lentiviral construct of wild type HA-SETD2, were probed with the indicated antibodies. (Upper panels-third line) RT-PCR reactions, using mRNA derived from the same cells, and oligonucleotide primers mapping in *U2AF2* exons 1 and 3 show that SETD2 does not rescue the shIWS1-induced exclusion of exon 2 from the U2AF2 mRNA (Middle panel) *U2AF2 E2/E3* ratio in HA-SETD2-transduced shIWS1, shIWS1/WT-R and shIWS1/MT-R cells, relative to HA-SETD2-transduced shControl cells. Data based on quantification of the RT-PCR products above. (Lower panel) The RT-PCR results were confirmed by quantitative RT-PCR. Bar graphs show again the E2/E3 ratio in HA-SETD2-transduced shIWS1, shIWS1/WT-R and shIWS1/MT-R cells, relative to HA-SETD2-transduced shControl cells ± SD. **B.** (Upper panels. first 6 lines) The listed H3K36 methyltransferases were efficiently knocked down in NCI-H522 and NCI-H1299 cells, by siRNA transfection, as determined by probing western blots of transfected cell lysates with the indicated antibodies. (Upper panels, lines 7 and 9) RT-PCR, using RNA isolated from these cells, and *U2AF2* exon 1 and exon 3 or exon 8 and 10 oligonucleotide primers shows that none of these methyltransferases control the splicing pattern of the *U2AF2* mRNA. (Middle panels) *U2AF2 E2/E3* ratio in the siRNA-transfected cells, relative to the siControl cells. Data based on quantification of the RT-PCR products above. (Lower panels) The RT-PCR results were confirmed by quantitative RT-PCR. Bar graphs show the *E2/E3* ratio in NCI-H522 and NCI-H1299 cells, after the knockdown of the indicated methyltransferases, relative to the siControl cells ± SD. **C.** (Upper Panels, first 3 lines) The listed H3K36 demethylases were overexpressed in NCI-H522 and NCI-H1299 cells, using viral constructs (pLX304 constructs for KDM4A and KDM4B and a pBabe-puro construct for KDM4C). Expression was determined

by probing western blots of transduced cell lysates with the indicated antibodies. (Upper panels 4th and 5th lines) RT-PCR, using RNA isolated from these cells, and *U2AF2* exon 1 and exon 3 or exon 8 and 10 oligonucleotide primers shows that none of these demethylases control the splicing pattern of the U2AF2 mRNA. (Middle panels) *U2AF2 E2/E3* ratio in the transduced cells, relative to the vector-transduced (pLX304 EV plus pBabe-puro EV) cells. Data based on quantification of the RT-PCR data above. (Lower panels) The RT-PCR results were confirmed by quantitative RT-PCR. Bar graphs show the *E2/E3 U2AF2* ratio in NCI-H522 and NCI-H1299 cells, after transduction with the indicated demethylases, relative to the Control cells ± SD. All assays in this figure were done in triplicate, on three biological replicates. n.s : non-significant *$p<0.05$, **$p<0.01$, ***$p<0.001$, ****$p<0.0001$. (one-side unpaired t-test) .

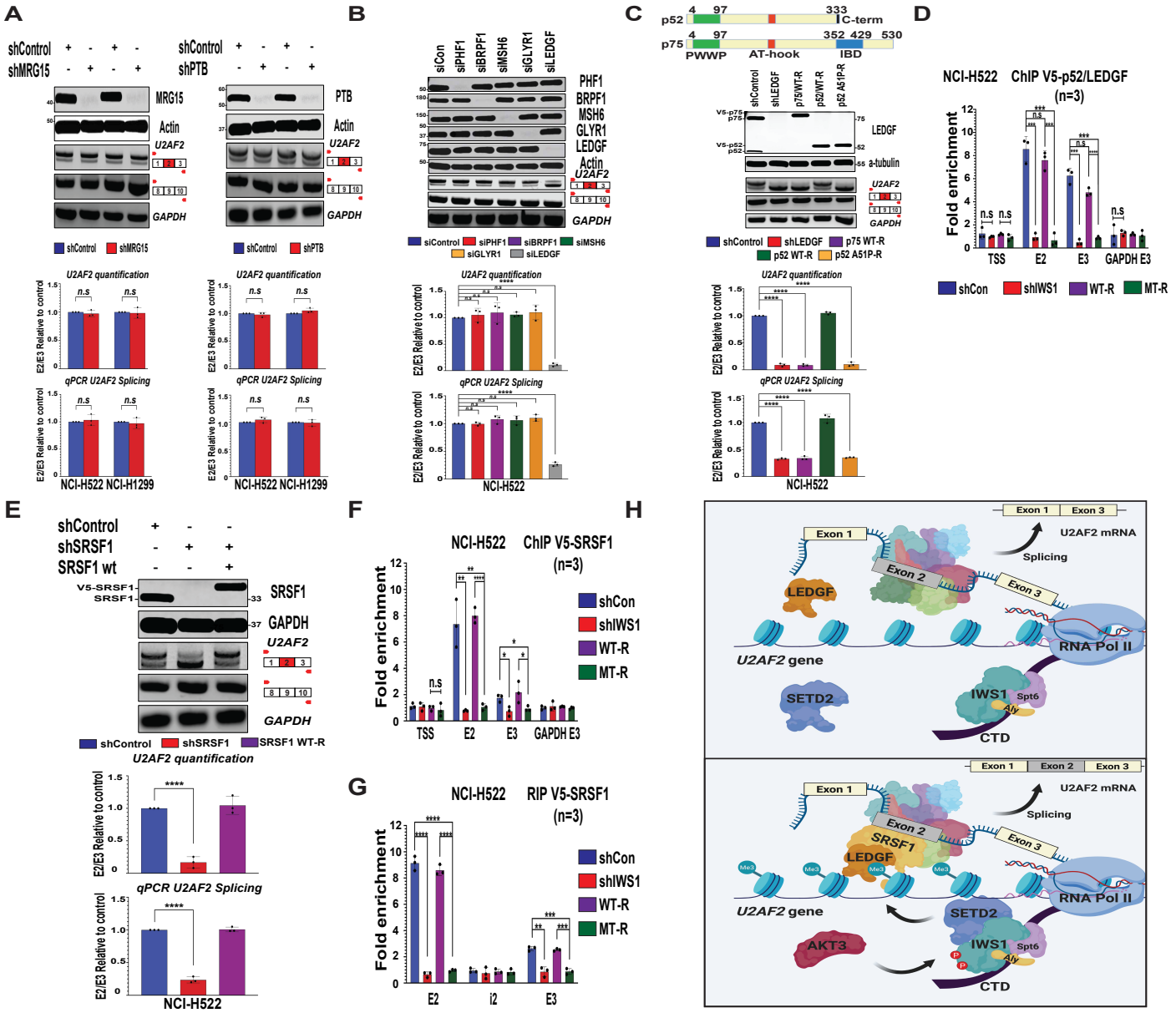

Figure 4. The regulation of the alternative splicing of the *U2AF2* exon 2 by IWS1 and IWS1 phosphorylation, depends on the p52 isoform of the H3K36me3 reader LEDGF and its splicing partner SRSF1.

A. *The H3K36me3 reader MRG15 and its binding partner PTB, play no role in the regulation of U2AF2 alternative RNA splicing.* (Upper panel) Western blots of lysates of NCI-H522 and NCI-H1299 cells transduced with shControl and shMRG15 (left) or shControl and shPTB (right) were probed with the indicated antibodies. RT-PCR, using RNA isolated from these cells and *U2AF2* exon 1 and exon 3 or exon

1363 8 and 10 oligonucleotide primers shows that the knockdown of neither MRG15 nor PTB affects the
1364 alternative splicing of *U2AF2*. (Middle and lower panel) The RT-PCR results were confirmed by quantitative
1365 RT-PCR. Bar graphs show the E2/E3 ratio in shMRG15 and shPTB NCI-H522 and NCI-H1299 cells, relative
1366 to the shControl ± SD. **B.** *The alternative splicing of the U2AF2 exon 2 is regulated by the H3K36me3*
1367 *reader LEDGF.* (Upper Panel) The listed H3K36me3 readers were efficiently knocked down by siRNA
1368 transfection of NCI-H522 cells, as determined by probing western blots of transfected cell lysates with the
1369 indicated antibodies. RT-PCR, using RNA isolated from these cells and *U2AF2* exon 1 and exon 3 or exon
1370 8 and 10 oligonucleotide primers shows that only the knockdown of LEDGF affects the alternative splicing
1371 of *U2AF2*. (Middle and lower panel) The RT-PCR results were confirmed by quantitative RT-PCR. Bar
1372 graphs show the *E2/E3 U2AF2* ratio in NCI-H522 cells, after the knockdown of the indicated readers,
1373 relative to the siControl ± SD. **C.** *The alternative RNA splicing of the U2AF2 exon 2 is regulated by the*
1374 *p52, but not the p75 isoform of LEDGF.*(Upper panel) Schematic representation of the p52 and p75 isoforms
1375 of LEDGF showing the position of the PWWP domain (green), the AT hook-like domain (red), the unique
1376 to p52 8 aa long C-terminal domain (black) and the unique to p75 integrase binding domain (IBD) (blue)
1377 (Ferris et al., 2010[54]). (Middle panel) Western blots of lysates of shControl, shLEDGF, shLEDGF/LEDGF-
1378 p75-R,shLEDGF/LEDGF-p52WT-R,shLEDGF/LEDGF-p52A51P-R NCI-H522 cells, were probed with the
1379 indicated antibodies. RT-PCR, using RNA isolated from these cells and *U2AF2* exons 1 and 3 or exons 8
1380 and 10 oligonucleotide primers shows that only the wild type p52 isoform of LEDGF rescues the alternative
1381 splicing of *U2AF2* in shLEDGF-transduced cells. The p75 isoform and the p52 mutant A51P, which does
1382 not bind H3K36me3, failed to rescue. (Lower panels) The RT-PCR results were confirmed by quantitative
1383 RT-PCR. Bar graphs show the *E2/E3 U2AF2* ratio in shLEDGF-transduced NCI-H522 cells, before and
1384 after the rescue with the indicated constructs, relative to the shControl ± SD. **D.** *The recruitment of*
1385 *p52/LEDGF to the U2AF2 gene depends on IWS1 phosphorylation.* ChIP assays showing the binding of
1386 p52/LEDGF to the *U2AF2* and *GAPDH* genes in shControl, shIWS1 shIWS1/WT-R and shIWS1/MT-R
1387 NCI-H522 cells, transduced with a lentiviral V5-p52/LEDGF construct. The bars show the mean fold
1388 enrichment in p52/LEDGF binding (anti-V5 IP, vs IgG control IP) to the indicated regions of the *U2AF2*
1389 gene, in shControl, shIWS1 shIWS1/WT-R and shIWS1/MT-R cells ±SD. Data were normalized relative to
1390 the input (2%). The expression of V5-p52/LEDGF is shown in figure S4D. **E.** *The alternative RNA splicing*
1391 *of the U2AF2 exon 2 depends on SRSF1.* (Upper panel) Western blots of lysates of shControl, shSRSF1
1392 and shSRSF1/SRSF1 WT-R NCI-H522 cells, were probed with the indicated antibodies. RT-PCR, using
1393 RNA isolated from these cells and *U2AF2* exons 1 and 3 or exons 8 and 10 oligonucleotide primers, shows
1394 that the knockdown of SRSF1 promotes a shift in the RNA splicing pattern of *U2AF2*, which favors the
1395 exclusion of exon 2 from the mature transcripts, and that wild type SRSF1 rescues the shift. (Lower panels)
1396 The RT-PCR results were confirmed by quantitative RT-PCR. Bar graphs show the E2/E3 ratio in shSRSF1-
1397 transduced NCI-H522 cells, before and after rescue with wild type SRSF1, relative to the shControl ±SD.
1398 **F.** *The recruitment of SRSF1 to the U2AF2 gene, depends on IWS1 phosphorylation.* ChIP assays showing
1399 the binding of SRSF1 to the *U2AF2* and *GAPDH* genes in shControl, shIWS1 shIWS1/WT-R and

shIWS1/MT-R NCI-H522 cells, transduced with a lentiviral V5-SRSF1 construct. The bars show the mean fold enrichment in SRSF1 binding (anti-V5 IP, vs IgG control IP) to the indicated regions of the *U2AF2* gene, in shControl, shIWS1 shIWS1/WT-R and shIWS1/MT-R cells ±SD. Data were normalized relative to the input (2%). The V5-SRSF1 expression is shown in Figure S4F. **G.** *The recruitment of SRSF1 to the U2AF2 RNA depends on IWS1 phosphorylation.* RIP assays showing the binding of SRSF1 to the *U2AF2* RNA in the NCI-H522 cells in Fig. 4F. The bars show the mean fold enrichment in SRSF1 binding in the indicated regions of the *U2AF2* RNA (anti-V5 IP, vs IgG control IP) ±SD. Data were normalized relative to the input (2%). All assays in this figure were done in triplicate, on three biological replicates. n.s : non-significant *p<0.05, **p<0.01, ***p<0.001, ****p<0.0001. (one-side unpaired t-test**) H.** *Model of the regulation of U2AF2 alternative RNA splicing by AKT3-mediated IWS1 phosphorylation at Ser720/Thr721.* The phosphorylation of IWS1 recruits SETD2 to the Spt6/IWS1/Aly complex in the CTD of RNA Pol II. SetD2 in the complex, trimethylates histone H3 at K36 during transcriptional elongation. p52/LEDGF and its RNA-binding partner SRSF1, bind histone H3K36me3. Binding of SRSF1 to exon 2 promotes inclusion of this exon in the mature *U2AF2* transcript.

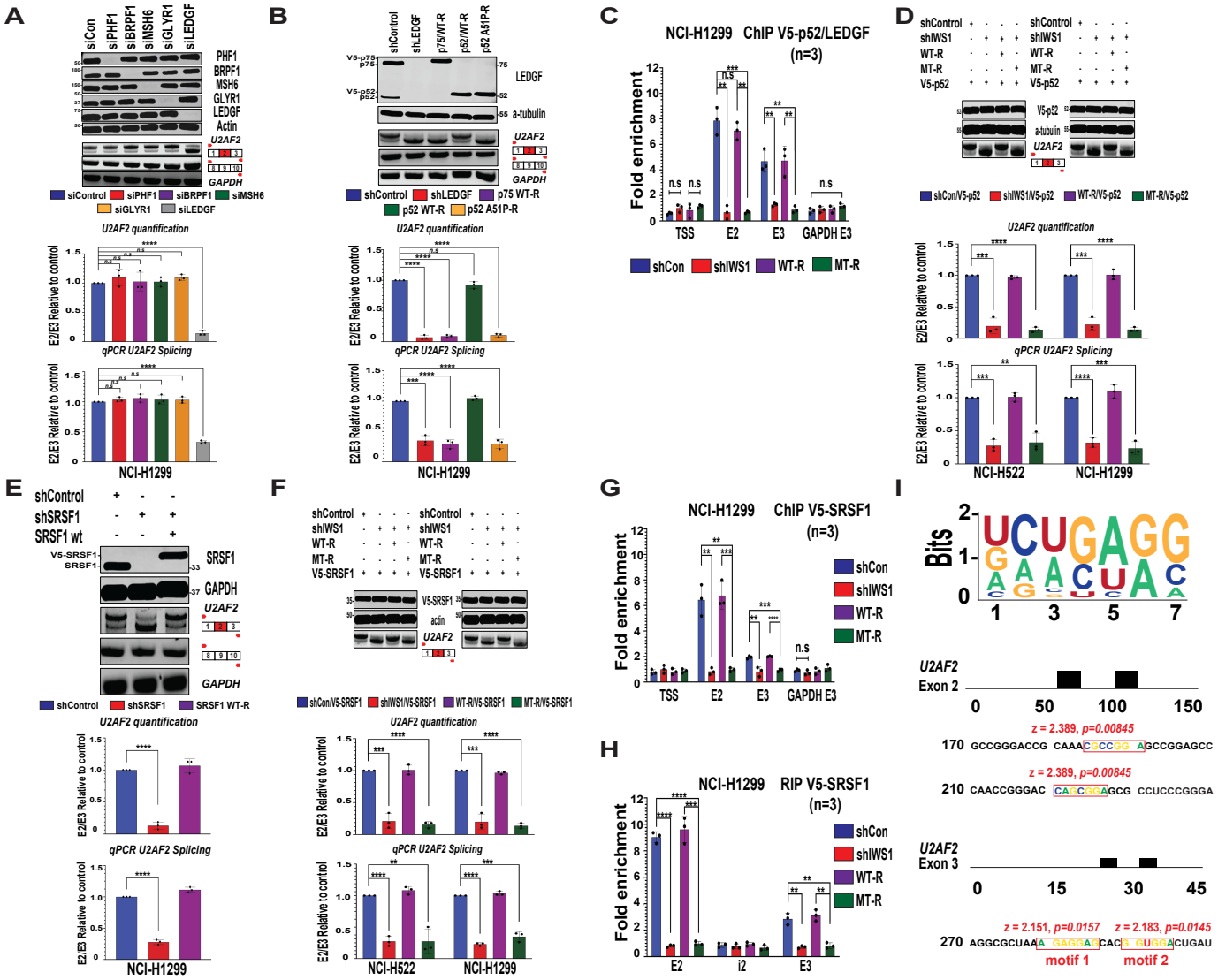

Figure S4 (relative to Figure 4). The regulation of the alternative splicing of the *U2AF2* exon 2 by *IWS1* and *IWS1* phosphorylation, depends on the p52 isoform of the H3K36me3 reader *LEDGF* and its splicing partner *SRSF1*.

A. The knockdown of the indicated histone H3K36me3 readers in NCI-H1299 cells confirmed that only the knockdown of LEDGF results the exclusion of exon 2 from the mature *U2AF2* mRNA transcript. This is a repeat of the experiment in figure 4B, which was done in NCI-H522 cells. The results confirmed that LEDGF controls the mRNA splicing of *U2AF2* in multiple cell lines. **B.** The expression of LEDGF-p75-WT, LEDGF-p52-WT and LEDGF-p52A51P (a LEDGF mutant, which has lost the ability to bind H3K36me3) in shLEDGF-transduced NCI-H1299 cells, confirmed that only LEDGF-p52-WT can rescue the shLEDGF-induced exclusion of exon 2 from the mature *U2AF2* mRNA transcript. This is a repeat of the experiment in

figure 4C, which was done in NCI-H522 cells. The results confirmed that the p52 isoform of wild type LEDGF controls the mRNA splicing of *U2AF2* in multiple cell lines. **C.** ChIP assays addressing the binding of V5-LEDGF-p52 in TSS, exon 2 and exon 3 of *U2AF2*, in shControl, shIWS1, shIWS1/WT-R and shIWS1/MT-R NCI-H1299 cells, confirmed the binding of this LEDGF isoform in both, exon 2 and exon 3. This is a repeat of the experiment in figure 4D, which was done in NCI-H522 cells. The results confirmed that the p52 isoform of wild type LEDGF controls the mRNA splicing of *U2AF2,* by binding the *U2AF2* exons 2 and 3, in multiple cell lines. **D.** *V5-LEDGF-p52 does not rescue the shIWS1 and shIWS1/MT-R U2AF2 alternative splicing phenotype.* (Upper panel-First two lines) shControl, shIWS1 shIWS1/WT-R and shIWS1/MT-R NCI-H522 (left panel) and NCI-H1299 (right panel) cells were transduced with a lentiviral construct of V5-p52/LEDGF. The expression of V5-p52-LEDGF was confirmed by probing lysates of these cells with an anti-V5 or an anti-α-tubulin (loading control) antibody. (Upper panel-Third line) RT-PCR, using RNA isolated from these cells and *U2AF2* exons 1 and 3 oligonucleotide primers shows that V5-p52-LEDGF does not rescue the shIWS1 and shIWS1/MT-R *U2AF2* alternative splicing phenotype. (Middle panel) Bars show the mean *E2/E3 U2AF2* RNA ratio in NCI-H522 and NCI-H1299 shIWS1, shIWS1/WT rescue and shIWS1/MT rescue cells, in the experiment in the top panel, normalized to the shControl cells ± SD (one-side unpaired t-test) (Lower panel) The RT-PCR results were confirmed by quantitative RT-PCR. **E.** *The alternative RNA splicing of the U2AF2 exon 2 depends on SRSF1.* (Upper panel) The experiment in figure 4E, which was carried out in NCI-H522 cells, was repeated in NCI-H1299 cells, with identical results. **F.** *V5-SRSF1-WT does not rescue the shIWS1 and shIWS1/MT-R U2AF2 alternative splicing phenotype.* (Upper panel-First two lines) shControl, shIWS1 shIWS1/WT-R and shIWS1/MT-R NCI-H522 (left panel) and NCI-H1299 (right panel) cells were transduced with a lentiviral construct of V5-SRSF1. The expression of V5-SRSF1 was confirmed by probing lysates of these cells with an anti-V5 or an anti-β-actin (loading control) antibody. (Upper panel-Third line) RT-PCR, using RNA isolated from these cells and *U2AF2* exons 1 and 3 oligonucleotide primers shows that V5-SRSF1 does not rescue the shIWS1 and shIWS1/MT-R *U2AF2* alternative splicing phenotype. (Middle panel) Bars show the mean *E2/E3 U2AF2* RNA ratio in NCI-H522 and NCI-H1299 shIWS1, shIWS1/WT-R and shIWS1/MT rescue cells, in the experiment in the top panel, normalized to the shControl cells ± SD (one-side unpaired t-test) (Lower panel) The RT-PCR results were confirmed by quantitative RT-PCR. **G.** The experiments in NCI-H522 cells, in figure 4F, was repeated in NCI-H1299 cells with identical results. **H.** The experiments in NCI-H522 cells, in figure 4G, was repeated in NCI-H1299 cells with identical results. **I.** (Upper panel) The 7-nt SRSF1 binding motif, involved in the regulation of alternative RNA splicing by SRSF1 (Anczuków et al., 2015[56]) (Middle and Lower panels) Boxes show the location of the SRSF1 binding motifs in *U2AF2* exons 2 and 3 and their nucleotide sequence. The height of the boxes is proportional to the *-log* (*p value*) and it is presented relative to the height of the box mapping between nucleotides 184 and 192. The binding scores (z-scores) and p values are calculated using the RBPmap pipeline (http://rbpmap.technion.ac.il/index.html)

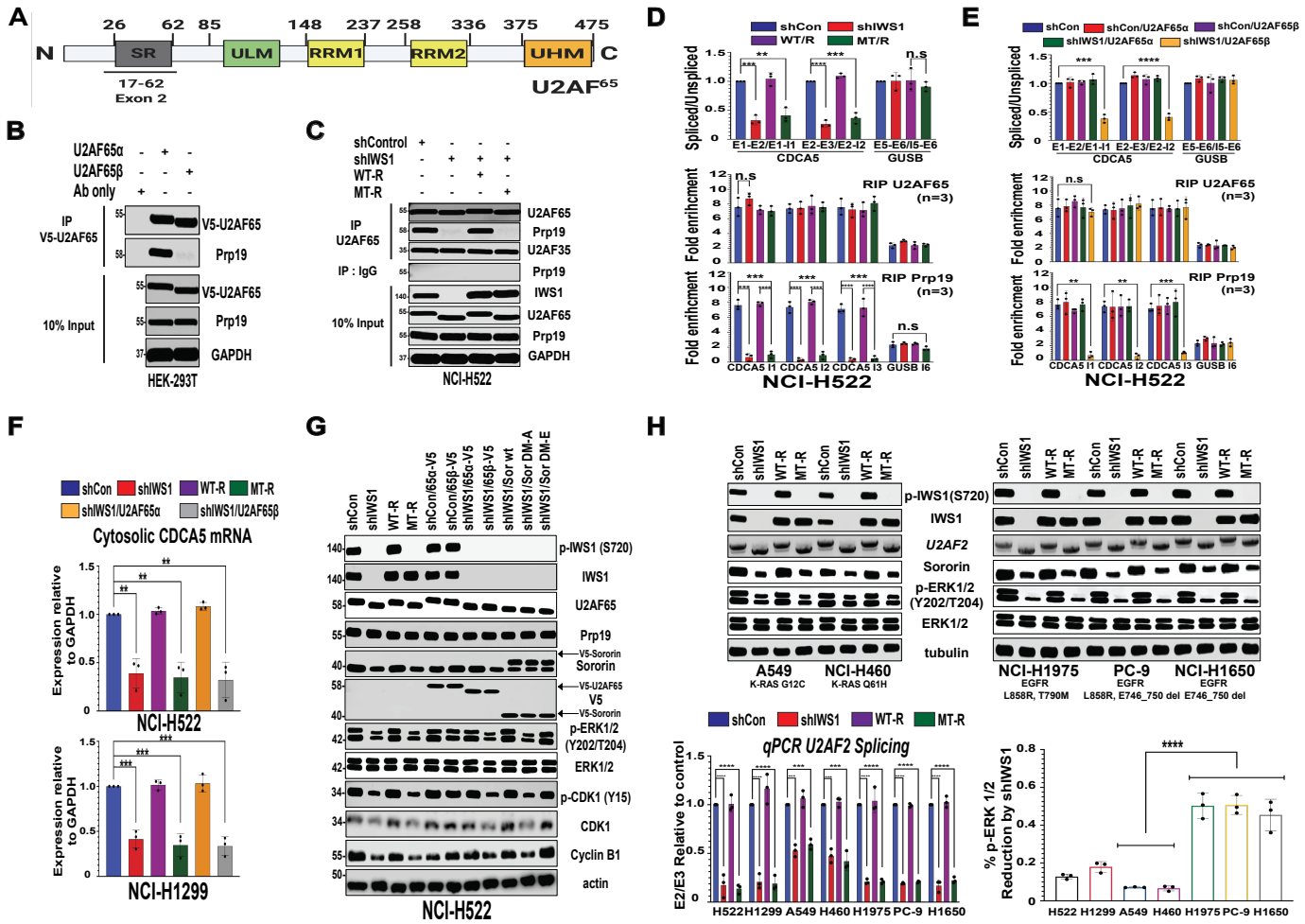

Figure 5. IWS1 phosphorylation controls the Sororin/ERK phosphorylation feedback loop, through *U2AF2* alternative RNA splicing.

A. Domain organization of the U2AF65 protein, showing the Serine/Arginine Rich (SR) domain, the U2AF-ligand motif (ULM), two RNA recognition motifs (RRMs) and the U2AF Homology Motif (UHM). Exon 2 encodes part of the N-terminal SR domain. U2AF65 and U2AF35 interact through the U2AF65 UHM domain. The numbers on top identify the amino acids at the boundaries of the indicated motifs. **B.** *The novel U2AF65β spliced variant, lacking exon 2, doesn't interact with Prp19.* HEK-293T cells were transduced with lentiviral constructs V5-U2AF65α, or V5-U2AF65β. Anti V5-U2AF65 immunoprecipitates from these cells were probed with anti-Prp19 or anti-V5-tag antibodies. (Lower panel). Western blots of the input lysates, probed with the indicated antibodies are also shown. **C.** *The U2AF65-Prp19 interaction depends on IWS1-phosphorylation.* (Upper panel) Anti-U2AF65 immunoprecipitated from lysates of shControl, shIWS1 shIWS1/WT-R and shIWS1/MT-R NCI-H522 cells were probed with anti-U2AF65, anti-Prp19, and anti-U2AF35 antibodies. Anti-IgG mouse isotype control immunoprecipitates were probed with the anti-Prp19 antibody. Western blots of the input lysates, probed with the indicated antibodies are also

1503 shown. **D.** *IWS1-phosphorylation controls CDCA5 RNA splicing.* (Upper panel). The ratio of spliced to
1504 unspliced *CDCA5* RNA transcripts was examined by quantitative RT-PCR, using total RNA isolated from
1505 shControl, shIWS1 shIWS1/WT-R and shIWS1/MT-R NCI-H522 cells and the listed oligonucleotide primers
1506 (E1-E2/E1-I1 and E2-E3/E2-I2). The same was done with the transcripts of a control gene (*GUSB*)
1507 (Oligonucleotide primers E5-E6/I5-E6). (Middle and lower panels) RIP assays in the same cells show that
1508 whereas the binding of Prp19 to the *CDCA5* RNA depends on the phosphorylation of IWS1, the binding of
1509 U2AF65 does not. The bars show the mean fold enrichment in U2AF65 and Prp19 binding in the indicated
1510 regions of the *CDCA5* pre-mRNA (anti-U2AF65 or anti-Prp19 IP, vs IgG control IP) ± SD. Data were
1511 normalized relative to the input (2%). The primer location within *CDCA5* and *GUSB* can be found in Figure
1512 S5B. **E.** *U2AF2 alternative RNA splicing, downstream of IWS1 phosphorylation controls CDCA5 splicing.*
1513 (Upper panel). The ratio of spliced to unspliced *CDCA5* RNA transcripts was examined in shControl NCI-
1514 H522 cells that were either not rescued, or rescued with U2AF65α, or U2AF65β, and in shIWS1 NCI-H522
1515 cells rescued with the same U2AF65α, or U2AF65β-encoding constructs. Quantitative RT-PCR was carried
1516 out and presented, as in Fig 5D. The *GUSB* gene was used again as the control. (Middle and lower
1517 panels) RIP assays in the same cells show that whereas U2AF65α rescues the binding of Prp19 to the
1518 *CDCA5* RNA in shIWS1 cells, U2AF65β does not. Moreover, U2AF65α and U2AF65β, bound equally to
1519 the *CDCA5* RNA. The presentation of the data was the same as in Fig 5D.
1520 **F.** *The abundance of mature CDCA5 mRNA in the cytoplasm is under the control of the IWS1-*
1521 *phosphorylation-dependent expression of U2AF65α.* The abundance of the cytosolic *CDCA5* mRNA was
1522 measured by quantitative RT-PCR in the cytosolic fraction of shIWS1, shIWS1/WT-R, shIWS1/MT-R,
1523 shIWS1/U2AF65α-R and shIWS1/U2AF5β-R NCI-H522 (upper panel) and NCI-H1299 (lower panel) cells.
1524 Bars show the mean cytosolic *CDCA5* mRNA expression normalized to *GAPDH* ± SD in NCI-H522 and
1525 NCI-H1299 shIWS1, shIWS1/WT-R, shIWS1/MT-R, shIWS1/U2AF65α-R and shIWS1/U2AF5β-R cells
1526 compared to shControl. The accuracy of the fractionation was validated with the experiment in Figure S5E.
1527 **G.** *CDCA5 and p-ERK, form a novel positive feedback loop, which is activated by IWS1 phosphorylation*
1528 *and U2AF2 alternative RNA splicing and promotes the expression of CDK1 and Cyclin B1.* Lysates of
1529 shControl, shIWS1, shIWS1/WT-R and shIWS1/MT-R NCI-H522 cells, along with shControl/U2AF65α,
1530 shControl/U2AF65β, shIWS1/U2AF65α-R, shIWS1/U2AF5β-R and shIWS1/Sororin-WT-R, shIWS1/
1531 Sororin -DM-A-R and shIWS1/ Sororin -DM-D-R NCI-H522 cells, were probed with the indicated antibodies.
1532 (DM-A is the S79/S209 Sororin mutant and DM-E is the S79/S209EE Sororin mutant). **H.** *IWS1*
1533 *phosphorylation controls the phosphorylation of ERK in cells harboring EGFR and K-RAS mutations.*
1534 Lysates of shControl, shIWS1, shIWS1/WT-R and shIWS1/MT-R *K-RAS* (upper left panels) and *EGFR*
1535 mutant cell lines were probed with the indicated antibodies. ERK phosphorylation was reduced in all
1536 shIWS1 and shIWS1/MT-R cells, including the ones with *K-RAS* and *EGFR* mutations. RT-PCR, using RNA
1537 isolated from these cells and *U2AF2* exon 1 and exon 3 oligonucleotide primers, confirmed the exclusion
1538 of exon 2 from the mature *U2AF2* mRNA, in all the shIWS1-transduced cells. (Lower left panel) The RT-
1539 PCR results were confirmed by quantitative RT-PCR. Bar graphs show the *E2/E3 U2AF2* ratio in all the

shIWS1, shIWS1/WT-R, and shIWS1/MT-R cells, relative to the shControl ± SD. (Lower right panel) Quantification of the reduction of ERK-phosphorylation (Y202/T204), induced by shIWS1 in the indicated cell lines. Bars show the percent reduction, normalized to tubulin. The comparison between the *K-RAS* mutant (A549 and NCI-H460) and *EGFR* mutant cells (NCI-H1975, PC-9, NCI-H1650) was performed with one-way ANOVA statistical test. All assays in this figure were done in triplicate, on three biological replicates. n.s : non-significant *p<0.05, **p<0.01, ***p<0.001, ****p<0.0001. (one-side unpaired t-test).

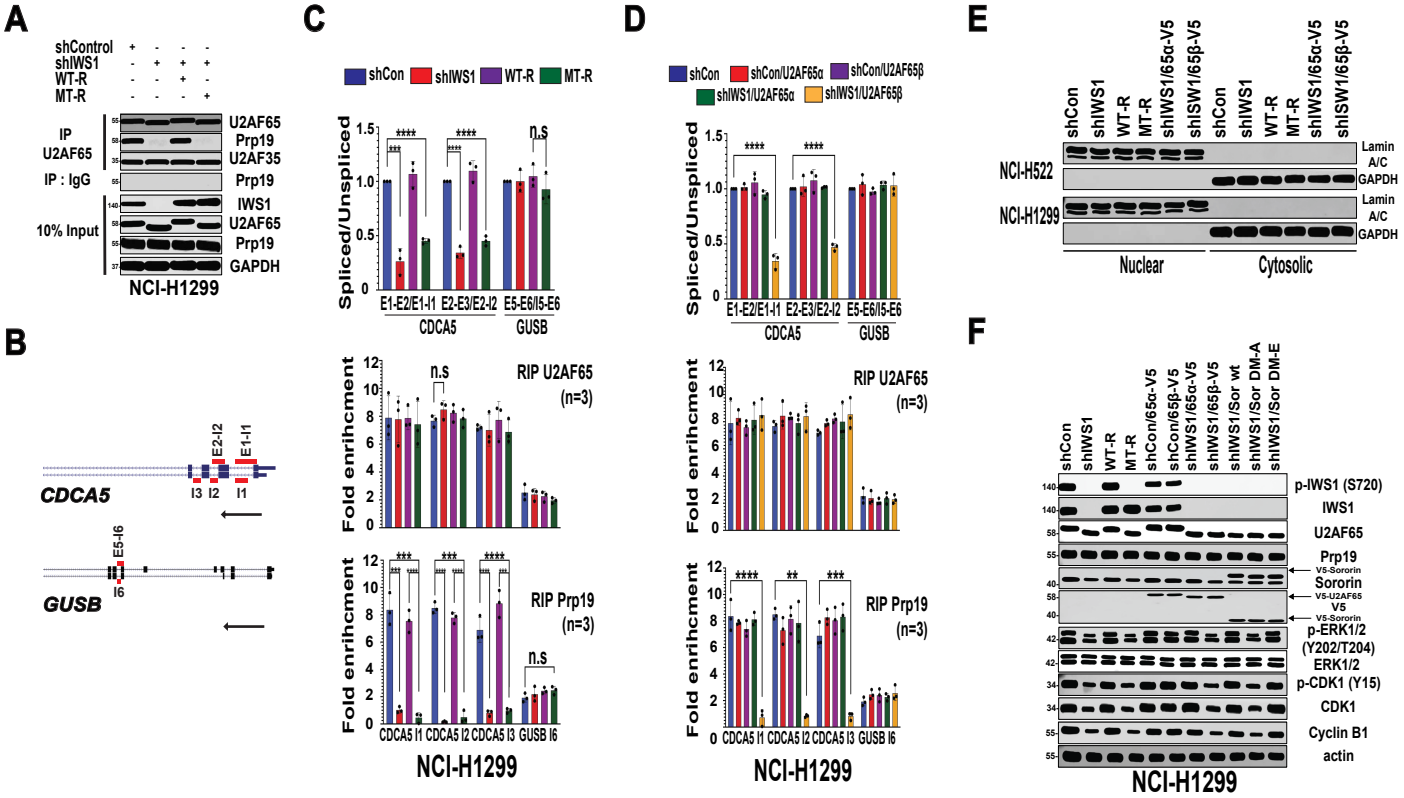

Figure S5 (relative to Figure 5). IWS1 phosphorylation controls the Sororin/ERK phosphorylation feedback loop, through *U2AF2* alternative RNA splicing.

A. The experiment in NCI-H522 cells, in figure 5C, was repeated in NCI-H1299 cells with identical results. **B.** UCSC browser snapshot showing the exon position of the relevant portions of the human *CDCA5* and *GUSB* genes. The map position of the sequences amplified by PCR is indicated with red lines. The arrows indicate the direction of transcription. **C.** The quantitative RT-PCR and RIP experiments in NCI-H522 cells, in figure 5D, were repeated in NCI-H1299 cells with identical results. **D.** The quantitative RT-PCR and RIP experiments in NCI-H522 cells, in figure 5E, were repeated in NCI-H1299 cells with identical results. **E.** The cytosolic and nuclear compartment of the indicated NCI-H522 (upper two lines) and NCI-H1299 cells (lower two lines) were probed with the indicated antibodies, to validate the fractionation. **F.** The experiment in NCI-H522 cells, in figure 5G, was repeated in NCI-H1299 cells with identical results.

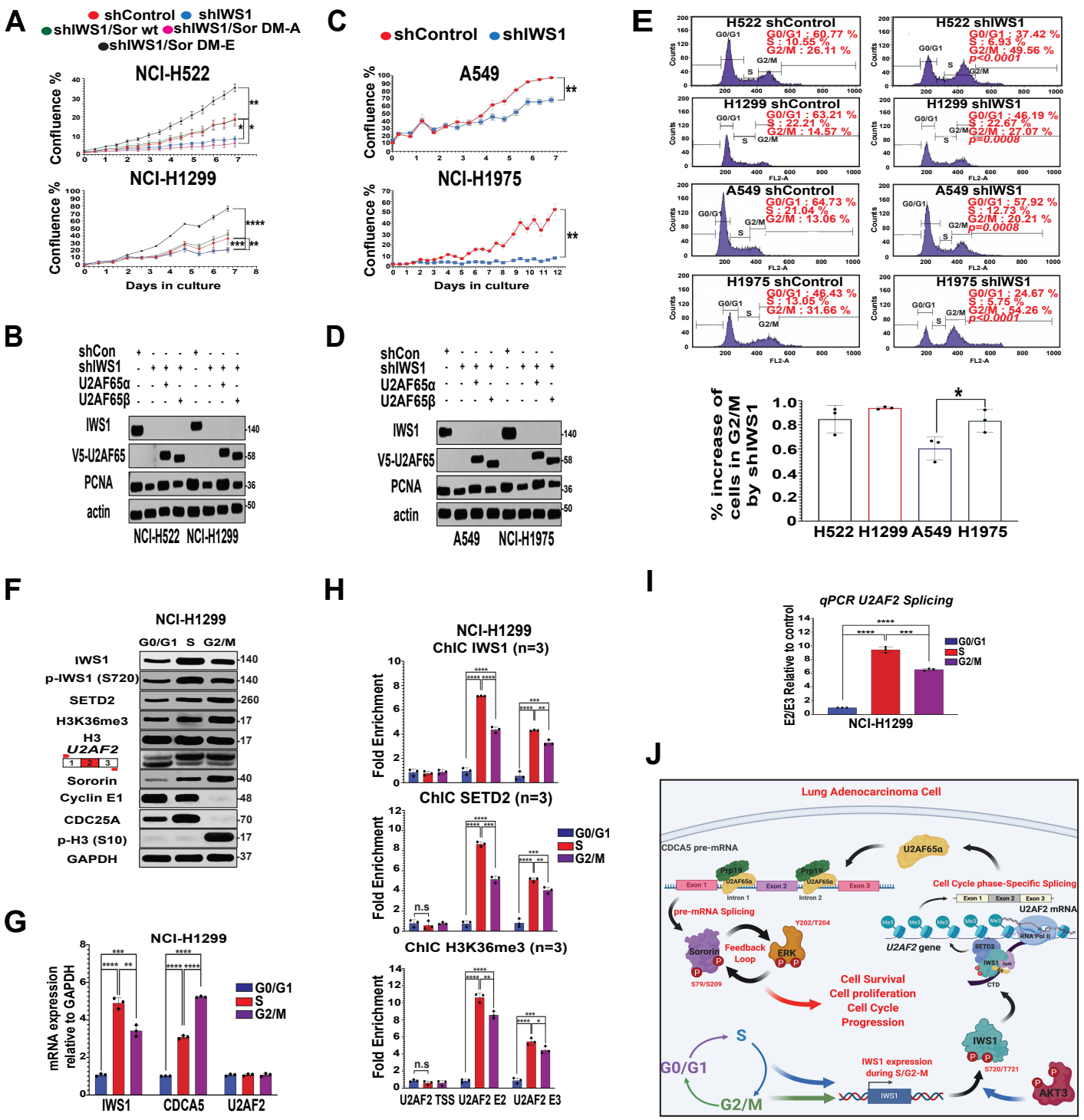

1559

1560

1561

1562 **Figure 6. IWS1 phosphorylation promotes cell proliferation by controlling the Sororin/ERK**
1563 **phosphorylation feedback loop, through *U2AF2* RNA splicing.**

1564 **A.** Growth curves of the indicated NCI-H522 (upper) and NCI-H1299 (lower) cells in media supplemented
1565 with 10% FBS. Cell proliferation was measured every 6 hours using an Incucyte live cell imager. Images of
1566 live cells in three independent cultures for each cell type were taken and analyzed using the native Incucyte
1567 confluence masking software. Results were expressed as confluence percentages ± SD. For simplicity, 12
1568 and not 6 hour time points are shown. P values were calculated for the endpoint measurements, using the
1569 one-side unpaired t-test. *p<0.05, **p<0.01, ***p<0.001, ****p<0.0001 **B.** *U2AF2 alternative RNA splicing*
1570 *affects cell proliferation.* Lysates derived from the indicated NCI-H522 and NCI-H1299 cells were probed
1571 with the indicated antibodies. In agreement with the data in A, PCNA was downregulated by shIWS1 in
1572 both cell lines, and its downregulation was rescued by U2AF65α, but not U2AF65β. **C.** *IWS1*
1573 *phosphorylation promotes cell proliferation more robustly in the EGFR mutant lung adenocarcinoma cell*
1574 *line NCI-H1975, than in the K-RAS mutant cell line A549.* Growth curves of shControl and shIWS1 A549
1575 (*K-RAS* mutant) and NCI-H1975 (*EGFR* mutant) cells in media supplemented with 10% FBS. Cell
1576 proliferation was measured as in A. **D.** Cell lysates derived from shControl and shIWS1 A549 and NCI-
1577 H1975 cells, before and after rescue with U2AF65α, or U2AF65β, were probed with the indicated
1578 antibodies. PCNA was again downregulated by shIWS1 in both cell lines, and its downregulation was
1579 rescued by U2AF65α, but not U2AF65β. **E.** *IWS1 phosphorylation regulates progression through the G2/M*
1580 *phase of the cell cycle.* Cell cycle profiles of the indicated propidium iodide (PI)-stained cell lines,
1581 transduced with shControl (left upper panels) or shIWS1 (Right upper panels) lentiviral constructs. The cells
1582 were plated in equal numbers and they were harvested from semi-confluent cultures 48 hours later. Figure
1583 shows one representative, out of three biological replicates for each cell line. Numbers in red show the
1584 mean percentage of cells in different phases of the cell cycle, measured based on the three biological
1585 replicates. The percent of cells in G2/M in shIWS1 cells was compared with the percent of cells in G2/M in
1586 shControl cells and the p value of the difference was calculated with the one-side unpaired t-test. (Lower
1587 panel) Bars show the shIWS1-induced percent change of the percentage of cells in G2/M in the indicated
1588 cell lines. The error bars show the SD of the percent change in 3 biological replicates. The percent change
1589 is smallest in the *K-RAS* mutant cell line A549. Supplemental Table S4 lists the data for all the replicates
1590 and all the conditions. The statistical analysis between the NCI-H1975 and A549 was performed using one-
1591 sided unpaired t-test. **F.** *IWS1 phosphorylation and U2AF2 alternative RNA splicing fluctuate during*
1592 *progression through the cell cycle.* Protein extracts derived from Exponentially growing NCI-H1299 cell
1593 cultures were separated into fractions enriched for cells in G0/G1, S and G2/M. Lysates of these cell
1594 fractions were probed with the indicated antibodies. RT-PCR, using RNA from the same cell fractions, and
1595 *U2AF2* exons 1 and 3 oligonucleotide primers, shows that *U2AF2* exon 2 inclusion in the mature U2AF2
1596 mRNA increases in cells in S and G2/M. **G.** The abundance of the *IWS1*, *CDCA5* and *U2AF2* mRNAs in
1597 the G0/G1, S and G2/M phases of the cell cycle in NCI-H1299 cells was measured by quantitative RT-PCR
1598 and is presented relative to the abundance of *GAPDH* ± SD. **H.** *IWS1 phosphorylation regulates the U2AF2*

1599 *alternative RNA splicing in a cell-cycle specific manner*. ChIC assays showing the binding of IWS1 and
1600 SETD2 (upper and middle panels respectively) and the abundance of H3K36me3 (lower panel) in the
1601 *U2AF2* gene, in NCI-H1299 cells in the G0/G1, S and G2/M phases of the cell cycle. The bars show the
1602 mean fold enrichment in IWS1 and SETD2 binding, and in H3K36me3 abundance, in the indicated regions
1603 of the *U2AF2* gene ±SD. **I.** Quantitative RT-PCR showing the *E2/E3 U2AF2* ratio in NCI-H1299 cells. Bars
1604 show the mean *E2/E3 U2AF2* ratio in NCI-H1299 cellular fractions enriched for cells in S and G2/M phase
1605 relative to G0/G1 enriched fractions. In 6G to 6I, the error bars show the SD of at least 3 biological
1606 replicates. *p<0.05, **p<0.01, ***p<0.001, ****p<0.0001. (one-side unpaired t-test) **J.** *Model of the*
1607 *regulation of the Sororin/ERK loop and cell cycle progression via the U2AF2 alternative RNA splicing,*
1608 *through the cell cycle.* IWS1 expression occurs specifically during the S and G2/M phase of the cell cycle.
1609 Following this cell cycle specific expression, IWS1 is phosphorylated by AKT3 at S720/T721 and
1610 orchestrates the assembly of epigenetic complexes on *U2AF2* gene, which translate the SETD2-mediated
1611 H3K36me3 signal into shifts of the alternative RNA splicing pattern of *U2AF2*, in a cell cycle specific
1612 manner. Subsequently, the U2AF65α isoform along with Prp19, facilitate the proper splicing of *CDCA5* pre-
1613 mRNA, leading to accumulation of Sororin during S and G2/M phase. Finally, Sororin forms a positive
1614 feedback loop with ERK phosphorylation. Activation of this loop plays an important role in the maintenance
1615 of ERK phosphorylation, and in the progression through the G2/M phase of the cell cycle in lung
1616 adenocarcinoma.

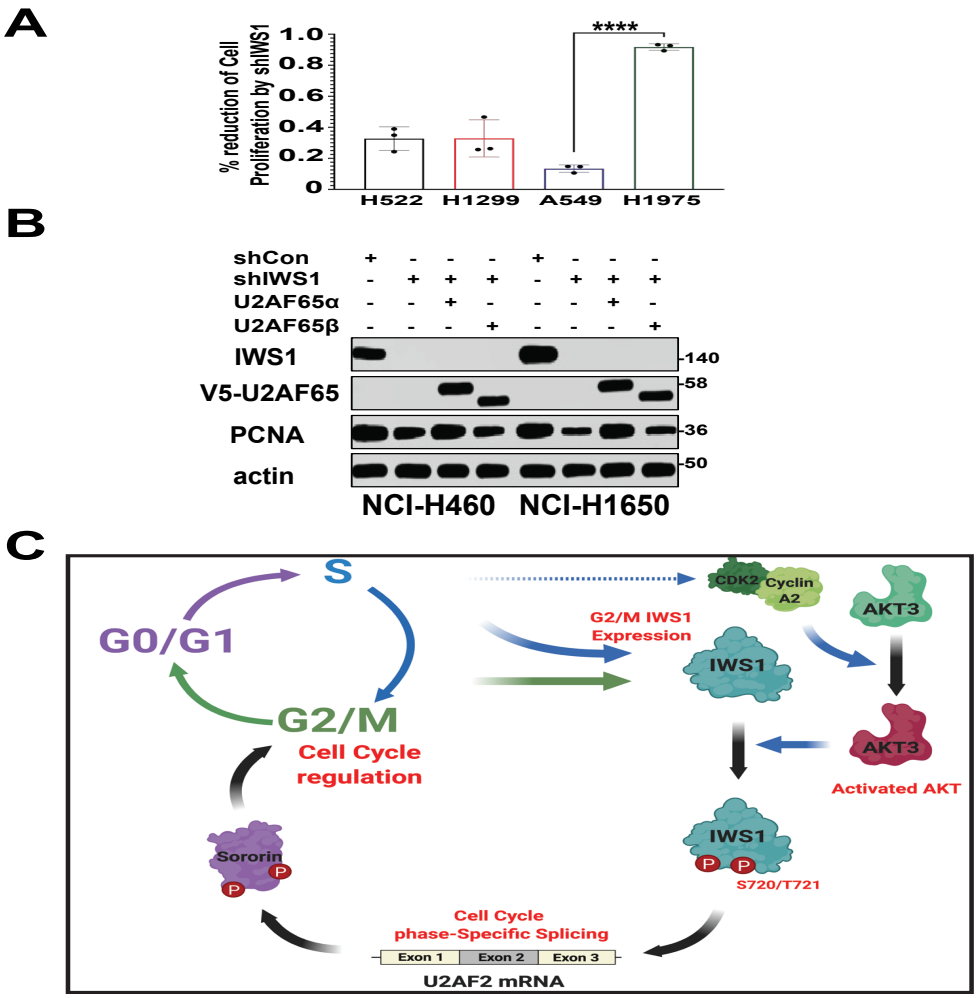

Figure S6 (relative to Figure 6). IWS1 phosphorylation promotes cell proliferation by controlling the Sororin/ERK phosphorylation feedback loop, through *U2AF2* RNA splicing.

A. Percent reduction of cell proliferation, induced by shIWS1 in the indicated cell lines. Bars show the mean reduction of cell proliferation, derived from the end-point data in Figure 6A and 6C. The error bars show the SD of at least 3 biological replicates. The statistics were performed using one-sided unpaired t-test (NCI-H522 vs A549 : p = 0.0225, NCI-H1299 vs A549 : 0.0493, A549 vs NCI-H1975 : p = 0.0001, NCI-H522 vs NCI-H1975 : p = 0.0174, NCI-H1299 vs NCI-H1975 : p = 0.0011). **B.** Cell lysates derived from the indicated NCI-H460 and NCI-H1650 cells, were probed with the indicated antibodies, in a repeat of the experiments in figures 6B and 6D, in two additional cell lines. **C.** *Model of the regulation of U2AF2 alternative RNA splicing, downstream of IWS1 phosphorylation, through the cell cycle.* IWS1 is expressed during S and G2/M (this report) and published data indicate that AKT is also activated as the cells enter S phase, via phosphorylation by CDK2/Cyclin A2. (Liu et al, 2014[73]) This induces a cell cycle specific alternative RNA splicing, resulting in inclusion of exon 2 in *U2AF2* mRNA. Subsequently, this isoform regulates the splicing and expression of Sororin, which in turn regulates the progression through the G2/M phase of the cell cycle.

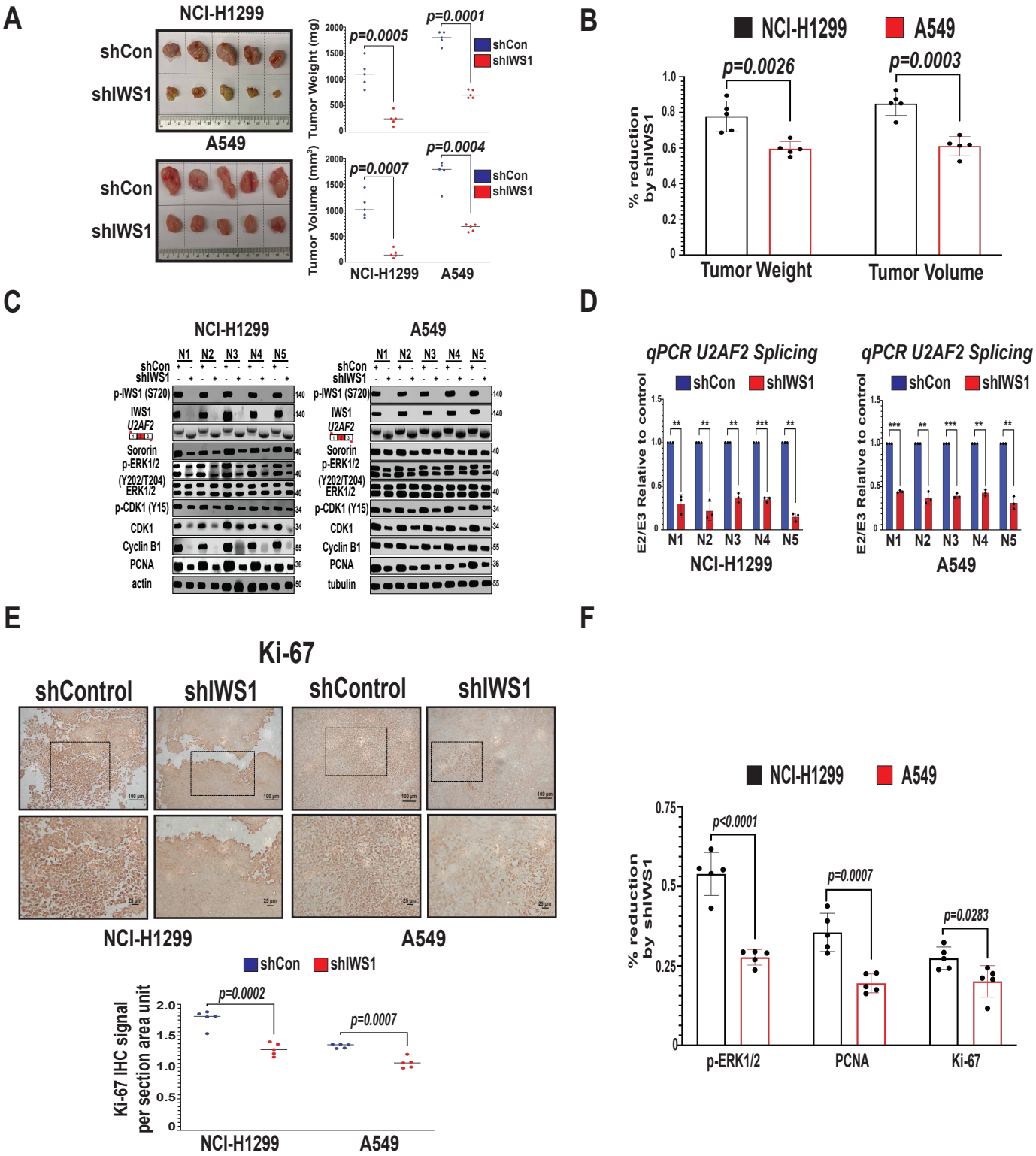

1632
1633
1634

1635 **Figure 7. IWS1 phosphorylation controls tumor growth *in vivo*, by regulating the**
1636 **U2AF2/Sororin/ERK axis.**

1637 **A.** *IWS1 phosphorylation at Ser720/Thr721 promotes tumor growth in xenograft lung adenocarcinoma*
1638 *model in NSG mice*. NSG mice were injected subcutaneously with shControl or shIWS1 NCI-H1299 or
1639 A549 cells. (N=5 mice/group). (Left panels) Images of the induced tumors, harvested at 4 weeks (NCI-
1640 H1299 cells) and 6 weeks (A549 cells) from the time of inoculation (Right panels) Scatter plots showing the
1641 tumor weight (up) and volume (down) of the harvested tumors. The horizontal lines indicate mean tumor
1642 weight or volume. Statistical analyses were done using the paired t-test. **B.** From the weight and volume of
1643 the tumors induced by shIWS1-transduced cells and shControl-transduced cells, we calculated the
1644 shIWS1-induced percent reduction of both tumor weight and volume. Bars show the mean percent
1645 reduction. The error bars show the SD of the percent reduction in each group. Statistical analyses were
1646 done using the one-sided unpaired t-test. **C.** *IWS1 phosphorylation controls the Sororin/ERK*
1647 *phosphorylation axis in vivo.* Cell lysates derived from NCI-H1299 and A549 (shControl and shIWS1)
1648 mouse xenografts, were probed with the indicated antibodies. RT-PCR, using RNA isolated from these
1649 xenografts and *U2AF2* exon 1 and exon 3 oligonucleotide primers shows that the knockdown of IWS1 in
1650 the xenografts results in *U2AF2* exon 2 exclusion. **D.** *IWS1 phosphorylation controls U2AF2 alternative*
1651 *RNA splicing in vivo.* Quantitative RT-PCR showing the *E2/E3 U2AF2* ratio using RNA derived from tumors
1652 in Fig 7C. Bars show the mean *E2/E3 U2AF2* in tumors derived from NCI-H1299 (left) or A549 (right)
1653 shIWS1 cells relative to those from shControl. The error bars are SD of at least 3 technical replicates.
1654 **p<0.001, ***p<0.001. (paired t-test) **E.** (Upper panels) Ki-67 staining of tumor xenografts of shControl and
1655 shIWS1-transduced NCI-H1299 (left) and A549 (right) cells. Formalin-fixed, paraffin-embedded tumor
1656 samples were stained with a Ki-67 antibody. Secondary antibody was HRP-labelled. The boxes delineate
1657 the area of higher magnification shown in the image below. Scale bar in the right corner of each image.
1658 (Lower panel) Scatter plots showing the Ki-67 IHC signal relative to the section area in shControl and
1659 shIWS1 NCI-H1299 and A549 tumors. The horizontal line shows the mean Ki-67 signal in the indicated
1660 groups of xenografts. Statistical analyses were performed, using the paired t-test. **F.** *K-RAS mutant tumors*
1661 *are more resistant to the loss of IWS1 in vivo.* Percentage of reduction of the described marker induced by
1662 shIWS1 in the tumors derived from the NCI-H1299 and A549 cell lines. Bars show the mean reduction of
1663 the markers, derived from the Western blots data in Figure 7C (p-ERK and PCNA) and IHC data in Figure
1664 7E (Ki-67). The error bars are SD of the values in each mice group. The statistics were performed with one-
1665 sided unpaired t-test.
1666
1667
1668
1669
1670
1671

1672

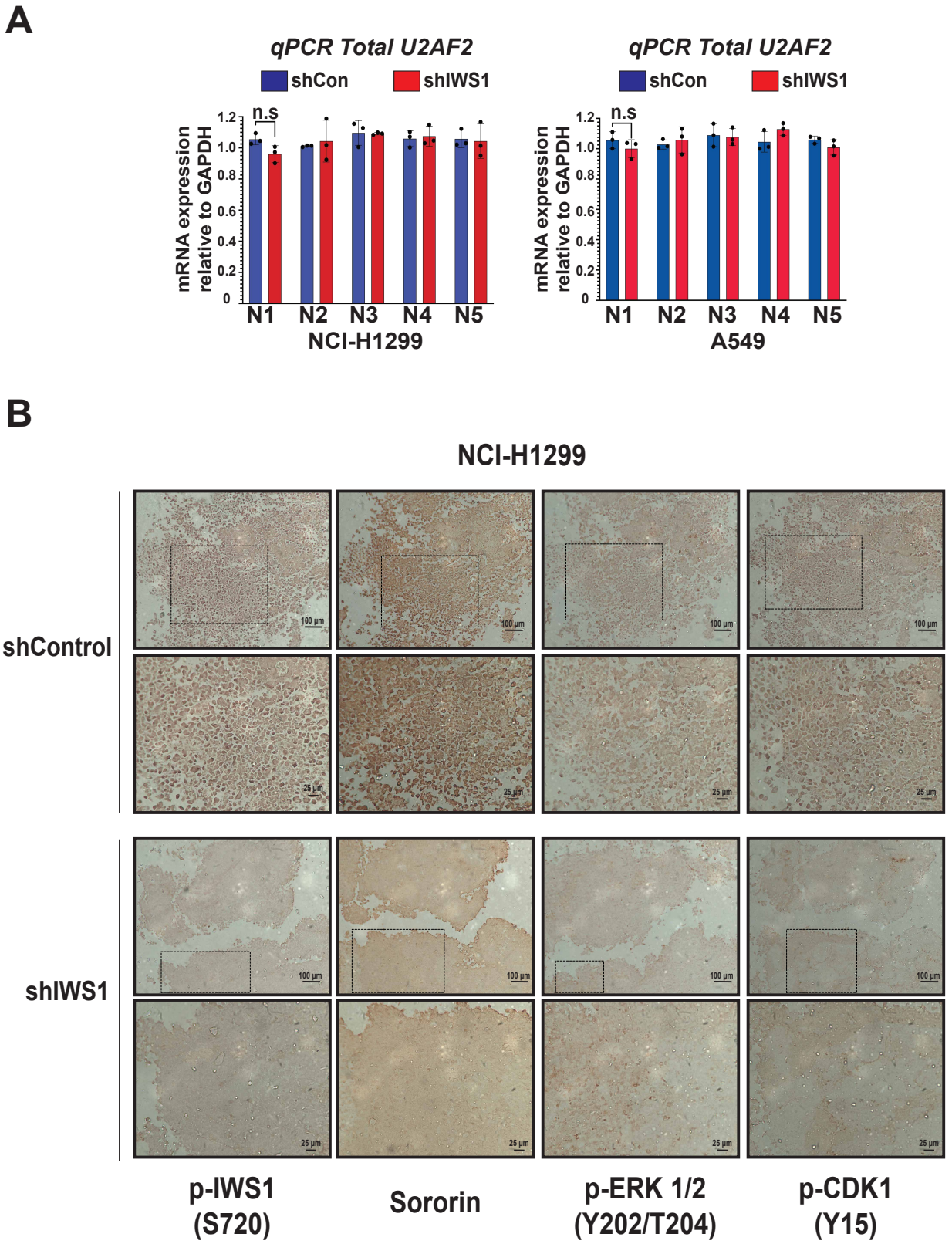
A
qPCR Total U2AF2
shCon
shIWS1
mRNA expression relative to GAPDH
n.s
1.2
1.0
0.8
0.6
0.4
0.2
0
N1
N2
N3
N4
N5
NCI-H1299
A549
B
NCI-H1299
shControl
shIWS1
100 µm
25 µm
p-IWS1 (S720)
Sororin
p-ERK 1/2 (Y202/T204)
p-CDK1 (Y15)

1673

1674

1675 **Figure S7 (Relative to Figure 7). IWS1 phosphorylation controls tumor growth *in vivo*, by regulating**
1676 **the U2AF2/Sororin/ERK axis.**

1677 **A**. Quantitative RT-PCR showing the total *U2AF2* in lysates derived from tumors in Fig 7C. Bars show the
1678 mean *U2AF2* levels, relative to *GAPDH*, in tumors derived from NCI-H1299 (left) or A549 (right) shControl
1679 and shIWS1 cells. The error bars are SD of at least 3 technical replicates. n.s : non-significant (paired t-
1680 test) **B.** *IWS1 controls the Sororin/ERK phosphorylation axis in vivo.* (Upper panels) Phospho-IWS1
1681 (Ser720), Sororin, phospho-ERK (Y202/T204) and phospho-CDK1 (Y15) staining, of NCI-H1299 shControl
1682 (upper) and shIWS1 (lower) tumor xenografts. Formalin-fixed, paraffin-embedded tumor samples from the
1683 experiment in Figure 7 were stained with the indicated antibodies. Secondary antibody was HRP-labelled.
1684 The staining of individual tumors with different antibodies was done, using sequential tumor sections, so
1685 that we could determine whether the expression and/or phosphorylation of proteins of interest spatially
1686 overlapped. Boxes delineate the area of higher magnification, shown in the image below. Scale in the right
1687 lower corner of each image.

1688
1689
1690
1691
1692
1693
1694
1695
1696
1697
1698
1699
1700
1701
1702
1703
1704
1705
1706
1707
1708
1709
1710
1711
1712
1713
1714

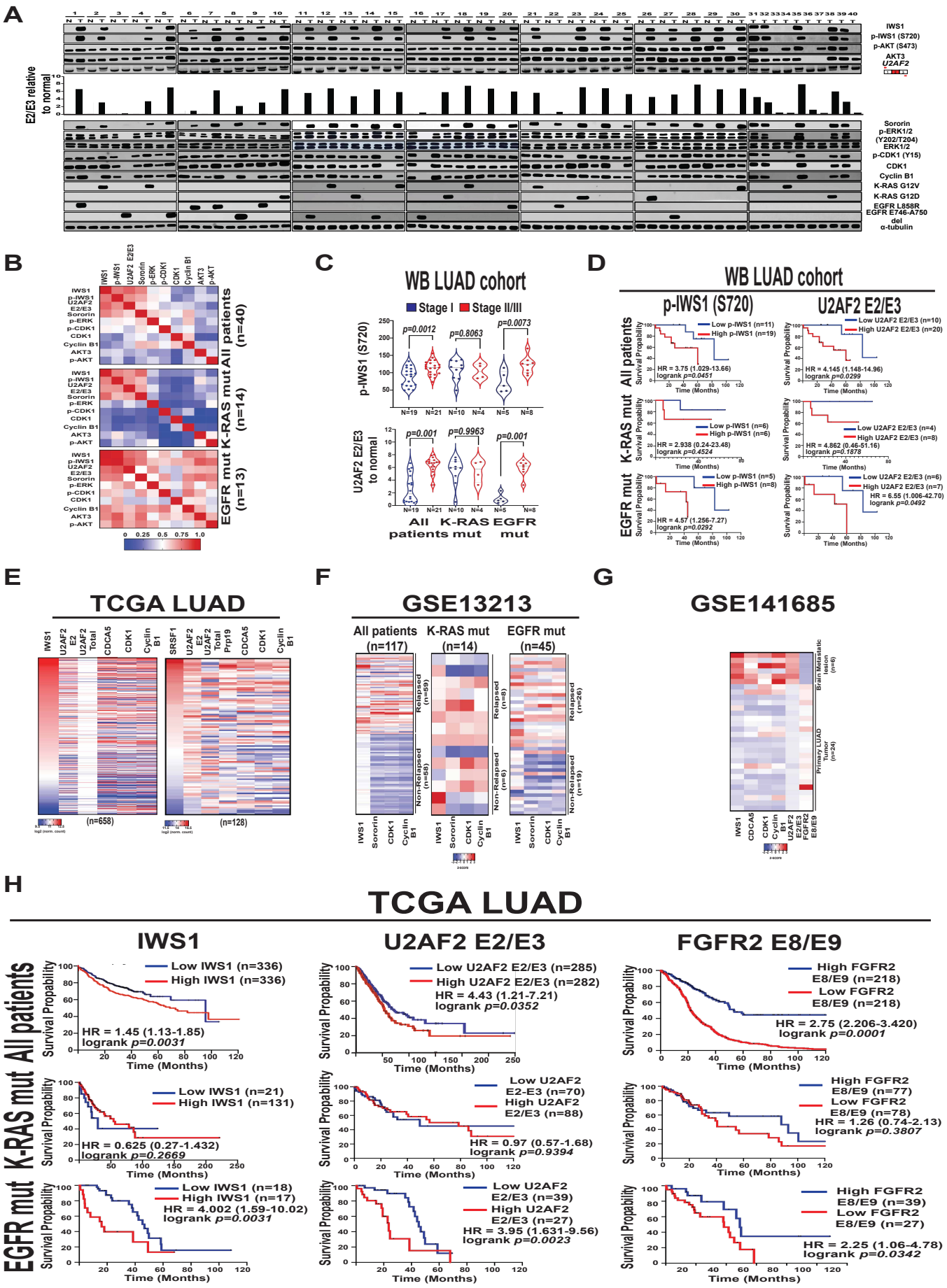
A
E2/E3 relative to normal
IWS1
p-IWS1 (S720)
p-AKT (S473)
AKT3
U2AF2
Sororin
p-ERK1/2 (Y202/T204)
ERK1/2
p-CDK1 (Y15)
CDK1
Cyclin B1
K-RAS G12V
K-RAS G12D
EGFR L858R
EGFR E746-A750 del
α-tubulin
B
All patients (n=40)
K-RAS mut (n=14)
EGFR mut (n=13)
C
WB LUAD cohort
Stage I
Stage II/III
p-IWS1 (S720)
U2AF2 E2/E3 to normal
All patients
K-RAS mut
EGFR mut
D
WB LUAD cohort
p-IWS1 (S720)
U2AF2 E2/E3
All patients
K-RAS mut
EGFR mut
Survival Propability
Time (Months)
E
TCGA LUAD
(n=658)
(n=128)
F
GSE13213
All patients (n=117)
K-RAS mut (n=14)
EGFR mut (n=45)
Relapsed
Non-Relapsed
G
GSE141685
Brain Metastatic lesion (n=6)
Primary LUAD tumor (n=24)
H
TCGA LUAD
IWS1
U2AF2 E2/E3
FGFR2 E8/E9
All patients
K-RAS mut
EGFR mut
Survival Propability
Time (Months)
Low IWS1 (n=336)
High IWS1 (n=336)
HR = 1.45 (1.13-1.85)
logrank p=0.0031
Low IWS1 (n=21)
High IWS1 (n=131)
HR = 0.625 (0.27-1.432)
logrank p=0.2669
Low IWS1 (n=18)
High IWS1 (n=17)
HR = 4.002 (1.59-10.02)
logrank p=0.0031
Low U2AF2 E2/E3 (n=285)
High U2AF2 E2/E3 (n=282)
HR = 4.43 (1.21-7.21)
logrank p=0.0352
Low U2AF2 E2-E3 (n=70)
High U2AF2 E2/E3 (n=88)
HR = 0.97 (0.57-1.68)
logrank p=0.9394
Low U2AF2 E2/E3 (n=39)
High U2AF2 E2/E3 (n=27)
HR = 3.95 (1.631-9.56)
logrank p=0.0023
High FGFR2 E8/E9 (n=218)
Low FGFR2 E8/E9 (n=218)
HR = 2.75 (2.206-3.420)
logrank p=0.0001
High FGFR2 E8/E9 (n=77)
Low FGFR2 E8/E9 (n=78)
HR = 1.26 (0.74-2.13)
logrank p=0.3807
High FGFR2 E8/E9 (n=39)
Low FGFR2 E8/E9 (n=27)
HR = 2.25 (1.06-4.78)
logrank p=0.0342

1716 **Figure 8. The p-IWS1/U2AF2 pathway is active in human lung adenocarcinomas and impacts tumor**
1717 **grade, stage, metastatic potential and treatment relapse in patients with *EGFR* mutant, but not *K-***
1718 ***RAS* mutant tumors.**

1719 **A.** Lysates form 30 LUAD samples, paired with NAT and 10 unpaired LUAD samples were probed with the
1720 indicated antibodies. (Fifth line from the top). RT-PCR, using RNA isolated from these tumors, and *U2AF2*
1721 exon 1 and exon 3 oligonucleotide primers, shows that phosphor-IWS1 correlates with U2AF2 exon 2
1722 inclusion, as expected. (Sixth line) *E2/E3 U2AF2* exon ratio in the tumors in the upper panel, relative to the
1723 average of the 30 normal lung samples. **B.** *IWS1 and phospho-IWS1 correlate with U2AF2 exon 2 inclusion*
1724 *and the activity of the Sororin/ERK axis, most robustly in EGFR mutant lung adenocarcinomas.* Heatmaps
1725 of the correlation coefficients between the indicated components of the IWS1 phosphorylation pathway, in
1726 the entire cohort (left), in *K-RAS* mutant (middle) and in *EGFR* mutant tumors (right). The correlation
1727 coefficients were calculated using simple linear regression. The values and the statistical confidence of all
1728 the comparisons can be found in Supplementary Table S5. **C.** Violin plots showing the abundance of IWS1
1729 phosphorylation (left) and the *E2/E3 U2AF2* ratio (right) in stage I and Stage II/III tumors. Data shown for
1730 all tumors in A and B, and selectively for *EGFR* or *K-RAS* mutant tumors. The horizontal black lines indicate
1731 mean values for p-IWS1 levels and *E2/E3 U2AF2* ratios. Statistical analyses were performed using the one-
1732 sided unpaired t-test. **D.** Kaplan-Meier Curves showing the impact of the abundance of phosphor-IWS1
1733 (left) and *E2/E3 U2AF2* ratio (right) on patient survival in the LUAD cohort in 8A. Separate curves are shown
1734 again for all the patients, or for the patients with *K-RAS* or *EGFR* mutant tumors. The effect of phosphor-
1735 IWS1 levels and *U2AF2* exon 2 inclusion on patient survival is again significant in *EGFR* mutant, but not in
1736 *K-RAS* mutant tumors. Statistical analyses were performed using the log rank test and Cox's proportional
1737 hazards model. **E.** Heat Maps showing the correlation of *IWS1* or *SRSF1* with components of the
1738 *IWS1/U2AF2* pathway in the TCGA LUAD database. The RNA-seq expression values from each individual
1739 patient were expressed as *log2* normalized counts and they were used to calculate the correlation
1740 coefficients. **F.** *The IWS1 phosphorylation axis correlated with relapse in lung adenocarcinoma patients*
1741 *harboring EGFR mutations.* Heatmaps showing the expression of IWS1, CDCA5, CDK1 and CCNB1 in
1742 relapsed and in non-relapsed tumors. Microarray analyses of lung adenocarcinomas in the entire cohort
1743 (left), *K-RAS* mutant (middle) or *EGFR* mutant (right) cohort in the GSE13213 dataset. For quantification of
1744 gene expression, we used the z-scores of the microarray signals. **G.** *IWS1 expression and the U2AF2 exon*
1745 *2 inclusion and FGFR2 exon 8 exclusion pathways correlate strongly with metastasis in lung*
1746 *adenocarcinomas.* Heat Maps showing the expression of IWS1 and its downstream targets in the
1747 IWS1/U2AF2 pathway in resected brain metastatic lesions and primary lung adenocarcinomas. RNA-seq
1748 data from the GSE141685 dataset and primary lung adenocarcinomas derived from TCGA LUAD database.
1749 The TCGA LUAD samples were picked randomly, independent of their clinical stage or mutational status.
1750 For quantification of gene expression, we used the z-scores of the normalized RNA-Seq reads. The primary
1751 tumors from the TCGA LUAD database are listed in Table S6. **H.** *The IWS1 phosphorylation axis defines*
1752 *poor survival in lung adenocarcinoma patients harboring EGFR mutations.* Kaplan-Meier Curves showing

the impact of IWS1 expression (left), *E2/E3 U2AF2* ratio (middle) and *FGFR2* E8/E9 ratio (right) on patient survival in patients in the TCGA LUAD database. Separate curves are shown for all the patients, or for the patients with *K-RAS* or *EGFR* mutant tumors. The effect of IWS1 levels and *U2AF2* exon 2 inclusion in patient survival is significant in *EGFR* mutant, but not in *K-RAS* mutant tumors. Statistical analyses were performed using the log rank test and Cox's proportional hazards model.

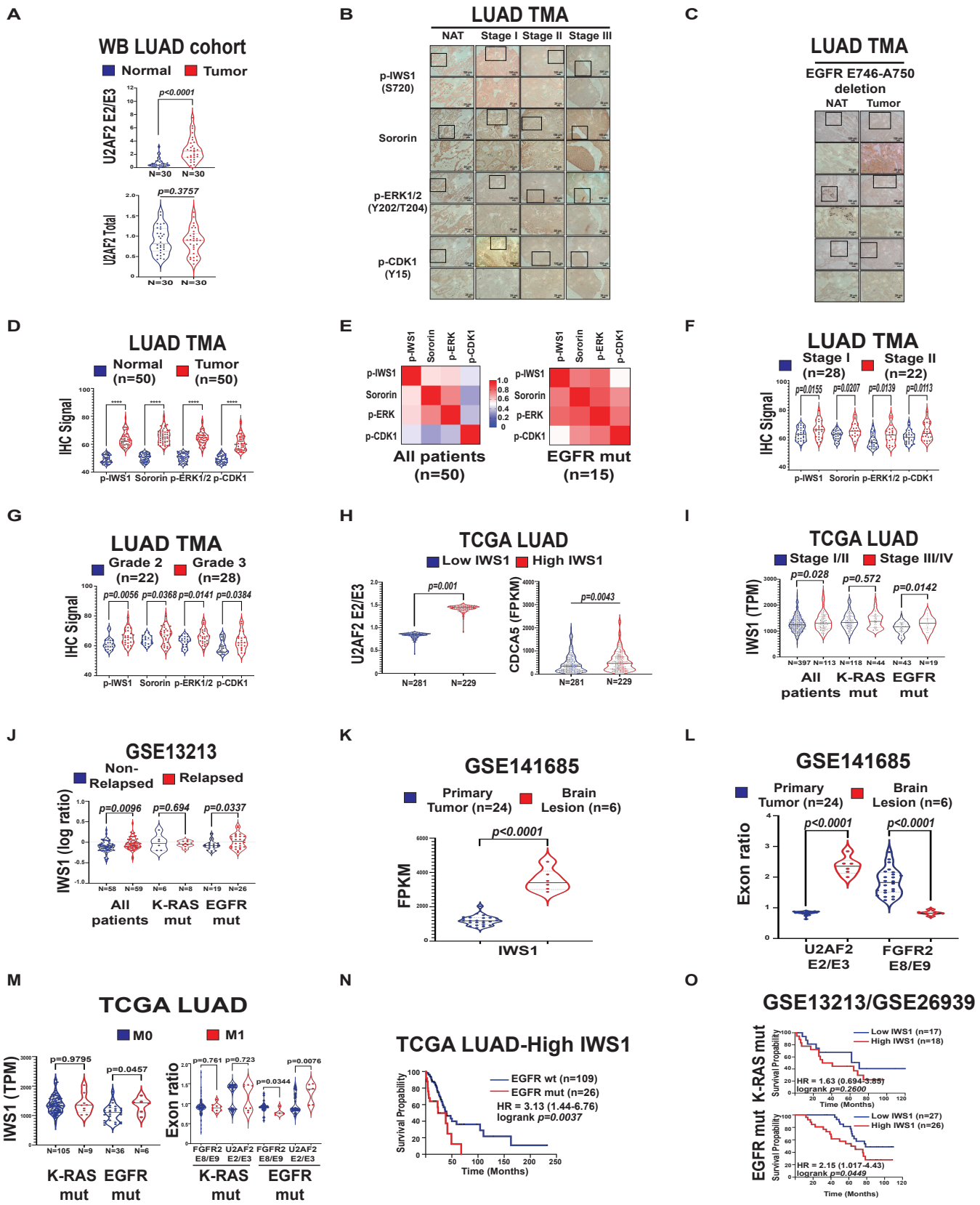
A
WB LUAD cohort
Normal
Tumor
U2AF2 E2/E3
p<0.0001
N=30
N=30
U2AF2 Total
p=0.3757
B
LUAD TMA
NAT
Stage I
Stage II
Stage III
p-IWS1 (S720)
Sororin
p-ERK1/2 (Y202/T204)
p-CDK1 (Y15)
C
LUAD TMA
EGFR E746-A750 deletion
NAT
Tumor
D
LUAD TMA
Normal (n=50)
Tumor (n=50)
IHC Signal
p-IWS1
Sororin
p-ERK1/2
p-CDK1
E
All patients (n=50)
EGFR mut (n=15)
F
LUAD TMA
Stage I (n=28)
Stage II (n=22)
p=0.0155
p=0.0207
p=0.0139
p=0.0113
G
LUAD TMA
Grade 2 (n=22)
Grade 3 (n=28)
p=0.0056
p=0.0368
p=0.0141
p=0.0384
H
TCGA LUAD
Low IWS1
High IWS1
U2AF2 E2/E3
p=0.001
N=281
N=229
CDCA5 (FPKM)
p=0.0043
I
TCGA LUAD
Stage I/II
Stage III/IV
IWS1 (TPM)
p=0.028
p=0.572
p=0.0142
N=397
N=113
N=118
N=44
N=43
N=19
All patients
K-RAS mut
EGFR mut
J
GSE13213
Non-Relapsed
Relapsed
IWS1 (log ratio)
p=0.0096
p=0.694
p=0.0337
N=58
N=59
N=6
N=8
N=19
N=26
All patients
K-RAS mut
EGFR mut
K
GSE141685
Primary Tumor (n=24)
Brain Lesion (n=6)
FPKM
p<0.0001
IWS1
L
GSE141685
Primary Tumor (n=24)
Brain Lesion (n=6)
Exon ratio
p<0.0001
p<0.0001
U2AF2 E2/E3
FGFR2 E8/E9
M
TCGA LUAD
M0
M1
IWS1 (TPM)
p=0.9795
p=0.0457
N=105
N=9
N=36
N=6
K-RAS mut
EGFR mut
Exon ratio
p=0.761
p=0.723
p=0.0344
p=0.0076
FGFR2 E8/E9
U2AF2 E2/E3
FGFR2 E8/E9
U2AF2 E2/E3
K-RAS mut
EGFR mut
N
TCGA LUAD-High IWS1
Survival Propability
EGFR wt (n=109)
EGFR mut (n=26)
HR = 3.13 (1.44-6.76)
logrank p=0.0037
Time (Months)
O
GSE13213/GSE26939
K-RAS mut
Low IWS1 (n=17)
High IWS1 (n=18)
HR = 1.63 (0.694-3.85)
logrank p=0.2600
EGFR mut
Low IWS1 (n=27)
High IWS1 (n=26)
HR = 2.15 (1.017-4.43)
logrank p=0.0449
Survival Propability
Time (Months)

1798

1799 **Figure S8 (relative to Figure 8). The AKT/p-IWS1/U2AF2 axis is active in human lung**
1800 **adenocarcinoma and affects the clinical outcome of *EGFR* mutant patients.**
1801 **A.** *The overall abundance of the U2AF2 mRNA in lung adenocarcinomas and the adjacent normal tissue is*
1802 *similar, but the E2/E3 ratio is higher in the tumors.* Quantitative RT-PCR showing the *U2AF2 E2/E3* ratio
1803 (top) and the total *U2AF2* mRNA (bottom) in lysates derived from the 30 LUAD samples and the paired
1804 normal adjacent tissue in Fig 8A. The black lines in the violin plots show the mean *U2AF2 E2/E3* ratio
1805 relative to the matching normal samples, or *U2AF2* levels, relative to *GAPDH*. Statistical analyses were
1806 done using the paired t-test. **B.** *IWS1 phosphorylation correlates with U2AF2 alternative RNA splicing and*
1807 *the Sororin/ERK axis in lung adenocarcinoma patients***.** Sections of a commercially available tissue
1808 microarray (TMA) of 50 LUAD with paired NAT, were probed with the indicated antibodies. Figure shows
1809 the staining of a representative NAT sample and representative samples of Stage I, II and III lung
1810 adenocarcinomas (one of each). Boxes delineate the area of higher magnification, shown in the image
1811 below. Scale in the right lower corner of each image. **C.** The TMA sections used before were stained with
1812 the specific monoclonal antibody against EGFR E746-A750 deletion. Figure shows three representative
1813 lung adenocarcinomas with EGFR deletion (E746-A750 deletion) and the corresponding NATs. Boxes
1814 delineate the area of higher magnification, shown in the image below. Scale in the right lower corner of
1815 each image. **D.** *The overall activity of the p-IWS1/Sororin is higher in human lung adenocarcinomas than*
1816 *in the adjacent normal tissue.* Violin plots showing the abundance of IWS1 phosphorylation, along with the
1817 abundance of Sororin, phospho-ERK and phospho-CDK1, in the LUAD and NAT samples in the tissue
1818 microarray in B and C. The black line indicates the mean p-IWS1, Sororin, p-ERK and p-CDK1 levels.
1819 Statistical analyses were done using the paired t-test. **E.** *IWS1 phosphorylation exhibits a more robust*
1820 *correlation with Sororin, phospho-ERK and phospho-CDK1 in lung adenocarcinomas with EGFR*
1821 *mutations.* Heatmaps showing the correlation coefficient between the indicated components of the IWS1
1822 phosphorylation pathway in the entire TMA cohort (left) and in the EGFR mutant cohort (right). The
1823 correlations were calculated using simple linear regression. The statistics and the p values for all the
1824 comparisons, can be found in Supplementary Table S5. **F.** *The activity of the p-IWS1/Sororin pathway*
1825 *correlates with tumor stage in human lung adenocarcinomas.* Violin plots comparing the phosphorylation
1826 of IWS1 and the abundance of Sororin, phospho-ERK and phospho-CDK1 in stage I and Stage II/III lung
1827 adenocarcinomas in the group of 50 tumors sampled in the commercial TMA described above. Statistical
1828 analyses were performed using the one-sided unpaired t-test. **G.** *The activity of the p-IWS1/Sororin*
1829 *pathway correlates with tumor grade in human lung adenocarcinomas.* Violin plots comparing the
1830 phosphorylation of IWS1 and the abundance of Sororin, phospho-ERK and phospho-CDK1 in histological
1831 grade 2 and grade 3 lung adenocarcinomas in the group of 50 tumors in the commercial TMA described
1832 above. Statistical analyses were performed using the one-sided unpaired t-test. **H.** The expression of IWS1
1833 correlates with Exon 2 inclusion in the *U2AF2* mRNA transcripts (upper panel) and with the expression of
1834 *CDCA5* (lower panel) in the TCGA LUAD dataset. The black line indicates the mean expression of *U2AF2*
1835 *E2/E3* ratio and *CDCA5*. Statistical analyses were performed using the one-sided unpaired t-test. **I.** Violin

1836 plots showing the abundance of IWS1 in stage I/II and in Stage III/IV tumors of patients in the TCGA LUAD
1837 database. Data shown for all tumors, and selectively for *EGFR* or *K-RAS* mutant tumors. The horizontal
1838 lines indicate mean values for IWS1 levels. Statistical analyses were performed using the one-sided
1839 unpaired t-test. **J.** Violin plots showing the abundance of IWS1 in relapsed and non-relapsed tumors of
1840 patients in the GSE13213 dataset. Data shown for all tumors, and selectively for *EGFR* or *K-RAS* mutant
1841 tumors. The horizontal lines indicate mean values for IWS1. Statistical analyses were performed using the
1842 one-sided unpaired t-test. **K.** The expression of *IWS1* is higher in brain metastases of lung
1843 adenocarcinomas than in primary tumors, while the *E8/E9* ratio in mature *FGFR2* transcripts (lower panel-
1844 right) is lower in brain metastases relative to primary tumors. The black lines indicate the mean expression
1845 of IWS1 and the mean *U2AF2 E2/E3* and *FGFR-2 E8/E9* ratio. Violin plots were based on the same data
1846 shown in Figure 8G. Statistical analyses were performed using the one-sided unpaired t-test. **L.** The *E2/E3*
1847 ratio in mature *U2AF2* mRNA transcripts are higher in the same patient group as Fig S8L. The black lines
1848 indicate the mean *U2AF2 E2/E3* and *FGFR2 E8/E9* ratio. Violin plots were based on the same data shown
1849 in Figure 8G. Statistical analyses were performed using the one-sided unpaired t-test. **M.** (Left panel) Violin
1850 plots showing the expression of IWS1 in transcripts per million (TPM) in *K-RAS* and *EGFR* mutant, primary
1851 and metastatic lung adenocarcinomas in the TCGA LUAD database. IWS1 expression is higher in tumors
1852 from patients with metastatic disease (M1) only if the tumors harbor *EGFR* mutations (Right panel). Exon
1853 E2/E3 ratio in the *U2AF2* mRNA and exon E8/E9 ratio in the *FGFR2* mRNA in *K-RAS* and *EGFR* mutant
1854 lung adenocarcinomas. E2/E3 ratio in the *U2AF2* mRNA is higher and the E8/E9 ratio in the *FGFR2* mRNA
1855 is lower in tumors from patients with metastatic disease (M1), only if the tumors harbor *EGFR* mutations.
1856 The black lines indicate the mean IWS1 expression, and the mean *U2FA2* E2/E3 and *FGFR2* E8/E9 ratios.
1857 Statistical analyses were performed using the one-sided unpaired t-test. **N.** *EGFR mutations predict poor*
1858 *survival in patients expressing high levels of IWS1.* Kaplan-Meier curves showing the impact of *EGFR*
1859 mutations on survival, in patients with lung adenocarcinomas expressing high levels of IWS1. Statistical
1860 analyses were performed using the log rank test and Cox's proportional hazards model. **O.** *The abundance*
1861 *of IWS1 has a stronger negative impact on the survival of patients with lung adenocarcinomas harboring*
1862 *EGFR, than those with lung adenocarcinomas harboring K-RAS mutations.* Kaplan-Meier curves showing
1863 the impact of the abundance of IWS1 on the survival of patients with lung adenocarcinomas harboring *K-*
1864 *RAS* mutations (upper panel) or *EGFR* mutations (lower panel) in the GSE13213/GSE26969 dataset.
1865 Statistical analyses were performed using the log rank test and Cox's proportional hazards model.
1866